行政院國家科學委員會補助專題研究計畫 ■成 果 報 告
□期中進度報告

整合傳統芬頓及氧化鐵過氧化程序處理毒性工業廢水

計畫類別：■ 個別型計畫 □ 整合型計畫
計畫編號：NSC 96－2628－E－041－001－MY3
執行期間： 96 年 8 月 1 日至 99 年 7 月 31 日

計畫主持人： 盧明俊 教授
共同主持人： Jin Anotai 教授
計畫參與人員：范竣程、李紘屹、蔡宜君、Nonglak Boonrattanakij、Pumis Thuptimdang,
蘇佳琪

成果報告類型(依經費核定清單規定繳交)：□精簡報告 ■完整報告

本成果報告包括以下應繳交之附件：
■赴國外出差或研習心得報告一份
□赴大陸地區出差或研習心得報告一份
■出席國際學術會議心得報告及發表之論文各一份
□國際合作研究計畫國外研究報告書一份

處理方式：除產學合作研究計畫、提升產業技術及人才培育研究計畫、列管計畫及下列情形者外，得立即公開查詢
□涉及專利或其他智慧財產權，□一年□二年後可公開查詢

執行單位： 嘉南藥理科技大學

中 華 民 國 九十九 年 八 月 十七 日

ABSTRACT

This research determined the rate constant between 2,6-dimethy-aniline (2,6-DMA) and hydroxyl radicals ($OH^{\bullet}$) by using Fenton reaction and competitive kinetics technique. Regardless of experimental conditions either batch or continuous mode, presence or absence of media, complete suspension or fluidized-bed reactor, the intrinsic 2^{nd}-order rate constant between 2,6-DMA and $OH^{\bullet}$ were found to be consistent in between 1.59×10^{10} and 1.80×10^{10} $M^{-1}sec^{-1}$ with the average and 95% confidence interval of $1.70\pm0.04\times10^{10}$ $M^{-1}sec^{-1}$. Aromatic intermediates from 2,6-DMA oxidation by $OH^{\bullet}$ were 2,6-dimethyl-nitrobenzene, 2,6-dimethy-phenol, 2,6-dimethyl-nitrophenol, 2,6-dimethyl-hydroquinone, 2,6-dimethyl-benzoquinone, and 2,6-dimethyl-3-hydroxy-benzoquinone indicating the methyl groups on the benzene ring were less susceptible to $OH^{\bullet}$ attack than the amino and hydroxide groups. Maleic, lactic, oxalic, acetic, and formic acids were also identified as the carboxylic intermediates. Degradation mechanism of 2,6-DMA oxidation by $OH^{\bullet}$ was also proposed.

Considering iron crystallization, it was found that ferrous (Fe^{2+}) was immediately transformed to ferric (Fe^{3+}) after the initiation of Fenton reaction and sequentially precipitated out in the form of $Fe(OH)_3$ due to its low solubility even in the acidic solution. However, if precipitation occurred in the labile zone, $Fe(OH)_3$ was formed via homogeneous nucleation and crystallized very slowly onto the fluidized media. On the other hand, if it happened in the metastable zone, $Fe(OH)_3$ crystallized onto the fluidized media more rapidly via heterogeneous nucleation and iron was removed significantly from the aqueous phase. Crystallization was controlled by the transport step rather than the surface interaction step. Rate of crystal growth followed the orthokinetic flocculation when the mixing was sufficiently provided; however, it became under the influence of molecular diffusion or perikinetic flocculation depending on the crystallite size under the stagnant conditions. Presence of organic intermediates which could form complex with Fe^{3+} increased the solubility of Fe^{3+} and sequentially deteriorated the crystallization process. Crystallization rate onto fluidized media decreased with time; thus, continuously replace certain portion of coated solids with fresh media will maintain satisfactory crystallization rate. Catalytic activity of the $Fe(OH)_3$-coated sand with 3.5% iron content by weight was only equivalent to 4% of the goethite.

CONTENTS

Page

ABSTRACT ……... I
CONTENTS……..II
LIST OF TABLES……V
LIST OF FIGURES…..…… VII
NOMENCLATURES…….....IX

CHAPTER I INTRODUCTION……1
1.1 Research Rationale…… 1
1.2 Objectives……..….. 3
1.3 Hypotheses……...3
1.4 Scope of the Research…….....3
1.5 Obtained Results…..…….4

CHAPTER II THEORIES AND LITERATURE REVIEWS..... 5
2.1 2,6-Dimethyl-aniline.....5
2.1.1 General Information.....5
2.1.2 Physical and Chemical Properties.....6
2.1.3 Toxicology…… 6
2.1.4 First Aid Measures…….....8
2.2 Advanced Oxidation Processes.....8
2.3 Fenton Process..... 9
2.3.1 Hydrogen Peroxide…..... 9
2.3.2 Ferrous…….. 10
2.3.3 Hydroxyl Radicals…….……..… 10
2.3.4 Fenton Reaction……..…..... 12
2.4 Fluidized-bed Fenton Process.....13
2.5 Reaction Rate Constant Determination.....14
2.6 Precipitation and Crystallization.....17
2.6.1 Rational…….....17
2.6.2 Nucleation…….....17
2.6.2.1 Homogeneous Nucleation.....18

2.6.2.2 Heterogeneous Nucleation..... 20
2.6.3 Crystal Growth..... 20
2.7 Literature Reviews……..... 24
2.7.1 Competitive Kinetics Technique..... 24
2.7.2 Degradation of 2,6-Dimethyl-aniline by AOPs..... 26
2.7.3 Removal of Organic Compounds in Heterogeneous Catalysis by H_2O_2..... 27
2.7.4 Iron Crystallization in Fluidized-bed Fenton Reactor...…….. 30

CHAPTER III METHODOLOGY……..... 33
3.1 Materials and Chemicals..... 33
3.1.1 Chemicals……..... 33
3.1.2 Batch Reactor……..... 33
3.1.3 Fluidized-bed Reactor..... 33
3.2 Experimental Procedures……..… 34
3.2.1 Kinetics of 2,6-Dimethyl-aniline Degradation…..... 34
3.2.1.1 Completely Mixed Reactor…… 34
3.2.1.2 Fluidized-bed Reactor…… 35
3.2.2 Iron Crystallization……..…….…….... 35
3.3 Experimental Scenarios…….…….…… 37
3.3.1 Kinetics of 2,6-Dimethyl-aniline Degradation…..... 37
3.3.2 Mechanism of 2,6-Dimethyl-aniline Oxidation…..... 40
3.3.3 Iron Precipitation and Crystallization…..... 41
3.4 Analytical Methods…….…….47
3.4.1 Measurement of Aromatic Compounds..... 47
3.4.2 Measurement of Iron……..... 48
3.4.3 Measurement of Hydrogen Peroxide Residual..... 48
3.4.4 Measurement of Total Organic Carbon..... 48
3.4.5 Identification and Measurement of Carboxylic Intermediates..48
3.4.6 Identification of Aromatic Intermediates…….…….....49
3.4.7 Solid Characterization…….....49

CHAPTER IV RESULTS AND DISCUSSION…….…….…… 50
4.1 Kinetics of 2,6-Dimethyl-aniline Degradation……..…..…… 50
4.1.1 Experimental Control..... 50

4.1.1.1 2,6-Dimethyl-aniline, n,n-Dimethyl-aniline and Aniline Oxidation by H_2O_2 and Volatilization..... 50
4.1.1.2 *o*-Toluidine Oxidation by H_2O_2 ……..... 50
4.1.2 Verification of Competitive Kinetics Technique.....52
4.1.3 Intrinsic Rate Constant of 2,6-Dimethyl-aniline with Hydroxyl Radical.....52
4.1.3.1 Batch Study in the Absence of Media.....52
4.1.3.2 Batch Study in the Presence of Media..... 55
4.1.3.3 Batch Study in the Fluidized-bed Reactor……..... 58
4.1.3.4 Continuous Study in the Absence of Media…….. 58
4.1.3.5 Overall Rate Constant and Confidence Interval…... 60
4.1.4 Effect of Fenton's Reagent on Organic Degradation.....60
4.1.5 Degradation Intermediates and Pathway……..... 62
4.2 Iron Crystallization…….……. 66
4.2.1 Iron Solubility…….....…… 66
4.2.2 $Fe(OH)_3$ Crystallization in Fluidized-bed Reactor…….. 69
4.2.3 $Fe(OH)_3$ Crystallization in Fluidized-bed Fenton Process…...70
4.2.4 Effect of $Fe(OH)_3$ Crystallites……..…..... 72
4.2.5 Effect of Iron Concentration…….....…… 74
4.2.6 Effect of Turbulence…… 77
4.2.7 Effect of Organic Compounds…….....80
4.2.8 Reusability of Iron-coated Construction Sand for Iron Crystallization……..……82
4.2.9 Catalytic Activity of Iron-coated Construction Sand….....86

CHAPTER V CONCLUSIONS……..... 92
5.1 Conclusions
5.1.1 Kinetics of 2,6-Dimethyl-aniline Degradation……..... 92
5.1.2 Iron Crystallization……..…… 92
5.2 Recommendations for Further Studies ……... 94

REFERENCES……...95
APPENDIX A 赴國外出差或研習心得報告……101
APPENDIX B 出席國際學術會議心得報告及發表之論文……126

LIST OF TABLES

Table		Page
2.1	Physical and chemical properties of 2,6-DMA	7
2.2	Oxidation potential of common oxidizing species	11
3.1	Conditions for the determination of H_2O_2 oxidation and volatilization of target compounds	37
3.2	Conditions for the determination of *o*-toluidine oxidation by H_2O_2	38
3.3	Conditions for verification of the competitive rate technique	38
3.4	Conditions for the rate constant determination under the batch operation	39
3.5	Conditions for the rate constant determination in the presence of solid media	39
3.6	Conditions for rate constant determination by the fluidized-bed Fenton process	40
3.7	Conditions for the rate constant determination under the continuous operation.	40
3.8	Conditions for oxidation pathway determination	41
3.9	Conditions for iron solubility study	41
3.10	Conditions for the effect of iron concentration	42
3.11	Conditions for the $Fe(OH)_3$ crystallization characterization in FBR	42
3.12	Conditions for the crystallization in fluidized-bed Fenton process	43
3.13	Conditions for the effect of $Fe(OH)_3$ crystallites	43
3.14	Conditions for the effect of iron concentration on crystallization	44
3.15	Conditions for the effect of mixing on crystal growth	44
3.16	Conditions for the effect of organo-ferric complex on Fe^{3+} solubility/crystallization in FBR	45
3.17	Conditions for the effect of organo-ferric complex on Fe^{3+} solubility/crystallization under dynamic state in fluidized-bed Fenton process	45
3.18	Conditions for the reusability of iron-coated CS for iron crystallization	46
3.19	Experimental scenarios for the catalytic ability of iron-coated construction sand on the oxidation of 2,6-DMA and AN	46
4.1	Intrinsic rate constants of 2,6-DMA obtained from various experimental conditions	56

4.2. Identified aromatic intermediates of 2,6-DMA oxidation by $OH^{\bullet}$……....62

.

LIST OF FIGURES

Figure		Page
2.1	Structure of 2,6-DMA……..……...6	
2.2	Fluidized-bed Fenton reactions.……14	
2.3	Schematic solubility isotherm of a solid electrolyte ……..……... 19	
2.4	Schematic representation of the ability of a solid substrate to catalyze the nucleation …… 21	
2.5	Attachment and detachment of an ion or molecule to and from a solid lattice…….... 21	
2.6	Concentration gradient in liquid phase for extreme cases of diffusion control and surface-interaction control……..… 23	
2.7	Reaction mechanism of benzoic acid (BA) oxidation by the fluidized-bed Fenton process…….... 32	
3.1	Fluidized-bed reactor. ……..……..… 34	
3.2	Experimental scheme for Fenton and fluidized-bed Fenton processes.…..…36	
3.3	Gas chromatography chromatogram……..……47	
4.1	Control experiment for direct H_2O_2 oxidation and volatilization …….... 51	
4.2	Control experiment for direct H_2O_2 oxidation of the internal standard (OT) 51	
4.3	Verification of competitive technique..…….…. 53	
4.4	Intrinsic rate constant determination of 2,6-DMA in batch mode…….… 54	
4.5	Intrinsic rate constant determination between 2,6-DMA and $OH^{\bullet}$ in a SiO_2-suspension reactor….……..… 57	
4.6	Intrinsic rate constant determination between 2,6-DMA and $OH^{\bullet}$ in a batch fluidized-bed reactor…….……..… 59	
4.7	Time-profile of 2,6-DMA and AN in continuous mode…… 60	
4.8	Effect of Fenton's reagent on the degradation of 2,6-DMA and AN in a batch mode without media…….. 61	
4.9	Proposed reaction pathway for the mineralization of 2,6-DMA by $OH^{\bullet}$…...64	
4.10	Intermediate products and TOC profiles of 10 mM of 2,6-DMA degradation by Fenton reaction……..…65	
4.11	Effect of ionic strength and pH on iron solubility at 25°C…… 66	
4.12	Theoretical Fe^{3+} solubility in an ideal solution……..67	

4.13 Ferric precipitation under different dissolved oxygen levels and turbulence condition (purging with O_2 and air versus stagnant condition in BOD bottle)……68
4.14 Effect of pH and fluidized-bed material on total iron removal……..70
4.15 Total iron removal in the fluidized-bed Fenton process with various solid materials and sizes…….71
4.16 Comparison between fully FBR and pre-CMR+FBR operations on total iron removal…….....73
4.17 Effect of Fe^{2+} concentration on iron removal in the fluidized-bed Fenton process under constant Fe^{2+}:H_2O_2 ratio scenario…….……..75
4.18 Effect of Fe^{2+} concentration on iron removal in the 1-hr pre-CMR+FBR under constant Fe^{2+}:H_2O_2 ratio scenario..……..76
4.19 Ferric precipitation under turbulence condition by purging with O_2 and air, and stagnant condition in BOD bottle (replotted of Figure 4.13 for 180 minutes)……...…77
4.20 Determination of the rate-limiting step controlling the crystallization process……..……...…79
4.21 Effect of organo-ferric complex on iron crystallization in FBR……80
4.22 Effect of organo-ferric complex on iron crystallization in fluidized-bed Fenton process in the presence of 2,6-DMA and AN……..……..81
4.23 Effect of organo-ferric complex on iron crystallization of 1 mM of 2,6-DMA and 1 mM of AN……... 83
4.24 Effect of organo-ferric complex on iron crystallization of 0.1 mM of 2,6-DMA and 0.1 mM of AN……..…….. 84
4.25 Reusability of iron-coated CS for iron crystallization……... 85
4.26 Comparison of iron profile between the 1^{st}- and 101^{st} –cycles……..86
4.27 XRD analysis of the 101^{st}-cycle iron-coated CS……... 87
4.28 Catalytic activity of iron-coated CS on organic degradation in heterogeneous Fenton process as compare to commercial goethite…….. 88
4.29 Iron leach ability of iron-coated CS and commercial goethite during the heterogeneous Fenton process……...…….. 90
4.30 Relationship between ln([2,6-DMA]/[2,6-DMA]$_0$) versus ln([AN]/[AN]$_0$) using the data from the experiment with 75 g/l of 101^{st}-cycle iron-coated CS ……..……..……91

NOMENCLATURES

AN	=	aniline
AOPs	=	advanced oxidation processes
CS	=	construction sand
2,6-DMA	=	2,4-dimethyl--aniline
n,n-DMA	=	n,n-dimethyl-aniline
2,6-DMB	=	2,6-dimethyl-benzoquinone
2,6-DMH	=	2,6-dimethyl-hydroquinone
2,6-DMN	=	2,6-dimethyl-nitrobenzene
2,6-DMP	=	2,6-dimethyl-phenol
M	=	molar
OT	=	*o*-toluidine
hr	=	hour
k	=	rate constant
mg/l	=	milligram/liter
min	=	minute
mM	=	millimolar
ml	=	milliliter
μm	=	micrometer

ABSTRACT

This research determined the rate constant between 2,6-dimethy-aniline (2,6-DMA) and hydroxyl radicals ($OH^{\bullet}$) by using Fenton reaction and competitive kinetics technique. Regardless of experimental conditions either batch or continuous mode, presence or absence of media, complete suspension or fluidized-bed reactor, the intrinsic 2^{nd}-order rate constant between 2,6-DMA and $OH^{\bullet}$ were found to be consistent in between 1.59×10^{10} and 1.80×10^{10} $M^{-1}sec^{-1}$ with the average and 95% confidence interval of $1.70\pm0.04\times10^{10}$ $M^{-1}sec^{-1}$. Aromatic intermediates from 2,6-DMA oxidation by $OH^{\bullet}$ were 2,6-dimethyl-nitrobenzene, 2,6-dimethy-phenol, 2,6-dimethyl-nitrophenol, 2,6-dimethyl-hydroquinone, 2,6-dimethyl-benzoquinone, and 2,6-dimethyl-3-hydroxy-benzoquinone indicating the methyl groups on the benzene ring were less susceptible to $OH^{\bullet}$ attack than the amino and hydroxide groups. Maleic, lactic, oxalic, acetic, and formic acids were also identified as the carboxylic intermediates. Degradation mechanism of 2,6-DMA oxidation by $OH^{\bullet}$ was also proposed.

Considering iron crystallization, it was found that ferrous (Fe^{2+}) was immediately transformed to ferric (Fe^{3+}) after the initiation of Fenton reaction and sequentially precipitated out in the form of $Fe(OH)_3$ due to its low solubility even in the acidic solution. However, if precipitation occurred in the labile zone, $Fe(OH)_3$ was formed via homogeneous nucleation and crystallized very slowly onto the fluidized media. On the other hand, if it happened in the metastable zone, $Fe(OH)_3$ crystallized onto the fluidized media more rapidly via heterogeneous nucleation and iron was removed significantly from the aqueous phase. Crystallization was controlled by the transport step rather than the surface interaction step. Rate of crystal growth followed the orthokinetic flocculation when the mixing was sufficiently provided; however, it became under the influence of molecular diffusion or perikinetic flocculation depending on the crystallite size under the stagnant conditions. Presence of organic intermediates which could form complex with Fe^{3+} increased the solubility of Fe^{3+} and sequentially deteriorated the crystallization process. Crystallization rate onto fluidized media decreased with time; thus, continuously replace certain portion of coated solids with fresh media will maintain satisfactory crystallization rate. Catalytic activity of the $Fe(OH)_3$-coated sand with 3.5% iron content by weight was only equivalent to 4% of the goethite.

CONTENTS

Page

ABSTRACT ……... I
CONTENTS……..II
LIST OF TABLES……V
LIST OF FIGURES…..…… VII
NOMENCLATURES…….....IX

CHAPTER I INTRODUCTION……1
1.1 Research Rationale…… 1
1.2 Objectives……..….. 3
1.3 Hypotheses……...3
1.4 Scope of the Research…….....3
1.5 Obtained Results…..…….4

CHAPTER II THEORIES AND LITERATURE REVIEWS..... 5
2.1 2,6-Dimethyl-aniline.....5
2.1.1 General Information.....5
2.1.2 Physical and Chemical Properties.....6
2.1.3 Toxicology…… 6
2.1.4 First Aid Measures…….....8
2.2 Advanced Oxidation Processes.....8
2.3 Fenton Process..... 9
2.3.1 Hydrogen Peroxide…..... 9
2.3.2 Ferrous…….. 10
2.3.3 Hydroxyl Radicals…….……..… 10
2.3.4 Fenton Reaction……..…..... 12
2.4 Fluidized-bed Fenton Process.....13
2.5 Reaction Rate Constant Determination.....14
2.6 Precipitation and Crystallization.....17
2.6.1 Rational…….....17
2.6.2 Nucleation…….....17
2.6.2.1 Homogeneous Nucleation.....18

2.6.2.2 Heterogeneous Nucleation..... 20
2.6.3 Crystal Growth..... 20
2.7 Literature Reviews……..... 24
2.7.1 Competitive Kinetics Technique..... 24
2.7.2 Degradation of 2,6-Dimethyl-aniline by AOPs..... 26
2.7.3 Removal of Organic Compounds in Heterogeneous Catalysis by H_2O_2..... 27
2.7.4 Iron Crystallization in Fluidized-bed Fenton Reactor...…….. 30

CHAPTER III METHODOLOGY……..... 33
3.1 Materials and Chemicals..... 33
3.1.1 Chemicals……..... 33
3.1.2 Batch Reactor……..... 33
3.1.3 Fluidized-bed Reactor..... 33
3.2 Experimental Procedures……..… 34
3.2.1 Kinetics of 2,6-Dimethyl-aniline Degradation…..... 34
3.2.1.1 Completely Mixed Reactor…… 34
3.2.1.2 Fluidized-bed Reactor…… 35
3.2.2 Iron Crystallization……..…….…….... 35
3.3 Experimental Scenarios…….…….…… 37
3.3.1 Kinetics of 2,6-Dimethyl-aniline Degradation…..... 37
3.3.2 Mechanism of 2,6-Dimethyl-aniline Oxidation…..... 40
3.3.3 Iron Precipitation and Crystallization…..... 41
3.4 Analytical Methods…….…….47
3.4.1 Measurement of Aromatic Compounds..... 47
3.4.2 Measurement of Iron……..... 48
3.4.3 Measurement of Hydrogen Peroxide Residual..... 48
3.4.4 Measurement of Total Organic Carbon..... 48
3.4.5 Identification and Measurement of Carboxylic Intermediates..48
3.4.6 Identification of Aromatic Intermediates…….…….....49
3.4.7 Solid Characterization…….....49

CHAPTER IV RESULTS AND DISCUSSION…….…….…… 50
4.1 Kinetics of 2,6-Dimethyl-aniline Degradation……..…..…… 50
4.1.1 Experimental Control..... 50

4.1.1.1 2,6-Dimethyl-aniline, n,n-Dimethyl-aniline and Aniline Oxidation by H_2O_2 and Volatilization..... 50
4.1.1.2 *o*-Toluidine Oxidation by H_2O_2 ……..... 50
4.1.2 Verification of Competitive Kinetics Technique.....52
4.1.3 Intrinsic Rate Constant of 2,6-Dimethyl-aniline with Hydroxyl Radical.....52
4.1.3.1 Batch Study in the Absence of Media.....52
4.1.3.2 Batch Study in the Presence of Media..... 55
4.1.3.3 Batch Study in the Fluidized-bed Reactor……..... 58
4.1.3.4 Continuous Study in the Absence of Media…….. 58
4.1.3.5 Overall Rate Constant and Confidence Interval…... 60
4.1.4 Effect of Fenton's Reagent on Organic Degradation.....60
4.1.5 Degradation Intermediates and Pathway……..... 62
4.2 Iron Crystallization…….……. 66
4.2.1 Iron Solubility…….....…… 66
4.2.2 $Fe(OH)_3$ Crystallization in Fluidized-bed Reactor…….. 69
4.2.3 $Fe(OH)_3$ Crystallization in Fluidized-bed Fenton Process…...70
4.2.4 Effect of $Fe(OH)_3$ Crystallites……..…..... 72
4.2.5 Effect of Iron Concentration…….....…… 74
4.2.6 Effect of Turbulence…… 77
4.2.7 Effect of Organic Compounds…….....80
4.2.8 Reusability of Iron-coated Construction Sand for Iron Crystallization……..……82
4.2.9 Catalytic Activity of Iron-coated Construction Sand….....86

CHAPTER V CONCLUSIONS……..... 92
5.1 Conclusions
5.1.1 Kinetics of 2,6-Dimethyl-aniline Degradation……..... 92
5.1.2 Iron Crystallization……..…… 92
5.2 Recommendations for Further Studies ……... 94

REFERENCES……...95
APPENDIX A 赴國外出差或研習心得報告……101
APPENDIX B 出席國際學術會議心得報告及發表之論文……126

LIST OF TABLES

Table		Page
2.1	Physical and chemical properties of 2,6-DMA	7
2.2	Oxidation potential of common oxidizing species	11
3.1	Conditions for the determination of H_2O_2 oxidation and volatilization of target compounds	37
3.2	Conditions for the determination of *o*-toluidine oxidation by H_2O_2	38
3.3	Conditions for verification of the competitive rate technique	38
3.4	Conditions for the rate constant determination under the batch operation	39
3.5	Conditions for the rate constant determination in the presence of solid media	39
3.6	Conditions for rate constant determination by the fluidized-bed Fenton process	40
3.7	Conditions for the rate constant determination under the continuous operation.	40
3.8	Conditions for oxidation pathway determination	41
3.9	Conditions for iron solubility study	41
3.10	Conditions for the effect of iron concentration	42
3.11	Conditions for the $Fe(OH)_3$ crystallization characterization in FBR	42
3.12	Conditions for the crystallization in fluidized-bed Fenton process	43
3.13	Conditions for the effect of $Fe(OH)_3$ crystallites	43
3.14	Conditions for the effect of iron concentration on crystallization	44
3.15	Conditions for the effect of mixing on crystal growth	44
3.16	Conditions for the effect of organo-ferric complex on Fe^{3+} solubility/crystallization in FBR	45
3.17	Conditions for the effect of organo-ferric complex on Fe^{3+} solubility/crystallization under dynamic state in fluidized-bed Fenton process	45
3.18	Conditions for the reusability of iron-coated CS for iron crystallization	46
3.19	Experimental scenarios for the catalytic ability of iron-coated construction sand on the oxidation of 2,6-DMA and AN	46
4.1	Intrinsic rate constants of 2,6-DMA obtained from various experimental conditions	56

4.2. Identified aromatic intermediates of 2,6-DMA oxidation by $OH^{\bullet}$……....62

.

LIST OF FIGURES

Figure		Page
2.1	Structure of 2,6-DMA……..……...6	
2.2	Fluidized-bed Fenton reactions.……14	
2.3	Schematic solubility isotherm of a solid electrolyte ……..……... 19	
2.4	Schematic representation of the ability of a solid substrate to catalyze the nucleation …… 21	
2.5	Attachment and detachment of an ion or molecule to and from a solid lattice…….... 21	
2.6	Concentration gradient in liquid phase for extreme cases of diffusion control and surface-interaction control……..… 23	
2.7	Reaction mechanism of benzoic acid (BA) oxidation by the fluidized-bed Fenton process…….... 32	
3.1	Fluidized-bed reactor. ……..……..… 34	
3.2	Experimental scheme for Fenton and fluidized-bed Fenton processes.…..…36	
3.3	Gas chromatography chromatogram……..……47	
4.1	Control experiment for direct H_2O_2 oxidation and volatilization …….... 51	
4.2	Control experiment for direct H_2O_2 oxidation of the internal standard (OT) 51	
4.3	Verification of competitive technique..…….…. 53	
4.4	Intrinsic rate constant determination of 2,6-DMA in batch mode…….… 54	
4.5	Intrinsic rate constant determination between 2,6-DMA and $OH^{\bullet}$ in a SiO_2-suspension reactor….……..… 57	
4.6	Intrinsic rate constant determination between 2,6-DMA and $OH^{\bullet}$ in a batch fluidized-bed reactor…….……..… 59	
4.7	Time-profile of 2,6-DMA and AN in continuous mode…… 60	
4.8	Effect of Fenton's reagent on the degradation of 2,6-DMA and AN in a batch mode without media…….. 61	
4.9	Proposed reaction pathway for the mineralization of 2,6-DMA by $OH^{\bullet}$…...64	
4.10	Intermediate products and TOC profiles of 10 mM of 2,6-DMA degradation by Fenton reaction……..…65	
4.11	Effect of ionic strength and pH on iron solubility at 25°C…… 66	
4.12	Theoretical Fe^{3+} solubility in an ideal solution……..67	

4.13 Ferric precipitation under different dissolved oxygen levels and turbulence condition (purging with O_2 and air versus stagnant condition in BOD bottle)……68
4.14 Effect of pH and fluidized-bed material on total iron removal……..70
4.15 Total iron removal in the fluidized-bed Fenton process with various solid materials and sizes…….71
4.16 Comparison between fully FBR and pre-CMR+FBR operations on total iron removal…….....73
4.17 Effect of Fe^{2+} concentration on iron removal in the fluidized-bed Fenton process under constant Fe^{2+}:H_2O_2 ratio scenario…….……..75
4.18 Effect of Fe^{2+} concentration on iron removal in the 1-hr pre-CMR+FBR under constant Fe^{2+}:H_2O_2 ratio scenario..……..76
4.19 Ferric precipitation under turbulence condition by purging with O_2 and air, and stagnant condition in BOD bottle (replotted of Figure 4.13 for 180 minutes)……...…77
4.20 Determination of the rate-limiting step controlling the crystallization process……..……...…79
4.21 Effect of organo-ferric complex on iron crystallization in FBR……80
4.22 Effect of organo-ferric complex on iron crystallization in fluidized-bed Fenton process in the presence of 2,6-DMA and AN……..……..81
4.23 Effect of organo-ferric complex on iron crystallization of 1 mM of 2,6-DMA and 1 mM of AN……... 83
4.24 Effect of organo-ferric complex on iron crystallization of 0.1 mM of 2,6-DMA and 0.1 mM of AN……..…….. 84
4.25 Reusability of iron-coated CS for iron crystallization……... 85
4.26 Comparison of iron profile between the 1^{st}- and 101^{st} –cycles……..86
4.27 XRD analysis of the 101^{st}-cycle iron-coated CS……... 87
4.28 Catalytic activity of iron-coated CS on organic degradation in heterogeneous Fenton process as compare to commercial goethite…….. 88
4.29 Iron leach ability of iron-coated CS and commercial goethite during the heterogeneous Fenton process……...…….. 90
4.30 Relationship between ln([2,6-DMA]/[2,6-DMA]$_0$) versus ln([AN]/[AN]$_0$) using the data from the experiment with 75 g/l of 101^{st}-cycle iron-coated CS ……..……..……91

NOMENCLATURES

AN	=	aniline
AOPs	=	advanced oxidation processes
CS	=	construction sand
2,6-DMA	=	2,4-dimethyl--aniline
n,n-DMA	=	n,n-dimethyl-aniline
2,6-DMB	=	2,6-dimethyl-benzoquinone
2,6-DMH	=	2,6-dimethyl-hydroquinone
2,6-DMN	=	2,6-dimethyl-nitrobenzene
2,6-DMP	=	2,6-dimethyl-phenol
M	=	molar
OT	=	*o*-toluidine
hr	=	hour
k	=	rate constant
mg/l	=	milligram/liter
min	=	minute
mM	=	millimolar
ml	=	milliliter
μm	=	micrometer

CHAPTER I
INTRODUCTION

1.1 Research Rationale

Nowadays, several chemicals which are highly persistent in the environment have been synthesized and used intensively and become hazardous wastes afterward. These chemicals cannot be degraded by traditional treatment processes due to their toxic and refractory property. Variation in the chemical composition leads to a need to develop a special and specific treatment method for each persistent pollutant. One group of the pollutants that is typically persistent and needs advanced treatment is the aromatic compounds.

2,6-dimethyl-aniline (2,6-DMA) is a metabolite of the xylidine group of anesthetics including lidocaine and can also be produced by the reduction of certain azo dyes by intestinal microflora. It may also enter the environment through degradation of certain pesticides. 2,6-DMA has been commercially produced and widely used as a chemical intermediate to produce many products such as pesticides, dyestuffs, antioxidants, pharmaceuticals and other products. 2,6-DMA-contaminated wastewaters from these manufacturers can pose adverse impacts in receiving waters due to its biorefractory and highly toxic properties. 2,6-DMA has been classified by International Agency for Research on Cancer (IARC) as group 2B carcinogens. As a result, appropriate and effective treatment technologies are needed to purify or clean up these contaminated wastewaters prior to discharge to the environment.

Advanced oxidation processes (AOPs) are one of the possible alternatives which can provide the destruction of refractory and hazardous organic compounds. Hydroxyl radicals ($OH^{\bullet}$), generated in the AOPs, are extremely reactive, short lived and unselective transient species which can readily oxidize organic/inorganic pollutants in water and wastewater and convert them into simple, relatively harmless substances. A number of methods can lead to the generation of $OH^{\bullet}$ including

H_2O_2/UV, O_3/H_2O_2, O_3/UV, TiO_2/UV, and Fenton's family which is of interest in this research.

Fenton process has been intensively studied for the treatment of biorefractory organic contaminants in aqueous waste streams, soils, and groundwater. The Fenton process is normally initiated by the addition of ferrous (Fe^{2+}) and hydrogen peroxide (H_2O_2) so called "Fenton's reagent". Conventional Fenton process is typically simple and effective, and requires no costly capital investment. It has been proven to be effective in treating various organic contaminants such as nitrophenol, dye, aromatic amines, polycyclic aromatic, ethers, and photographic wastewater (Ewa et al., 1991). The Fenton's reagent as an oxidant for wastewater treatment is attractive due to the facts that iron is a highly abundant and non-toxic element and H_2O_2 is easy to handle and kindly environmental making (Munter, 2001; Pignatello, 1992). This reaction is typically performed under an acidic condition to raise the iron solubility and to enhance the oxidative character of the $OH^{\bullet}$. A neutralization step is required after treatment to eliminate ferric ions by hydroxide precipitation and to comply with the effluent standard. This neutralization step can generate an enormous amount of ferric hydroxide sludge which requires further separation and disposal. The use of fluidized-bed reactor can overcome or lessen this problem. Ferric ions resulted from the Fenton reaction can precipitate and crystallize onto the carriers' surface; hence, significantly reducing the formation of iron puffy sludge (Chou and Huang, 1999). In addition, it was also found that these crystallized iron oxides could catalyze the decomposition of H_2O_2 to generate $OH^{\bullet}$ which further enhancing the removal of pollutant (Lin and Gurol, 1998).

Although the oxidation of 2,6-DMA by $OH^{\bullet}$ has been investigated previously by Ting et al. (2009) and Masomboon et al (2010), no intrinsic kinetic rate constant of the reaction between 2,6-DMA and $OH^{\bullet}$ have been reported. This constant is a very important and useful scientific and engineering parameter and is deserved to be investigated. As a result, this research project focused on the determination of the intrinsic second-order rate constant between 2,6-DMA and $OH^{\bullet}$. In addition, this research also characterize the iron crystallization onto the carriers in a fluidized-bed reactor in order to provide a better understanding on iron removal mechanism in the fluidized-bed Fenton process which is very valuable in field practice.

1.2 Objectives

The main objectives of this study are:

1. To characterize the kinetics of 2,6-DMA oxidation by $OH^{\bullet}$ using Fenton and fluidized-bed Fenton processes.
2. To characterize the iron precipitation and crystallization in the fluidized-bed Fenton process.

The first objective led to the determination of the intrinsic kinetic rate constant between 2,6-DMA and $OH^{\bullet}$ and the oxidation pathway of 2,6-DMA. The second objective provided the fundamental understanding on the characteristics of iron crystallization onto the carrier's surface in the fluidized-bed Fenton process as well as the catalytic ability of iron-coated media on H_2O_2 decomposition to generate $OH^{\bullet}$.

1.3 Hypotheses

1. Oxidation of 2,6-DMA by $OH^{\bullet}$ is a second-order reaction.
2. 2,6-Dimethyl-aniline decomposition by ordinary and fluidized-bed Fenton processes depends on system pH and chemical dosages.
3. Metal oxide can effectively serve as a medium for iron crystallization in the fluidized-bed Fenton process.
4. Iron concentration as well as 2,6-DMA and its intermediates have an effect on iron crystallization in fluidized-bed Fenton process.

1.4 Scope of the Research

1. Using lab scale reactors of 1.35 liter for the fluidized-bed Fenton and 0.5 liter for the ordinary Fenton.
2. Using a synthetic wastewater.
3. For the fluidized-bed Fenton process, the carriers were either silica dioxide, aluminum oxide, or construction sand.
4. Working at 25°C under room condition.
5. Operating in both batch and continuous modes.

1.5 Obtained Results

1. Intrinsic kinetic rate constant for 2,6-DMA oxidation by $OH^{\bullet}$.
2. Intermediates and pathway of 2,6-DMA oxidation by $OH^{\bullet}$.
3. Characteristics of iron crystallization onto the carriers' surface in the fluidized-bed Fenton process.
4. Catalytic ability of iron-coated media on H_2O_2 decomposition to generate $OH^{\bullet}$.

CHAPTER II
THEORIES AND LITERATURE REVIEWS

2.1 2,6-Dimethyl-aniline

2.1.1 General Information

2,6-dimethyl-aniline (2,6-DMA) is one of the six dimethyl-aniline isomers of which their molecular formula are $(CH_3)_2C_6H_3NH_2$. 2,6-dimethyl-aniline has two methyl groups positioned on both sides of the amino group on the benzene ring (at both ortho-positions) as shown in Figure 2.1. 2,6-dimethyl-aniline can be either obtained as a by-product in the fractional distillation of the coal tar or synthesized by heating aniline hydrochloride with methanol at 220 °C. Furthermore, 2.6-DMA is a metabolite of the xylidine group of anaesthetics including lidicaine and is produced by the reduction of certain azo dyes by intestinal microflora. It may also enter the environment through degradation of certain pesticides. 2,6-dimethyl-aniline is an aniline homologue and has similar properties of aromatic amine. 2,6-dimethyl-aniline is sparingly soluble in water but miscible with ethanol and diethyl ether and is sensitive to air and light and tends to darken on storage. 2,6-dimethyl-aniline is used to manufacture many products including pesticides, dyestuffs, antioxidants, pharmaceuticals and other products.

2,6-dimethyl-aniline damages hemoglobin, a protein that normally transports oxygen in the blood, so that oxygen cannot be transported to cells and tissues causing them to lack oxygen for their metabolisms. This condition is known as “methemoglobinemia”. Methaemoglobinemia causes headache, cardiac arrhythmia, blood pressure drop, dyspnoea, spasms, and cyanosis (blue coloration of the blood). Sensitization with allergic manifestations in predisposed persons. Direct contact with 2,6-DMA can also produce skin and eye irritation. 2,6-dimethyl-aniline is released into the environmental primarily from industrial uses, and may cause long-term adverse effects in the aquatic environment (NTP, 2002).

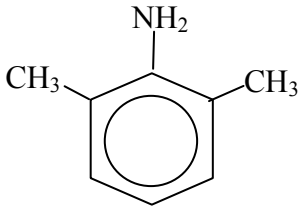

Figure 2.1 Structure of 2,6-DMA.

2.1.2 Physical and Chemical Properties

Physical state and appearance of 2,6-DMA is in a liquid form, colorless to reddish-yellow, clear liquid. It has a melting point of 11.2 °C and a boiling point of 216 °C. 2,6-dimethyl-aniline is slightly soluble in water and freely soluble in ether and alcohol. The density is 0.979 g/cm^3 at 20 °C. The substance has a flash point of 91 °C. 2,6-dimethyl-aniline is quite stable in the environment except under excessive heat exposure or contact with incompatible materials such as oxidizing agents and acids including acid chlorides, halogens, acid anhydrides, hypochlorite, and chloroformates. Addition physical and chemical properties of 2,6-DMA are presented in Table 2.1

2.1.3 Toxicology

Human can expose to 2,6-DMA via many routes. 2,6-dimethyl-aniline can be absorbed through skin, dermal contact, eye contact, inhalation and ingestion. It may cause skin irritation, eye irritation, and respiratory tract (nose and throat) irritation with coughing and/or shortness of breath. It causes gastrointestinal tract irritation with nausea, vomiting and diarrhea. Exposure through skin, inhalation and ingestion induces methemoglobinemia which affects behavior/central nervous system (CNS depression), respiration, heart, urinary system (kidneys), and blood. Symptoms of methemoglobinemia include hypoxia, apnea, cyanosis (a bluish discoloration of the skin due to deficient oxygenation of the blood), headache, fatigue, dizziness, weakness, lethargy, loss of coordination, dyspnea, coma, and death. Additional signs

Table 2.1 Physical and chemical properties of 2,6-DMA.

Property	**Data**
Molecular formula	$C_8H_{11}N$
Molecular weight	121.18 g/mol
Appearance	Yellow liquid, with characteristic odor and turn brown on exposure to air
Density	0.979 g/cm^3
Boiling point	216 °C
Melting point	11.2 °C
Water solubility	35 g/l @ 25°C
Specific gravity	0.9842 @ 20°C
Vapor pressure	< 0.1 kPa @ 20 °C
Ignition temperature	520°C
Flash point (closed cup)	91°C
Octanol/water partition Coefficient (log K_{ow})	1.96

and symptoms of exposure may include photophobia, visual disturbances, sluggish pupillary reaction, tinnitus, speech disturbances, anorexia, nausea, colicky pain, muscle pain, faintness, paresthesias of the extremities, tremor, seizures, cardiacarrhythmias, tachycardia, and heart block. Urinary signs and symptoms may include painful micturition, hemoglobinuria, methemoglobinuria, hematuria, oliguria, and renal insufficiency, and chocolate-brown blood. In case of chronic potential health effects, a Heinz-body hemolytic crisis may follow the development of methemoglobinemia. Heart, kidney, and liver damage may occur, possibly as secondary effects of hemolysis (NTP, 2002). In addition, 2,6-DMA may also cause mutagenic effects for bacteria and/or yeast; however, there is currently no solid evidence that 2,6-DMA is human mutagen. 2,6-DMA has been classified as group 2B carcinogens (possible for human) by International Agency for Research on Cancer (IARC).

2.1.4 First Aid Measures

In case of eye contact, immediately flush eyes with plenty of water for at least 15 minutes by warm water and get medical attention if irritation occurs. For the skin contact, wash with soap and water and cover the irritated skin with an emollient. If irritation develops or becomes worsen, the patient needs to seek for medical care. If inhaled, remove to fresh air. If not breathing, give artificial respiration. If breathing is difficult, give oxygen supply. In case of ingestion, do not induce vomiting unless directed to do so by medical personnel. Never give anything by mouth to an unconscious person. If large quantities of this material are swallowed, call a physician immediately. Loosen tight clothing such as a collar, tie, belt or waistband.

2.2 Advanced Oxidation Processes

Advanced oxidation processes (AOPs) have been known since the 1970's. The widely accepted definition for AOPs came from Glaze et al. (1987) which stated "advanced oxidation processes are defined as those which involve the generation of hydroxyl radicals ($OH^{\bullet}$) in sufficient quantity to affect water purification". Hydroxyl radicals is one of the most active oxidant known, it is nonselective for oxidizing compounds and able to operate at normal temperature and pressure (Tchobanoglous et al., 2003).

There are many processes able to generate the highly reactive $OH^{\bullet}$ species including heterogeneous photocatalytic, photo and non-photocatalytic homogeneous processes. In heterogeneous photocatalysis, $OH^{\bullet}$ is generated at the surface of a semiconductor (usually TiO_2) in the presence of UVA. Ozone/UV, $O_3/H_2O_2/UV$ and H_2O_2/UV are common photocatalytic combinations which can also generate $OH^{\bullet}$. The non-photocatalytic processes include "peroxone" (H_2O_2/O_3) and Fenton process (H_2O_2/Fe^{2+}) (Rodger and Bunce, 2001); however, this study emphasized on the latter.

2.3 Fenton Process

Fenton's reagent was discovered in 1894 by its inventor Henry J. Fenton, but its application as an oxidizing process for destroying toxic organics was applied in the late 1960s (Huang et al., 1993). Fenton reaction is one kind of AOPs used to generate $OH^{\bullet}$ for degradation of pollutants. This reaction involves chemical reagents called "Fenton's reagent", which are the combination of hydrogen peroxide (H_2O_2) and a ferrous ion (Fe^{2+}). Fenton's reagent is an effective and simple oxidant of various types of organic contaminants.

2.3.1 Hydrogen Peroxide

Hydrogen peroxide is an aqueous solution which has clear, colorless, water-like in appearance, and can be mixed with water in any proportion. It is miscible with cold water and is soluble in alcohol and ether. At high concentration, it has a slightly pungent or acidic odor. The chemical formula is H_2O_2 and it has a molecular weight of 34.015 g/mole and is non-flammable at any concentrations. Hydrogen peroxide is a diprotic acid with K_{A1} and K_{A2} equal to $10^{-11.8}$ and $<10^{-14}$, respectively.

Although pure H_2O_2 is fairly stable, it significantly decomposed into water and oxygen when heated above about 60°C or in the presence of reducing agents. Aqueous solution of H_2O_2 is mainly used for oxidation reactions, including bleaching process, chemical syntheses, and for water and wastewater treatment. In drinking water purification, Hydrogen peroxide is used to pre-oxidized organic constituents and to eliminate iron and manganese ions. Furthermore, by dissociation into oxygen and water, H_2O_2 can also supply oxygen to microorganism in biological treatment facilities and in the bioremediation of contaminated sites. It can be used as a disinfecting agent in the control of undesirable biofilm growth. Since the oxygen concentration is generally limiting factor during the in-situ biodegradation of organic contaminants, many applications using injection of H_2O_2 into the subsurface have been successfully applied to enhance the biodegradation activity. The decomposition of H_2O_2 to water and oxygen can be toward enzymatic and non-enzymatic routes.

Hydrogen peroxide also catalytically decomposes in the presence of numerous catalysts, e.g., most transition-metal ions such as Fe^{2+}, Cu^{+}, Cr^{2+}, Co^{2+}, or UV irradiation via different route to form a highly-oxidative $OH^{\bullet}$.

2.3.2 Ferrous

Iron (Fe) is the most abundant element on Earth and is the cheapest and most important of all metals. Iron is used to manufacture steel and other alloys important in construction and manufacturing. It also plays a vital role in the functioning of living organisms by transporting oxygen in blood via the hemoglobin molecule (an iron-complex organic compound). Its oxidation number varies from -2 to +6; however, most general states typically found in the environment are ferrous (Fe^{2+}) and ferric (Fe^{3+}). Iron exists in the ferrous state under reducing conditions such as those in anaerobic environment. Ferrous iron will be rapidly oxidized to ferric state when exposed to oxidizing agents; hence, it is not stable in the atmospheric environment where oxidative oxygen gas is present (21% by volume).

As mentioned previously that several transition-metal ions can catalyze the decomposition of H_2O_2 to form $OH^{\bullet}$, Fe^{2+} is the most preferred and environmental friendly among all transition-metal catalysts. Iron(II) sulfate is the most common form of ferrous salt commercially available in the market and can be found in various states of hydration; however, the heptahydrate or so called “green vitriol or copperas” ($FeSO_4 \cdot 7H_2O$) is the most common. This greenish crystalline compound is used as a pigment, fertilizer, medicine in the treatment of iron deficiency, coagulant for coagulation process, and catalyst in the Fenton process.

2.3.3 Hydroxyl Radicals

Hydroxyl radical is extremely reactive, short-lived, and non-selective transient species. It is a strong oxidant which has a very high oxidizing capacity equaling 2.8 V (Prengle, 1978; Masten and Davies, 1994). Table 2.2 shows the oxidation potential of $OH^{\bullet}$ compared to other oxidants (Parsons, 2004). It can be seen that $OH^{\bullet}$ is the second

Table 2.2 Oxidation potential of common oxidizing species.

Oxidant	Oxidation Potential (V)
Fluorine	3.03
Hydroxyl radical	2.80

Ozone	2.07
Hydrogen peroxide	1.78
Potassium permanganate	1.68
Chlorine dioxide	1.59
Chlorine	1.36

strongest oxidant, which is inferior only to fluorine. Hydroxyl radical can decompose the organic compounds relatively unselective with the rate constants ranging from 10^9-10^{10} $M^{-1}s^{-1}$ (Buxton, et al., 1988).

Hydroxyl radical is generated among various AOPs in the reaction mixture and has been used for achieving the treatment of a myriad of contaminated waters and industrial wastewaters. Hydroxyl radical can react in aqueous solution by different types of reactions (Eqs. 2.1 to 2.4) depending on target compounds, wastewater composition, and environmental conditions (Hoigné, 1998):

Electron transfer reaction: $OH^{\bullet} + M^n \Rightarrow M^{n+1} + (OH^-)_{(aq)}$ (2.1)

Hydrogen abstraction: $OH^{\bullet} + R\text{-}H \Rightarrow R^{\bullet} + H_2O$ (2.2)

Electrophilic addition: $OH^{\bullet} + R_2C{=}CR_2 \Rightarrow {}^{\bullet}CR_2\text{-}C(OH)R_2$ (2.3)

Radical interaction: $OH^{\bullet} + OH^{\bullet} \Rightarrow H_2O_2$ (2.4)

For complex or large aliphatic hydrocarbons, $OH^{\bullet}$ will oxidize via electrophilic addition to form carbon-center radicals which immediately further react in a bimolecular reaction with dissolved oxygen to produce peroxyl radicals and sequentially stable oxidation products. On the other hand, $OH^{\bullet}$ tends to react with small aliphatic compounds by the hydrogen abstraction mean in which carbon dioxide can be formed as the final product (complete mineralization). The oxidation of aromatic compounds by $OH^{\bullet}$ is more complex than aliphatic hydrocarbons and could involve hydrogen abstraction, electrophilic addition, and radical interaction. Direct electron transfer normally occurs with inorganic pollutants. In addition, $OH^{\bullet}$ itself can react with another $OH^{\bullet}$ to combine or to disproportionate to form a stable product (Peres et al., 2003).

2.3.4 Fenton Reaction

Fenton process and its modified versions are being increasingly used in the treatment of contaminated water and soil. The conventional "dark" Fenton process involves the use of an oxidizing agent (usually H_2O_2) and a catalyst (usually Fe^{2+}) to generate highly reactive $OH^{\bullet}$. Once the Fenton's reagent is combined together, its sequential reactions are very complicated but well specified as shown in Eqs. (2.5) to (2.16) (Pignatello, 1992; Lu et al., 1999; Chen et al., 2001).

$Fe^{2+} + H_2O_2$	$\rightarrow$	$Fe^{3+} + {}^{\bullet}OH + OH^-$;	$k_1 = 76\ M^{-1}s^{-1}$	(2.5)
H_2O_2	$\leftrightarrow$	$HO_2^- + H^+$;	$K_2 = 1.59\times10^{-12}$ M	(2.6)
$Fe^{3+} + H_2O_2$	$\rightarrow$	$Fe^{2+} + HO_2^{\bullet}$;	$k_3 = 0.02\ M^{-1}s^{-1}$	(2.7)
$HO_2^{\bullet}$	$\leftrightarrow$	$O_2^{\bullet-} + H^+$;	$K_4 = 1.6\times10^{-5}$ M	(2.8)
$Fe^{2+} + {}^{\bullet}OH$	$\rightarrow$	$Fe^{3+} + OH^-$;	$k_5 = 4.3\times10^{6}\ M^{-1}s^{-1}$	(2.9)
$Fe^{2+} + O_2^{\bullet-}$	$\rightarrow$	$Fe^{3+} + O_2^-$;	$k_6 = 1\times10^{7}\ M^{-1}s^{-1}$	(2.10)
$Fe^{2+} + HO_2^{\bullet}$	$\rightarrow$	$Fe^{3+} + HO_2$;	$k_7 = 1.2\times10^{6}\ M^{-1}s^{-1}$	(2.11)
$H_2O_2 + {}^{\bullet}OH$	$\rightarrow$	$HO_2^{\bullet} + H_2O$;	$k_8 = 2.7\times10^{7}\ M^{-1}s^{-1}$	(2.12)
$HO_2^{\bullet} + HO_2^{\bullet}$	$\rightarrow$	$H_2O_2 + O_2$;	$k_9 = 8.3\times10^{5}\ M^{-1}s^{-1}$	(2.13)
${}^{\bullet}OH + {}^{\bullet}OH$	$\rightarrow$	H_2O_2;	$k_{10} = 5.3\times10^{9}\ M^{-1}s^{-1}$	(2.14)
$RH + {}^{\bullet}OH$	$\rightarrow$	$RH^{\bullet} + OH^- \rightarrow \rightarrow \rightarrow$ products or $CO_2 + H_2O$		(2.15)
$Fe^{3+} + 3OH^-$	$\rightarrow$	$Fe(OH)_{3(s)}$;	$K_{sp} = 4\times10^{-38}$	(2.16)

Although Fe^{2+} is acting as a catalyst in the Fenton reaction series, it can be seen that the consumption rate of Fe^{2+} in Eq. (2.5) is almost 3,800 times faster than the regeneration rate of Fe^{2+} from Fe^{3+} in Eq. (2.7). As a result, the pollutant degradation in Fenton process typically proceeds in two sequential steps. In the first step, the pollutant disappears rapidly under sufficient Fe^{2+} leading to the $OH^{\bullet}$ excessive environment whereas, in the slower second step, the oxidation rate of the pollutant is controlled by Eq. (2.7) which is known as "Fenton-like process" (Lunar et al., 2000). After treatment with Fenton process, the mixture is typically neutralized to

comply with the effluent standard and the ferric hydroxide will precipitate out as illustrated in Eq. (2.16). This ferric hydroxide sludge will cause a burden for further separation and disposal which is a major drawback for ordinary Fenton process.

2.4 Fluidized-bed Fenton Process

As mentioned previously, the major disadvantage of Fenton process is the production of a substantial amount of iron precipitation. To overcome and/or ease this problem, the fluidized-bed reactor (FBR) is one of the possible alternatives. The ferric ion generated from Eq. (2.5) can precipitate and crystallize onto the carriers' surface in the form of iron oxide; hence, reducing the production of puffy ferric hydroxide sludge. In FBR, several important and complicated processes occur simultaneously including: 1) homogeneous chemical oxidation (H_2O_2/Fe^{2+}); 2) heterogeneous chemical oxidation (H_2O_2/ iron oxide); 3) fluidized-bed crystallization; and 4) reductive dissolution of iron oxides. Factors influencing iron oxide crystallization on the surfaces of fluidized-bed carriers operated in FBR are pH, specific iron loading, H_2O_2/Fe^{2+}, and superficial velocity (Chou, et al., 2004). Figure 2.2 illustrates the fluidized-bed Fenton mechanisms in details. The Fenton's reagent can produce the non-selective oxidant $OH^{\bullet}$ via homogeneous reaction (a). Then, this strong oxidant attacks the aromatic hydrocarbon to initiate ring opening as reaction (b). After that, the intermediate products from previous reaction appears, these lead into further oxidation (reaction (c)). From this Fenton's reaction, Fe^{3+} is form (reaction (d)). The Fe^{3+} can be converted back to Fe^{2+} and initiate Fenton reaction further as in reaction (h). However, in the presence of solid carriers, the ferric hydrolysis product of Fenton's reaction can also crystallize and grow on the surface of the carriers (reaction(e)); hence, decreasing the precipitation of puffy ferric hydroxide forms

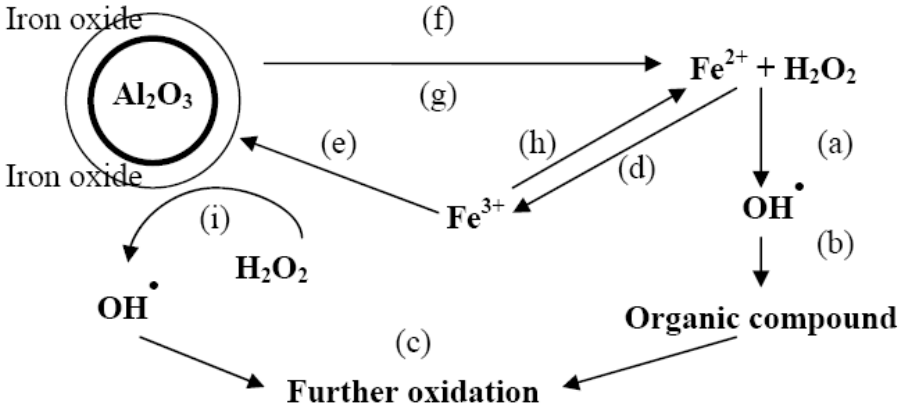

Figure 2.2 Fluidized-bed Fenton reactions.

(Chou and Huang, 1999). At the same time, the crystallized ferric oxide can also serve as a catalyst for hydrogen peroxide decomposition in a heterogeneous reaction (i) (Chou et al., 2003). Considering iron oxide on the surface carriers, it can re-dissolve via reductive dissolution (reaction (g)) and/or heterogeneous reaction (f) to form Fe^{2+}. However, these reactions which are similar to Eq. (2.7) are still slower than Eq. (2.5) (Pignatello, 1992). Key factors in the design of fluidized-bed Fenton process are: selection of carrier, including the material, specific gravity, and particle size; design of bed expansions; superficial velocity; feed mode and dosage of Fenton's reagent; and size, configuration, and recycle ratio of reactor.

2.5 Reaction Rate Constant Determination

In this research, the intrinsic second-order rate constant of the reaction between 2,6-DMA and $OH^{\bullet}$ was determined by using a technique of competitive kinetics between 2,6-DMA and a reference compound in the presence of $OH^{\bullet}$. This reference compound has to have the intrinsic rate constant with $OH^{\bullet}$ reported. Buxton et al. (1988) have compiled many rate constants between various organic compounds and $OH^{\bullet}$ some of which were used in this study. Aniline (AN) was selected as the reference compound with the rate constant with $OH^{\bullet}$ of 4.8×10^{9} $M^{-1}sec^{-1}$ (Buxton et al., 1988). The competitive kinetics as described later is a very useful yet simple tool to estimate the unknown rate constant of a compound without any complexity in experimental setup and equipments. It is well established that $OH^{\bullet}$ will react with any compound in a second-order manner. Hence, the reaction rate in a batch operation could be written as shown in Eqs (2.17) and (2.18) and could be further derived for the competition reaction manner as illustrated below:

$$\frac{d[2,6-DMA]}{dt} = -k_{2,6-DMA}[2,6-DMA][OH^{\bullet}] \quad (2.17)$$

$$\frac{d[AN]}{dt} = -k_{AN}[AN][OH^{\bullet}] \quad (2.18)$$

$$\frac{Eq(2.16)}{Eq(2.17)} = \frac{\frac{d[2,6-DMA]}{dt}}{\frac{d[AN]}{dt}} = \frac{-k_{2,6}[2,6-DMA][OH^{\bullet}]}{-k_{AN}[AN][OH^{\bullet}]} \quad (2.19)$$

$$\frac{\frac{1}{[2,6,DMA]}d[2,6-DMA]}{\frac{1}{[AN]}d[AN]} = \frac{k_{2,6-DMA}}{k_{AN}} \quad (2.20)$$

$$\frac{\int_0^i \frac{1}{[2,6,DMA]}d[2,6-DMA]}{\int_0^i \frac{1}{[AN]}d[AN]} = \frac{k_{2,6-DMA}}{k_{AN}} \quad (2.21)$$

$$\frac{\ln[2,6-DMA]_i - \ln[2,6-DMA]_0}{\ln[AN]_i - \ln[AN]_0} = \frac{k_{2,6-DMA}}{k_{AN}} \quad (2.22)$$

$$\frac{\ln\frac{[2,6-DMA]_i}{[2,6-DMA]_0}}{\ln\frac{[AN]_i}{[AN]_0}} = \frac{k_{2,6-DMA}}{k_{AN}} \quad (2.23)$$

$$\ln\left(\frac{[2,6-DMA]_i}{[2,6-DMA]_0}\right) = \frac{k_{2,6-DMA}}{k_{AN}}\ln\frac{[AN]_i}{[AN]_0} \quad (2.24)$$

where $[2,6\text{-DMA}]_0$, $[AN]_0$, and [2,6-DMA], [AN] are concentrations of 2,6-DMA, AN before and after the reaction, respectively; $[OH^{\bullet}]$ is concentration of the hydroxyl radical; $k_{2,6\text{-DMA}}$, k_{AN} are the rate constants of $OH^{\bullet}$ reacting with 2,6-DMA and AN, respectively. This final equation is similar to the one used by Shen et al. (2008) in the determination of the rate constant between *p*-chloronitrobenzene and $OH^{\bullet}$. According

to the Eq. (2.24), the plot between $\ln([2,6\text{-DMA}]_i/[2,6\text{-DMA}]_0)$ versus $\ln([AN]_i/[AN]_0)$ should result in a linear relationship and the slope will represent the ratio of the rate constant between aniline and 2,6-DMA.

In addition to the batch study, this research also determined the intrinsic rate constant of 2,6-DMA in the continuous mode in order to confirm the results. The reaction rate equations between 2,6-DMA and $OH^{\bullet}$ under the continuous mode could be derived as follows:

$$\frac{d[2,6-DMA]}{dt} = -k_{2,6-DMA}[2,6-DMA][OH^{\bullet}] + Q\left([2,6-DMA]_{in} - [2,6-DMA]_{out}\right) \quad (2.25)$$

$$\frac{d[AN]}{dt} = -k_{AN}[AN][OH^{\bullet}] + Q([AN]_{in} - [AN]_{out}) \quad (2.26)$$

At steady state $\Rightarrow$ $\frac{d[2,6-DMA]}{dt} = 0$, $\frac{d[AN]}{dt} = 0$

$$\frac{k_{2,6-DMA}[2,6-DMA][OH^{\bullet}]}{k_P[AN][OH^{\bullet}]} = \frac{Q([2,6-DMA]_{in} - [2,6-DMA]_{out})}{Q([AN]_{in} - [AN]_{out})} \quad (2.27)$$

$$\frac{k_{2,6-DMA}}{k_{AN}} = \frac{([2,6-DMA]_{in} - [2,6-DMA]_{out})}{([AN]_{in} - [AN]_{out})} \cdot \frac{[AN]}{[2,6-DMA]} \quad (2.28)$$

where $[2,6\text{-DMA}]_{in}$, $[AN]_{in}$, and $[2,6\text{-DMA}]_{out}$, $[AN]_{out}$ are influent and effluent concentrations of 2,6-DMA, AN at the steady state, respectively; $[OH^{\bullet}]$ is concentration of the hydroxyl radical; $k_{2,6\text{-DMA}}$ and k_{AN} are the rate constant of $OH^{\bullet}$ reacting with 2,6-DMA and AN, respectively; and Q is the flow rate in and out of the reactor.

2.6 Precipitation and Crystallization

2.6.1 Rational

Precipitation phenomenon is very important in both water and wastewater treatment processes. It is the formation of a solid in a solution and involves several

physical and chemical processes. Reverse process of precipitation is called "dissolution." Since these two processes are reversible but sometimes progress very slowly, both equilibrium and kinetics considerations are important. Knowledge of equilibrium relationships permits the calculation of equilibrium concentrations of cation(s) and anion(s) from the dissolution/precipitation of any salts. Nonetheless, in some heterogeneous systems, the equilibrium calculation may only provide the boundary conditions of the system rather than the situation that truly exists because the equilibrium is slowly established. In such cases, the kinetics consideration which is more complicated will play a major role in predicting the system behavior.

2.6.2 Nucleation

Once the product of cation(s) and anion(s) according to the solubility equation exceeds the dissociation constant, the solution will be oversaturated and a solid phase will be simultaneously formed. Various processes are involved in the solid formation; however, only three steps are believed to control the overall process. The first step is the interaction between ions or molecules leads to the formation of a critical cluster or nucleus or so called "nucleation" as shown in Eqs. (2.29) to (2.32). These nuclei can serve as the centers from which spontaneous growth of crystals can occur. The nucleation process determines the size and distribution of crystal produced. The second step is the formation of crystallites (crystal growth) as a result from sequential deposition of material on the nuclei formed from the first step as shown in Eq. (2.33). The last step is the formation of large crystals from the crystallites by a process called "ripening" as shown in Eq. (2.34)

$$X + X \leftrightarrow X_2 \quad (2.29)$$

$$X_2 + X \leftrightarrow X_3 \quad (2.30)$$

$$X_{j-1} + X \leftrightarrow X_j \text{ (critical cluster)} \quad (2.31)$$

Nucleation: $X_j + X \leftrightarrow X_{j+1}$ (2.32)

Crystallite formation: $X_j + X \leftrightarrow X_{j+1} \rightarrow$ crystal growth (2.33)

Crystal formation: $X_{j+1} + X \leftrightarrow X_{j+1} \rightarrow$ crystal ripening (2.34)

Nucleation can be divided into two types, i.e., homogeneous and heterogeneous nucleation, depending on the number of phases during the initial step of solid

formation. Figure 2.3 shows the schematic solubility isotherm of a solid electrolyte, where "S" is the saturation ratio (a/a_0), "a" is the actual concentration, and "a_0" is the concentration at solubility equilibrium of the solutes that characterize the solubility. Line "S = 1" divided the graph into two areas, i.e., undersaturated (no precipitation occurs) and oversaturated zones (precipitation should occur theoretically). Within the oversaturated zone, "S_M" is the minimum supersaturation ratio in which the precipitation could occur simultaneously without a need for the surface-catalytic seeds which called "homogeneous nucleation." In other word, solid precipitation will proceed spontaneously within the labile zone (above the "S_M-line"). Between the unsaturation and labile zones is a metastable zone where the nucleation rate is virtually zero or extremely slow even though the solution is already oversaturation; hence, the solutes can be stable for long periods without precipitation.

2.6.2.1 Homogeneous Nucleation

If the concentration of a solution is gradually increased until exceeding the solubility product with respect to a solid phase, the new solid phase will be theoretically formed. Nonetheless, in real practice, the new solid phase will not be formed within a specific amount of time until a certain degree of supersaturation has been achieved and accelerate the precipitation process. This phenomenon can be explained by chemical thermodynamics principle.

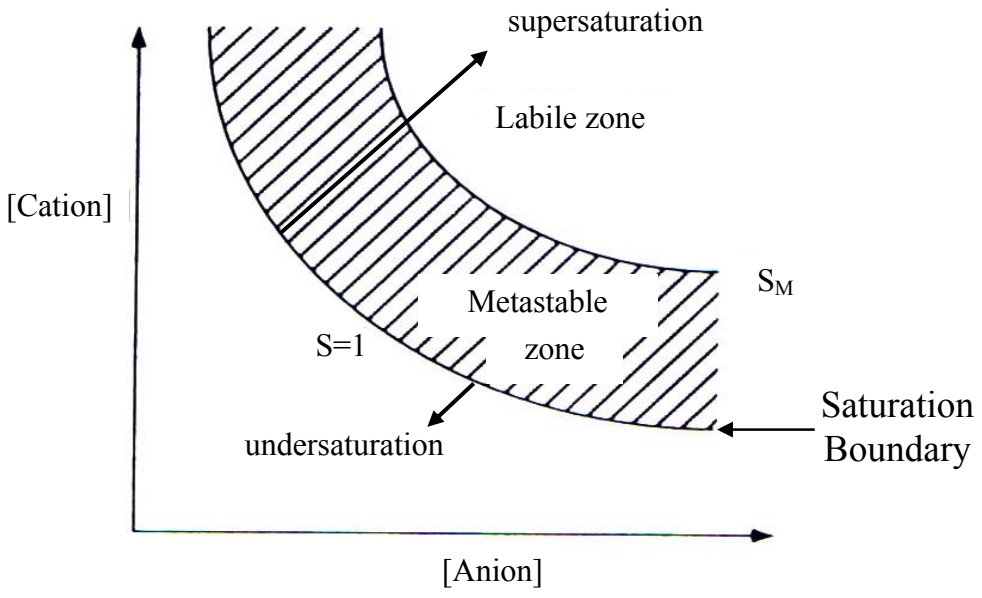

Figure 2.3 Schematic solubility isotherm of a solid electrolyte (Adapted from Stumm and Morgan, 1996).

A nucleus will be formed if total Gibb's free energy of the system decreases as a result from the formation of a new solid phase from an aqueous phase. In other word, the change in free energy of the formation of a nucleus (ΔG_f) has to be negative. The "ΔG_f" is the summation of free energy in the system which has two parts, i.e., free energy from bulk phase (ΔG_{bulk}) and free energy from solid phase ($\Delta G_{surface}$). The "ΔG_{bulk}" is a function of supersaturation degree in the aqueous phase and is always negative for a supersaturation solution. On the other hand, the "$\Delta G_{surface}$" is related to the interfacial energy between the surface of the solid being formed and the solvent; hence, is always positive. Then, the "ΔG_f" will be negative if the negative quantity of "ΔG_{bulk}" is greater than the positive quantity of "$\Delta G_{surface}$" and; thus, the nucleus formation can be thermodynamically favorite. As a result, a large supersaturation must be exceeded before the pure solid nucleus can be formed from the homogeneous oversaturated solution by itself or so called "homogeneous nucleation".

2.6.2.2 Heterogeneous Nucleation

Heterogeneous nucleation is in many cases the predominant formation process for crystals in natural waters. In the presence of foreign solid particles, the "$\Delta G_{surface}$" is reduced due to the interference of the interfacial energy of the external seeds (should match well with the crystal to be formed), thus reducing the formation free energy, and sequentially allow the nucleation to proceed more easily (Figure 2.4). In other words, these foreign solids are serving as the catalyst to reduce the energy barrier of the nucleation process similar to chemical catalysts which reduce the activation energy for chemical reaction. Theoretically, with proper matching between the foreign solid and the crystal to be precipitate, the nucleation may take place at a lower saturation ratio (in the metastable zone in Figure 2.3) on the solid surface than in solution (homogeneous nucleation).

In fluidized-bed Fenton process, the media, normally SiO_2 or construction sands, will be fluidized in the reactor and serve as the foreign solids on which the iron oxide can precipitate; hence, the nucleation process follows the heterogeneous mechanism. According to the nucleation principle mentioned previously, to optimize iron crystallization onto the media in fluidized-bed Fenton process, the saturation ratio has to be maintained within the metastable zone of Figure 2.3.

2.6.3 Crystal Growth

After the nucleation process (i.e., the initial formation of solid nuclei), spontaneous growth of crystal will occur. The attachment of a molecule/nucleus to another nucleus to form a solid lattice which includes the transportation of materials to the surface of these nuclei and surface deposition will become very important and should follow the mechanism of solid-solution interface at the molecular level. Four steps are believed to get involve in the attachment of solutes/nuclei to the solid surface of foreign particles or other nuclei as shown in Figure 2.5: 1) diffusion through the bulk solution and the water layer adjacent to nuclei (bulk diffusion); 2) adsorption-desorption reaction on the solid surface; 3) migration on the surface to or

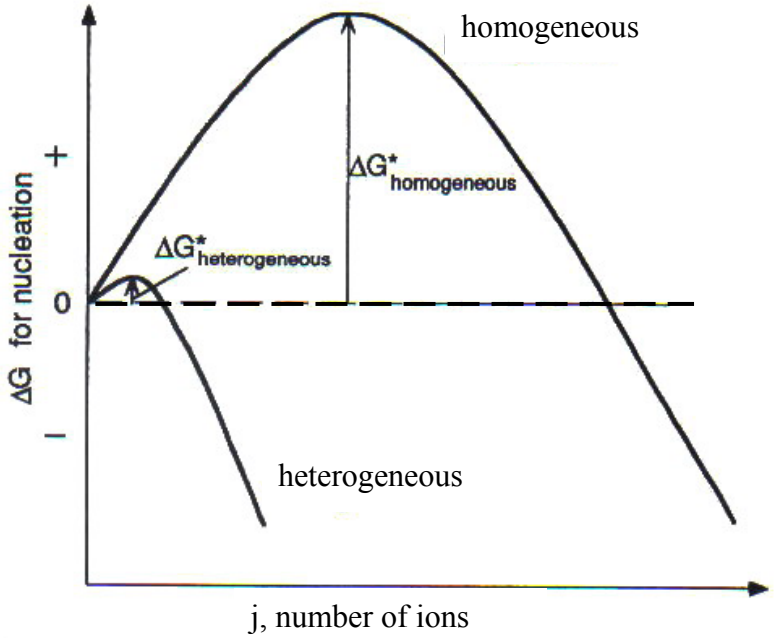

Figure 2.4 Schematic representation of the ability of a solid substrate to catalyze the nucleation (Stumm and Morgan, 1996).

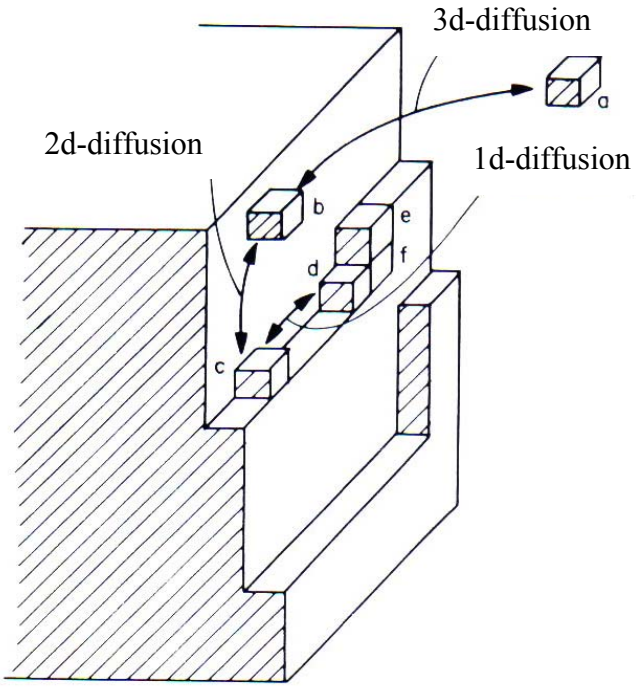

Figure 2.5 Attachment and detachment of an ion or molecule to and from a solid lattice (Morel and Hering, 1993).

from a step edge (surface diffusion); and 4) migration along a step edge to or from a kink (edge diffusion). Considering on the precipitation part, the ion or molecule will be more stable (lower free energy) as it embeds deeper into the solid matrix: a < b < c < d < e < f. If step 1 only is limiting, the kinetics are said to be diffusion or transport controlled. In this case, there is a concentration gradient in a liquid layer adjacent to the solid surface as shown in Figure 2.6. The liquid-film thickness depends on the mixing condition. On the other hand, if step 2, 3 and/or 4 only are limiting, the kinetics are said to be surface-interaction control and there will be no concentration gradient in the liquid adjacent to the solid surface. If the growth of crystal is controlled by the surface interaction; then, a zero-order rate law could be applied if the steady-state conditions at the surface prevail (Stumm and Morgan, 1996):

$$\frac{dC}{dt} = -k_S A \qquad (2.35)$$

where "k_S" is the surface-reaction rate constant normalized to solid surface area and "A" is the surface area of the solid. On the other hand, for transport control

mechanism, Stumm and Morgan (1996) proposed a parabolic rate law for the diffusion at the solid interface at the ionic or molecular level as:

$$\frac{dC}{dt} = -k_p t^{-\frac{1}{2}} \qquad (2.36)$$

where k_p is the rate constant. Integrating equation (2.36) will yield:

$$C = C_0 - 2k_p t^{\frac{1}{2}} \qquad (2.37)$$

Since, this research used a 0.22-μm membrane filter to differentiate the soluble species from the particulate species, the solutes may not be in the molecular level but can be in the colloidal particles with the diameters less than 0.22 μm. In other word, due to the limitation in measurement procedure, the iron particles with the sizes less than 0.22 μm such as the crystallites would be considered as soluble iron. According to literatures, diameters of colloids can vary from 0.001 to 100 μm which also cover the range of crystallite size. Therefore, the agglomeration or reduction of these

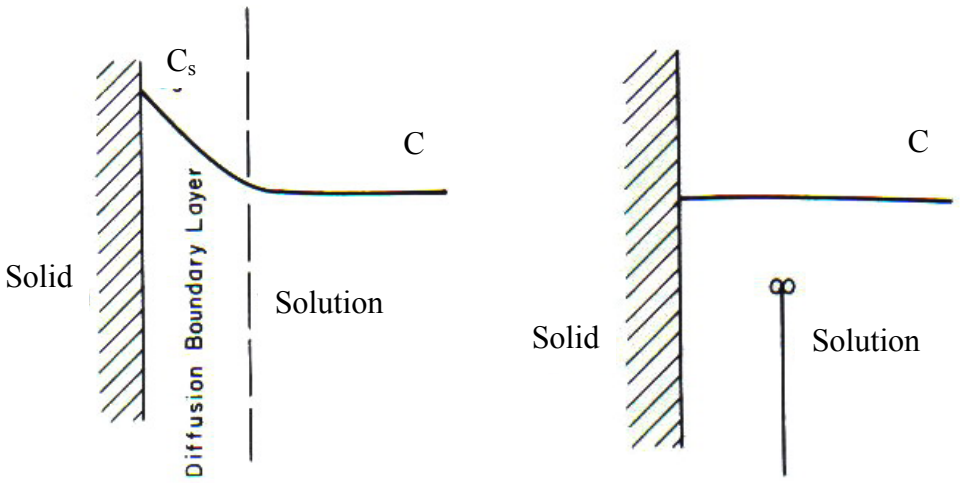

(a) diffusion control (b) surface-interaction control

Figure 2.6 Concentration gradient in liquid phase for extreme cases of diffusion control and surface-interaction control (Morel and Hering, 1993).

crystallites during the crystal growth stage as a result from colloidal transport and collision could be described by the second-order rate law as proposed by O'Melia and Tiller (1993), who studied on the aggregation of colloids as follows:

$$\frac{dN}{dt} = -k_a N^2 \qquad (2.38)$$

or

$$\frac{1}{N} = \frac{1}{N_0} + k_a t \qquad (2.39)$$

where "N" is the number concentration of particles in suspension at time "t" and "k_a" is a second-order rate constant which is a function of physical and chemical properties of the system including mass transport coefficient and collision efficiency factor. The second-order rate law of Eq. (2.38) is comparable to the very well-known rate of change in the concentration of colloidal particles during the flocculation process both in perikinetic (random diffusion control) and orthokinetic (movement of solvent or velocity gradient control) manners.

In this study, both transport equations (Eqs. (2.36) and (2.38)) were used to characterize the behavior of crystal formation in order to provide a better understanding on the crystallization process.

2.7 Literature Reviews

2.7.1 Competitive Kinetics Technique

Leitner and Roshani (2010) determined the rate constant of benzotriazole (BT) by the reaction of direct ozonation and $OH^{\bullet}$ at different pH. They accessed the kinetics information by 2 approaches, i.e., the log-reduction of BT in the case which ozone was present in excess (1^{st}-model) and the competition kinetic technique in the case which a reference compound was co-existed (2^{nd}–model). The results showed that the 2^{nd} order rate constant of BT with molecular ozone at pH 2 by the 1^{st}-model was 36.4±3.8 $M^{-1}s^{-1}$ as compared to 18.4±0.8 $M^{-1}s^{-1}$ for the 2^{nd}-model. With the 2^{nd}-model, the 2^{nd} order rate constant at pH 5 was found to be 22.0±0.2 $M^{-1}s^{-1}$. In a second stage, the reaction of BT and $OH^{\bullet}$ was carried out by using the 2^{nd}–model

involving 2 probe compounds during the ozonation at pH values ranging from 2 to 10.2. They found that the 2nd order rate constant of BT and $OH^{\bullet}$ were found to vary from 6.2×10^{9} $M^{-1}s^{-1}$ at pH 10.2 to 1.7×10^{10} $M^{-1}s^{-1}$ at pH 2.

Balci et al. (2009) investigated the kinetic and mechanism of atrazine degradation by in-situ electrochemically generated Fenton's reagent. They found the intrinsic rate constant of the reaction between atrazine and $OH^{\bullet}$ by competition kinetics technique to be $2.54\pm0.22\times10^{9}$ $M^{-1}s^{-1}$. The atrazine disappearance rate and solution mineralization efficiency were very rapid at the beginning of the reaction, but became slow down as the reaction proceeded. High mineralization rate of 82% was obtained by TOC and IC analysis. The oxidation pathway of atrazine degradation by $OH^{\bullet}$ was also proposed.

Kwon et al. (2009) determined the second order rate constants of $OH^{\bullet}$ with 14 organics and inorganic solutes such as chloride, carbonate, sulfate, bromide, etc., by using a simple competitive kinetics in a continuous flow system in the UV/H_2O_2 process. *p*-Nitroso-dimethyl-aniline (PNDA) was selected as the reference probe. They found that the $OH^{\bullet}$ rate constants obtained for 14 solutes selected in this study were consistent with values reported in the literatures using the more complicated pulse radiolysis method.

Shen et al. (2008) investigated the kinetics and mechanism of *p*-chloronitrobenzene (*p*CNB) degradation by ozone. With reference compounds, nitrobenzene (NB) and chlorobenzene (CB), the reaction rate constants of *p*CNB with O_3 and $OH^{\bullet}$ were measured by means of competition kinetics (mixture of *p*CNB and NB, or *p*CNB and CB) and found to be 1.6×10^{9} and 2.6×10^{9} $M^{-1}s^{-1}$, respectively. The increases in chloride and nitrate concentrations nearly equaled to the decrease in *p*CNB concentration. The degradation pathway for the ozonation of *p*CNB was also proposed.

Mazellier et al. (2007) investigated the degradation of fenuron by hydroxyl and carbonate radicals in aqueous solution by using the competitive method.

Photolysis of H_2O_2 at 254 nm was used to generate $OH^{\bullet}$ and carbonate radicals were generated by the photolysis of $Co(NH_3)_5CO_3^+$ at 254 nm. Atrazine was used as the reference compound for both processes. The results found that the 2nd order rate constant of fenuron with $OH^{\bullet}$ and carbonate radicals were found to be $7\pm1\times10^9$ $M^{-1}s^{-1}$ and $7\text{-}12\pm3\times10^6$ $M^{-1}s^{-1}$, respectively. The intermediates of fenuron oxidized by hydroxyl and carbonate radicals were also identified by LC-MS.

Einschlag et al. (2003) determined the rate constant of a set of nitroaromatic compounds with $OH^{\bullet}$ using competition experiment in the UV/H_2O_2 process. For a given pair of substrates S_1 and S_2, the relative reactivity β (defined as k_{S1}/k_{S2}) was calculated from the slope of the plot between ln[S_1] VS ln[S_2]. This method allows a better estimation of the relative reactivity than the plot of ln[S_1] and ln[S_2] against time. The rate constants of nitroaromatic substrates with $OH^{\bullet}$ were found to be in between 0.33×10^9 and 8.6×10^9 $M^{-1}s^{-1}$.

Spanggord et al. (2000) examined the kinetics of aminodinitrotoulenes (2-amino-4,6-dinitrotoluene (2-ADNT) and 4-amino-2,6-dinitrotoluene (4-ADNT)) by using the competition kinetics in a peroxone (ozone and H_2O_2) oxidizing system where both $OH^{\bullet}$ and ozone are important oxidants. The results found that the rate constant of 2- and 4-ADNT with ozone by using resorcinol as a reference compound were around 1.45×10^5 and 1.8×10^5 $M^{-1}s^{-1}$, respectively. For $OH^{\bullet}$ oxidation, determined using *p*-nitoracetophenone (PNAP) as the reference compound, the rate constants were found to be 1.6×10^9 and 1.9×10^9 $M^{-1}s^{-1}$ for 2-, and 4-ADNT, respectively. Although rate constants for $OH^{\bullet}$ oxidation were much higher than those for ozone, the kinetics modeling revealed that ozone was the dominant oxidant for ADNTs oxidation in the peroxone mixture, except when the ADNTs were below 1 μM (200 ppb).

2.7.2 Degradation of 2,6-Dimethyl-aniline by AOPs

Masomboon et al. (2010) determined the oxidation of 2,6-DMA be electro-Fenton process at pH 2. They found that 1 mM of Fe^{2+}, 20 mM of H_2O_2 and current density of 15.89 Am^{-2} were the optimum operating parameters for completely degrading 1 mM of 2,6-DMA. Furthermore, the degradation pathway of 2,6-DMA was also proposed.

Masomboon et al. (2009) investigated the effect of reaction conditions including the dosages of Fenton's reagent and initial pH on 2,6-DMA degradation and COD removal. They found that 70% removal efficiency was achieved under the optimum conditions of 2 mM of Fe^{2+}, 20 mM of H_2O_2 and pH 2 after 3 hrs. Moreover, they also proposed the intermediates and pathway of 2,6-DMA degradation.

Ting et al. (2009) investigated the kinetics of 2,6-DMA oxidation by photoelectron-Fenton process using different electrochemical cells. Effect of initial pH, Fe^{2+} concentration, H_2O_2 loading, and current density were explored to validate the kinetics model. The results showed that when pH was higher than 2, amorphous $Fe(OH)_{3(s)}$ was generated and the degradation of 2,6-DMA increased with increasing of Fe^{2+} and current density from 1.0 to 1.5 mM and 3.5 to 10.6 A/m^2, respectively, and the optimal H_2O_2 concentration for 2,6-DMA oxidation under the studied condition was 25 mM.

2.7.3 Removal of Organic Compounds in Heterogeneous Catalysis by H_2O_2

Flores et al. (2008) demonstrated that H_2O_2 could be activated in the presence of a heterogeneous catalyst (Fe^{3+}-containing ashes) to generate a powerful radical oxidant. The result from leaching test indicated that more of the 99 % by weight of the iron ion still stayed in the solid catalysts and the presence of H_2O_2 did not alter this relation. It is concluded that radical species (HO_2•) are formed and could be further transformed to $OH^{\bullet}$ when the H_2O_2 was activated by the immobilized Fe^{3+}. The results showed that it was possible to oxidize reactive black 5 dye using a

stoichiometric amount of H_2O_2. After 2 hours of treatment, reactive dye solutions were effectively decolorized and 80% of the original COD was removed.

Zelmanov and Semiat (2008) investigated the catalytic behavior of iron-based nano-catalysts on ethylene glycol and phenol treatment in the advanced oxidation processes. The results showed that the Fenton-like reaction using iron (III) oxide-based nano-catalysts in the presence of H_2O_2 could degrade both substances efficiently.

Dantas et al. (2006) evaluated the use of new composites as the adsorbents and/or heterogeneous catalysts for Fenton process to treat textile wastewater. The efficiency of the process was explored as a function of the experimental parameters: pH, H_2O_2 concentration and iron oxides content. The composites with high iron oxide content could effectively adsorb the contaminants in textile wastewater, and the adsorptive capacity increased with the iron content. These solids were also applied as the catalyst in the heterogeneous Fenton reaction and found to be very effective at pH 3.0 with the consumption of H_2O_2 lower than those required by the homogeneous Fenton process.

Baldrian et al. (2006) used the heterogeneous catalysts based on magnetic mixed iron oxides to decolorize several synthetic dyes. All the catalysts could catalyze H_2O_2 to produce highly reactive $OH^{\bullet}$ which able to decolorize the synthetic dyes effectively. The most effective catalyst was $FeO.Fe_2O_3$ which provided more than 90% decolorization. The fastest decomposition proceeded during the first hour of the reaction. In addition to dye decolorization, all the catalysts also caused a significant decrease in COD. These catalysts were active in the pH range of 2–10 depending on their structures and able to perform sequential catalytic cycles with low metal leaching.

Christopher et al. (2005) studied Fenton-mediated oxidation in the presence and absence of oxygen. The experiment showed that the oxidation of formic acid could occur effectively under a variety of experiment conditions by Fenton process. The intermediates generated during formic acid oxidation were found to increase the

oxidation efficiency, especially at high initial organic concentrations, by contributing in the redox cycling of iron. In the presence of oxygen, however, such improvement was attenuated through competition for the organic intermediates.

Lu et al. (2002) investigated how surface dissolution of goethite affected 2-chlorophenol oxidation in the goethite/H_2O_2 process. The results showed that ligand and reductant could enhance the dissolution rate of goethite which was a surface-controlled mechanism. Furthermore, the result from this study indicated that 2-chlorophenol could be effectively degraded by Fenton-liked reaction using the goethite as a catalyst at acidic pH. The extent of 2-chlorophenol degradation increased with increasing goethite dosage which providing more surface sites for the reductive dissolution.

Huang et al. (2001) examined the catalyzed decomposition of H_2O_2 and 2-chlorophenol in the presence of iron oxides. The catalytic activity for H_2O_2 decomposition was the highest for ferrihydrite, less for goethite, and much less for hematite based on mass and surface area basis. However, hematite exhibited the highest activity in catalyzing 2-chlorophenol oxidation. The oxidation efficiency of 2-chlorophenol corresponded with the inverse sequence of specific area and pH_{pzc} of the iron oxides.

Lu (2000) investigated the effect of goethite particle size, goethite dosage, Fe^{2+} and Fe^{3+} concentrations on the 2-chlorophenol oxidation. It was found that 2-chlorophenol could be decomposed with H_2O_2 catalyzed by goethite and the oxidation rate increased with decreasing goethite particle size. 2-Chloropheol degradation was almost retarded with 0.8 g/l of goethite because Fe^{2+} could not be produced at this condition. Addition of Fe^{2+} and Fe^{3+} can enhance the oxidation efficiency in the presence of goethite and H_2O_2. In conclusion, the essential mechanisms of goethite catalyzing H_2O_2 to decompose 2-chlorophenol may be due to the catalysis of ferrous ion and goethite surface. The reaction mechanisms are shown in Eqs. (2.40) to (2.42):

$$\alpha\text{-}FeOOH_{(s)} + 2H^+ + \tfrac{1}{2}H_2O_2 \rightarrow Fe^{II} + \tfrac{1}{2}O_2 + 2H_2O \qquad (2.40)$$

$$Fe^{II} + H_2O_2 \rightarrow Fe^{III} + OH^{\bullet} + OH^{-} \quad (2.41)$$

$$Fe^{III} + H_2O + OH^{-} \rightarrow \alpha\text{-}FeOOH_{(s)} + 2H^{+} \quad (2.42)$$

Chou and Huang (1998) studied on the oxidation of benzoic acid (BA) via Fenton-liked reaction using an innovative supported γ-FeOOH catalyst. Oxidation of BA by H_2O_2 was performed to understand the effects of initial pH and H_2O_2 dosage. The removal efficiency of BA at an initial pH of 3.2 was higher than at initial pH of 6.0 and 10.0; this result can be partly explained by reductive dissolution of γ-FeOOH. Therefore, the extent of heterogeneous catalysis was evaluated and found that the majority of mineralization of BA takes place on the catalyst surface while some occur in the aqueous phase due to iron dissolution of the catalyst.

Lin and Gurol (1998) described the kinetics, mechanism, and implication on the catalytic decomposition of H_2O_2 with granular size goethite ($\propto$-FeOOH) particles in aqueous solution. The results showed that the decomposition rate of H_2O_2 over goethite surface can be explained by the 2nd-order kinetic expression and the apparent reaction rate was dominated by the intrinsic reaction rates on the oxide surface rather than the mass transfer rate of H_2O_2 to the surface. The reaction mechanism for the decomposition of H_2O_2 on goethite surface was proposed on the basis of the fundamental reactions explaining the surface complexation chemistry for iron oxide and interaction of H_2O_2 with the surface sites as shown in Eqs. (2.43) to (2.47):

$$\equiv Fe^{III}OH + H_2O_2 \leftrightarrow (H_2O_2)_s \quad (2.43)$$

$$(H_2O_2)_s \rightarrow \equiv Fe^{II} + H_2O + HO_2^{\bullet} \quad (2.44)$$

$$\equiv Fe^{II} + H_2O_2 \rightarrow \equiv Fe^{III}OH + OH^{\bullet} \quad (2.45)$$

$$HO_2^{\bullet} \rightarrow H^{+} + O_2^{\bullet -} \quad (2.46)$$

$$\equiv Fe^{III}OH + HO_2^{\bullet}/O_2^{\bullet -} \rightarrow \equiv Fe^{II} + H_2O/OH^{-} + O_2 \quad (2.47)$$

Lin et al. (1996) investigated on the possibility of using mixture of H_2O_2 and iron oxide (goethite, α-FeOOH) particles as a chemical oxidant for wastewater

treatment by using BuCl as a studied compound. The oxidation rate of BuCl was closely related with degradation rate of H_2O_2. The results showed that BuCl was oxidized effectively by $OH^{\bullet}$ generated from the interaction of H_2O_2 with FeOOH particles.

2.7.4 Iron Crystallization in Fluidized-bed Fenton Reactor

Hsueh et al. (2006) used a novel supported iron oxide, prepared in a fluidized-bed reactor (FBR), as a catalyst for the heterogeneous photo-assisted Fenton degradation of azo-dye Reactive Black 5 (RB5). This catalyst was much cheaper than Nafion-based catalysts, and could markedly accelerate the degradation of RB5 under irradiation by UVA (@ 365 nm). The effects of the molar concentration of H_2O_2, the pH of the solution and the catalyst loading on the degradation of RB5 were elucidated. A simplified mechanism of RB5 decomposition which was consistent with the experimental findings for a solution with the pH of up to 7.0 was proposed. Approximately 70% decolorization was obtained and 45% of the total organic carbon was eliminated on the surface of the iron oxide at pH 7.0 after 480 minutes in the presence of 0.055 mM RB5, 5.0 g iron oxide/L, 29.4 mM H_2O_2, under 15W UVA.

Chou et al. (2004) determined the effect of operational pH, superficial velocity, specific iron loading, and influent H_2O_2 concentration on the crystallization efficiency of FeOOH. Two types of FeOOH catalysts were synthesized: FeOOH I was prepared at pH 3.5 (70% amorphous FeOOH and 30% γ-FeOOH), and FeOOH II was formed by aging FeOOH I at pH 13 (30% amorphous FeOOH and 70% γ-FeOOH). The results demonstrated that all these parameters were found to significantly influence the crystallization efficiency. The FeOOH II catalyst presented higher reactivity to ward H_2O_2 but lower stoichiometric efficiency in oxidizing benzoic acid than FeOOH I, similar to the result from the commercial goethite. Furthermore, the performance of catalytic oxidation was significantly depended on the crystalline property.

Chou et al. (2001) applied a novel supported γ-FeOOH catalyst to oxidize benzoic acid (BA) in a circulating fluidized-bed reactor by H_2O_2 and to determine the effects of homogeneous and heterogeneous catalysis. They found that the degradation rate of H_2O_2 was proportional to its concentration and the BA decomposition depended on both BA and H_2O_2. Conclusively, although heterogeneous catalysis contributed primarily to the oxidation of BA at pH 4.4-7.0, the homogeneous catalysis was of increasing importance below pH 4.4.

Chou and Huang (1999) investigated on the effect of Fe^{2+} on the catalytic oxidation of benzoic acid (BA) in the FBR applying supported γ-FeOOH as the carrier. They found that both mineralization of organics and crystallization of Fe^{3+} were simultaneously well performed under proper condition. Moreover, the reductive and the crystallization of γ-FeOOH as well as the oxidation of BA was proposed based on the experiment results. The reaction mechanism is shown in Figure 2.7

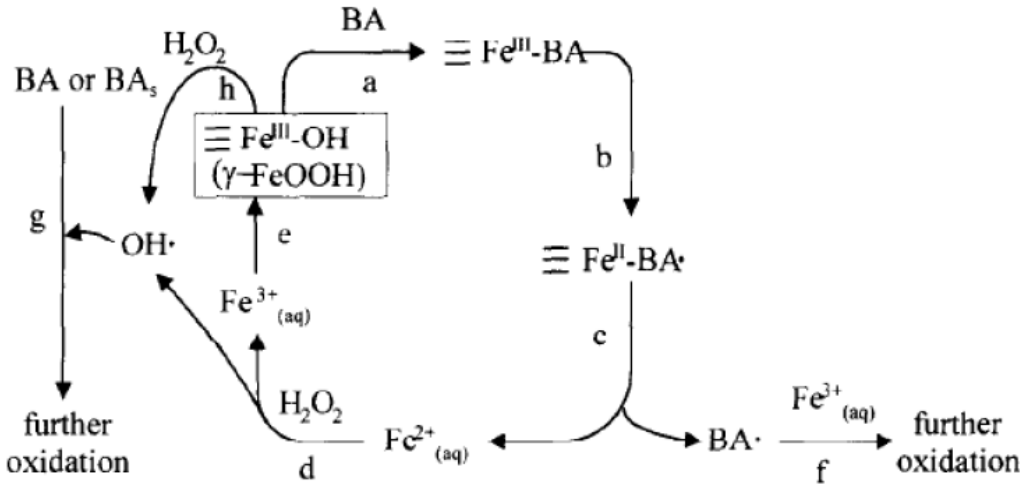

Figure 2.7 Reaction mechanism of benzoic acid (BA) oxidation by the fluidized-bed Fenton process: (A) reductive dissolution: reactions a, b, and c; (B) synthesis of Fe(III) hydroxide: reactions d and e; (C) oxidation of BA: reactions f, g, and h; BAx(5) denotes the surface complex of BA and γ-FeOOH (Chou and Huang, 1999).

Tai (1999) studied the crystal growth kinetics of a two-step growth process in liquid fluidized-bed crystallizers. A reliable method has been proposed to determine the parameters of the two-step growth. For sparingly soluble salts, the growth process was more complicated, but the two-step model could still be applied successfully under a similar environment of pH, ionic strength, and species ratio.

CHAPTER III
METHODOLOGY

3.1 Materials and Chemicals

3.1.1 Chemicals

2,6-DMA, n,n-dimethyl-aniline (n,n-DMA), aniline (AN), 2,6-dimethyl-phenol (2,6-DMP), 2,6-dimethyl-nitrobenzene (2,6-DMN), 2,6-dimethyl-benzoquinone (2,6-DMB), $FeSO_4 \bullet 7H_2O$, H_2O_2, and all chemical substances used in this work were analytical reagent grade. Fluidized media were quartz sand (SiO_2), construction sand (CS), and aluminum oxide (Al_2O_3). Except stated otherwise, the diameter sizes of SiO_2 and CS were 0.42 to 0.59 mm by using the sieves #30 & #40 (passing #30 but retained on #40) whereas the size of Al_2O_3 was 2.5 mm which was the smallest size commercially available. All media were soaked in HCl solution at pH 1 for 24 hours, washed with de-ionized water until the solution pH was 7, and then oven dried at 103°C (Lo and Chen, 1997). De-ionized water from a Millipore system with a resistivity of 18.2 MΩ/cm was used for preparing all solutions.

3.1.2 Batch Reactor

For the batch experiments both for 2,6-DMA degradation kinetics study and iron precipitation/crystallization study, a 0.5-liter Pyrex beaker in a water bath for temperature control at 25±0.2°C was used as the reactor (as shown in Appendix A).

3.1.3 Fluidized-bed Reactor

A 1.35-liter glass-cylinder reactor with an inlet, outlet, and a recirculation pump as shown in Figure 3.1 was used as the fluidized-bed reactor (FBR). The carrier used in this study was either quartz sand, construction sand, or aluminum oxide. The

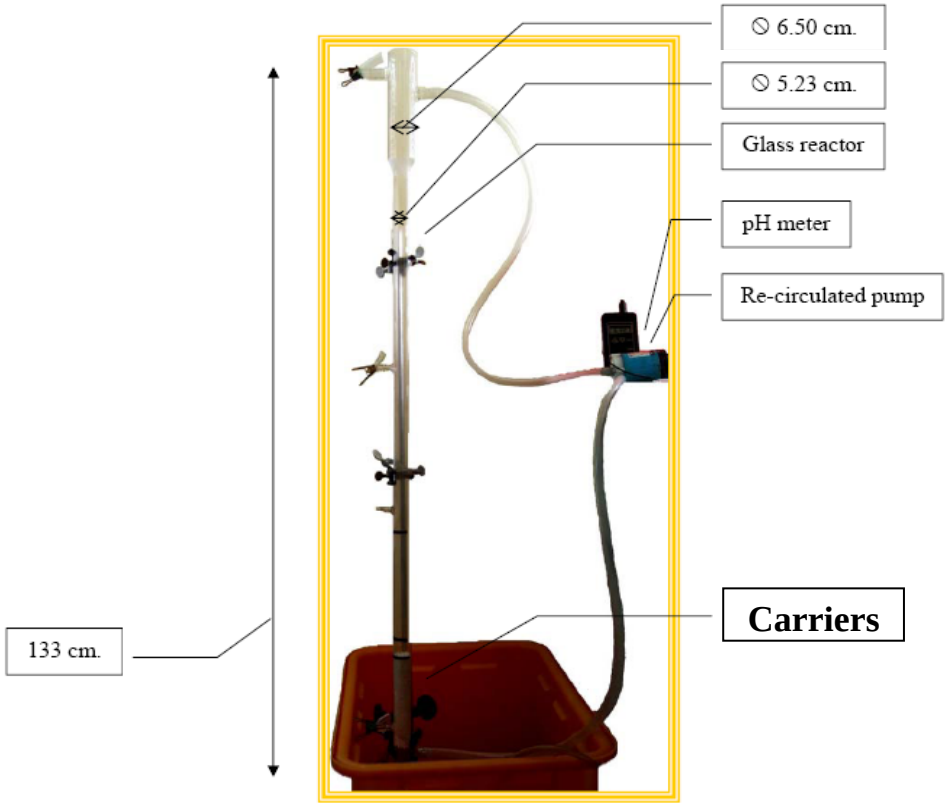

Figure 3.1 Fluidized-bed reactor.

bed expansion was kept constant at 50% from the original bed level by adjusting the internal recirculation rate. The FBR was controlled at 25±0.2°C by air recirculation from 2 air conditioners.

3.2 Experimental Procedures

3.2.1 Kinetics of 2,6-Dimethyl-aniline Degradation

3.2.1.1 Completely Mixed Reactor

For the batch study, the synthesis wastewater was prepared in the beaker using reagent grade chemicals diluted with de-ionized water to the desired concentration. A calculated amount of $FeSO_4 \bullet 7H_2O$ was added as the source of Fe^{2+}. Next, the stirrer was turned on to mix the solution and completely dissolve the ferrous salt. After that, the pH was adjusted to 3.0±0.1 by 1+3 H_2SO_4. H_2O_2 solution was added and the

reaction was simultaneously started. At selected time interval, an appropriate amount of aliquot was taken from the reactor for analysis. To stop further Fenton reaction, an appropriate amount of 0.1 N NaOH was added to the sample to raise the pH to alkaline range. After that, the solution was filtered by a 0.22-μm cellulose acetate membrane filter to separate precipitated iron before analysis. Solution pH was controlled constantly by the addition of 1+3 H_2SO_4 or 1 or 6 N NaOH whenever necessary. All experimental activities are described in Figure 3.2.

For the continuous study, the synthetic wastewater with Fe^{2+} dissolution and H_2O_2 solution were separately, but continuously and equally (18 ml/min), fed into the 0.5-liter beaker by a peristaltic pump. The effluent characteristics were monitored until the steady state has been reached. All other procedures were similar to the batch study.

3.2.1.2 Fluidized-bed Reactor

For fluidized-bed Fenton experiment, the synthetic wastewater with desired Fe^{2+} concentration was prepared in a beaker before pouring into the FBR. After that, 300 gm (300 g per 1.3 L) of carriers was filled into the reactor. The internal recirculation pump was switched on to mix the solution and suspend the carrier at 50% bed expansion. The pH was adjusted to 3.0±0.1 by 1+3 H_2SO_4. Next, H_2O_2 solution was added and the reaction was simultaneously started. Solution pH was controlled constantly by the addition of 1+3 H_2SO_4 or 1 or 6 N NaOH whenever necessary. At selected time interval, an appropriate amount of aliquot was taken from the FBR for analysis. Pretreatment step was similar to the case of Fenton experiment. Experimental steps are summarized in Figure 3.2.

3.2.2 Iron Crystallization

All experimental procedures and setup for completely mixed reactor and fluidized-bed reactor in this part were similar to those in the kinetics study.

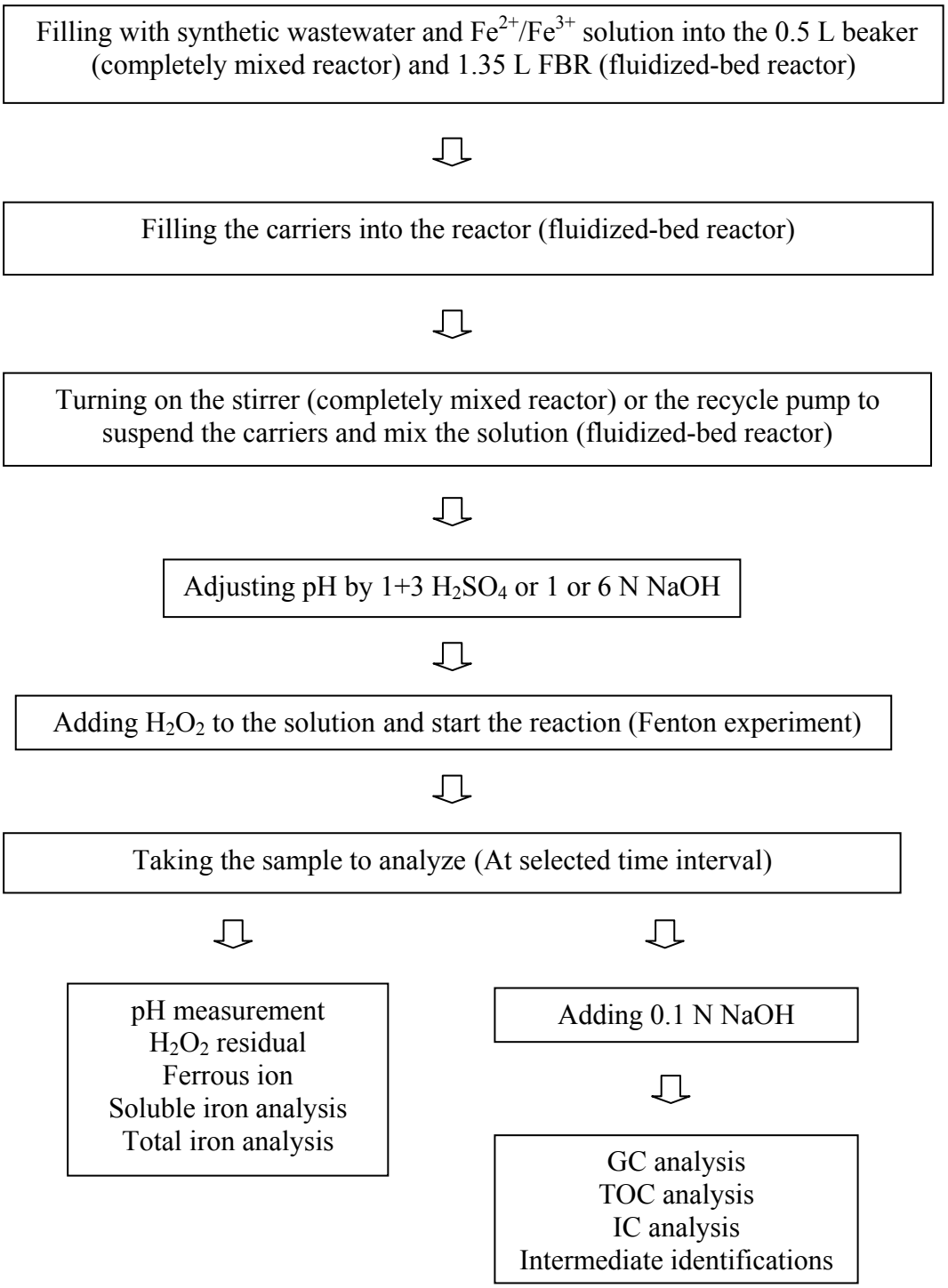

Figure 3.2 Experimental scheme for Fenton and fluidized-bed Fenton processes.

3.3 Experimental Scenarios

This research study was divided mainly into two parts. The first part aimed to determine the kinetics and mechanism of 2,6-DMA degradation by $OH^{\bullet}$. Various experimental scenarios, including batch and continuous modes, with and without solid media, were performed to determine the intrinsic 2^{nd}-order rate constant between 2,6-DMA and $OH^{\bullet}$ to ensure the accuracy of the obtained values. For mechanism determination, several extra experiments were performed using the initially identified aromatic intermediates, i.e., 2,6-DMP, 2,6-DMN and 2,6-DMB, as the target compounds for cross-checking purpose. In the second part, the behavior of the iron precipitation and crystallization onto the media in the FBR was investigated.

3.3.1 Kinetics of 2,6-Dimethyl-aniline Degradation

To determine the intrinsic 2^{nd}-order rate constant between 2,6-DMA and $OH^{\bullet}$, 6 experimental scenarios (Scenarios B to G) were set up and carried out. In addition, one control experiment was also performed for system control (Scenario A).

Scenario A

Determination of the effect of volatilization and H_2O_2 on the disappearance of 2,6-DMA, n,n-dimethylaniline, and aniline in a batch reactor under the conditions as shown in Table 3.1. This experiment was conducted to observe the reactivity of all target compounds with H_2O_2 as well as their ability to volatile to the atmosphere under the studied conditions.

Table 3.1 Conditions for the determination of H_2O_2 oxidation and volatilization of target compounds.

2,6-DMA (mM)	AN (mM)	n,n-DMA (mM)	H_2O_2 (mM)	pH
1	1	1	20	3

Scenario B

Determination of the effect of H_2O_2 on the degradation of *o*-toluidine in a batch reactor with the condition as shown in Table 3.2. This experiment aimed to verify the H_2O_2–resistivity of the *o*-toluidine which was used as an internal standard for GC analysis.

Table 3.2 Conditions for the determination of *o*-toluidine oxidation by H_2O_2.

o-toluidine (mM)	H_2O_2 (mM)	pH
0.1	2	11

Scenario C

Verification of the competitive rate technique in a batch reactor with the conditions as shown in Table 3.3. This part aimed to verify the feasibility and accuracy of the competition rate technique in determining the reaction rate constant by using two organics, i.e., AN and n,n-DMA of which the rate constants with $OH^{\bullet}$ have been already reported.

Table 3.3 Conditions for verification of the competitive rate technique.

n,n-DMA (mM)	AN (mM)	Fe^{2+} (mM)	H_2O_2 (mM)	pH	Number of run
1	1	1	20	3	3

Scenario D

Determination of intrinsic rate constant by ordinary Fenton process in a batch reactor in the absence of solid carriers with the conditions as shown in Table 3.4. This part aimed to determine the 2^{nd}-order rate constant between 2,6-DMA and $OH^{\bullet}$ by the competitive rate technique using AN as a reference compound.

Table 3.4 Conditions for the rate constant determination under the batch operation.

2,6-DMA (mM)	AN (mM)	Fe^{2+} (mM)	H_2O_2 (mM)	pH	Number of run
1	1	1	20	3	3
0.5	1	1	20	3	1
1	0.5	1	20	3	1
0.5	0.5	1	20	3	1
1	1	1.5	30	3	1
1	1	2	40	3	1
1	1	1	30	3	1

Scenario E

Determination of intrinsic rate constant by ordinary Fenton process in the presence of SiO_2 in the batch reactor with the conditions as shown in Table 3.5. This part aimed to investigate the effect of solid media on the disappearance rate and rate constant of 2,6-DMA simulating of those occurred the fluidized-bed Fenton process.

Table 3.5 Conditions for the rate constant determination in the presence of solid media.

2,6-DMA (mM)	AN (mM)	Fe^{2+} (mM)	H_2O_2 (mM)	pH	SiO_2 (g/l)
1	1	1	20	3	37.04

Scenario F

Determination of intrinsic rate constant by fluidized-bed Fenton process with the conditions as shown in Table 3.6. This part aimed to investigate the effect of FBR operation on the oxidation rate and rate constant of 2,6-DMA.

Table 3.6 Conditions for rate constant determination by the fluidized-bed Fenton process.

2,6-DMA (mM)	AN (mM)	Fe^{2+} (mM)	H_2O_2 (mM)	pH	CS (g/l)	Number of run
1	1	1	20	3	230.77	2

Scenario G

Determination of intrinsic rate constant by ordinary Fenton process in the continuous mode with the conditions as shown in Table 3.7. The objective of this part was similar to those of Scenario D; however, the operation was changed from a batch mode to continuous mode.

Table 3.7 Conditions for the rate constant determination under the continuous operation.

2,6-DMA (mM)	AN (mM)	Fe^{2+} (mM)	H_2O_2 (mM)	pH	Number of run
1	1	1	20	3	2

3.3.2 Mechanism of 2,6-Dimethyl-aniline Oxidation

To determine the oxidation pathway of 2,6-DMA by $OH^{\bullet}$, the Fenton reaction of 2,6-DMA and its potential intermediates was studied in the batch reactor.

Scenario H

Determination of the mechanism of 2,6-DMA oxidation by $OH^{\bullet}$ with the conditions as shown in Table 3.8.

Table 3.8 Conditions for oxidation pathway determination.

2,6-DMA (mM)	2,6-DMB (mM)	2,6-DMN (mM)	2,6-DMP (mM)	Fe^{2+} (mM)	H_2O_2 (mM)	pH
10	-	-	-	10	200	3
-	10	-	-	5	100	3
-	-	10	-	5	100	3
-	-	-	10	5	100	3

3.3.3 Iron Precipitation and Crystallization

Since the precipitation and crystallization of solid particles occur simultaneously and simultaneously, this research decided to investigate all the conditions involving in these two processes.

Scenario I

Preliminary study on the effect of pH on iron solubility with the conditions as shown in Table 3.9. Since Fe^{2+} is one of the Fenton's reagent and Fe^{3+} is the oxidize product from Fenton reaction, it is important to determine the aqueous solubility of both iron species. This can ensure that all $FeSO_4 \bullet 7H_2O$ being added could completely dissolve in the water and the precipitation of Fe^{3+} can be understood.

Table 3.9 Conditions for iron solubility study.

Iron (mM)	pH	$NaClO_4$ (M)
1 mM of Fe^{2+}	1-12	-
		0.1
1 mM of Fe^{3+}	1-12	0.1

Scenario J

Determination the effect of iron concentration on iron solubility at different pH with the condition as shown in Table 3.10. This part aimed to provide a better understanding in the solubility behavior of Fe^{2+} and Fe^{3+} in aqueous phase.

Table 3.10 Conditions for the effect of iron concentration.

Iron	pH	$NaClO_4$ (M)
1 & 2 mM Fe^{2+}	1-12	0.1
1 & 2 mM Fe^{3+}		

Scenario K

Determination of $Fe(OH)_3$ crystallization with the conditions as shown in Table 3.11. The behavior of $Fe(OH)_3$ crystallization onto solid media under supersaturated was investigated in this part which can lead to a better understanding on the removal of iron in the fluidized-bed Fenton process.

Table 3.11 Conditions for the $Fe(OH)_3$ crystallization characterization in FBR.

Fe^{3+} (mM)	pH	CS (g/l)	SiO_2 (g/l)	Al_2O_3 (g/l)
1	7	230.77	-	-
1	7	-	230.77	-
1	7	-	-	230.77
1	3	230.77	-	-

Scenario L

Determination of crystallization under Fenton reaction with the conditions as shown in Table 3.12. This part aimed to determine the natural behavior of iron crystallization in the fluidized-bed Fenton process in the absence of organic matters.

Table 3.12 Conditions for the crystallization in fluidized-bed Fenton process.

Fe^{2+} (mM)	H_2O_2 (mM)	pH	CS (g/l)	SiO_2 (g/l)
1	20	3	230.77	-
			-	230.77
			230.77 (passing #30)	-

Scenario M

Determination of effect of $Fe(OH)_3$ crystallites on crystallization process with the conditions as shown in Table 3.13. In this part, the Fenton reaction was allowed to proceed in a completely mixed reactor (CMR) for 1 hour without any medium before transferring into the FBR for crystallization for 3 hours (1-hr pre-CMR+FBR). This scenario was different from previous in term of the crystallite formation. In previous scenario, the iron crystallites were formed and the crystallization onto the sand surface occurred simultaneously. On the other hand, the crystallites were allowed to ripen for 1 hour (the crystals became larger) before the crystallization in the FBR could happen.

Table 3.13 Conditions for the effect of $Fe(OH)_3$ crystallites.

Fe^{2+} (mM)	H_2O_2 (mM)	pH	CS (g/l)	Operating Mode
1	20	3	230.77	fully FBR
				1-hr pre-CMR+FBR
3	60	3	230.77	5-min pre-CMR+FBR

Scenario N

Determination of effect of iron concentration on iron crystallization with the conditions as shown in Table 3.14. As the iron concentration increased, the supersaturated condition became more prevailed even though the pH was the same; hence, the effect of supersaturation on iron crystallization could be obtained without compromising the effect of pH. In this part, various Fe^{2+} concentrations were used to

observe the behavior of iron crystallization both under the typical FBR mode and 1-hr pre-CMR+FBR mode.

Table 3.14 Conditions for the effect of iron concentration on crystallization.

Fe^{2+} (mM)	H_2O_2 (mM)	pH	CS (g/l)	Operating Mode
1	20	3	230.77	fully FBR
				1-hr pre-CMR+FBR
2	40			fully FBR
				1-hr pre-CMR+FBR
3	60			fully FBR
				1-hr pre-CMR+FBR

Scenario O

Determination of effect of mixing on crystal growth with the conditions as shown in Table 3.15. This part aimed to provide a better understanding on the mechanism of crystallite formation and crystal growth.

Table 3.15 Conditions for the effect of mixing on crystal growth.

Fe^{3+} (mM)	pH	Operating Conditions
3	3	Purging with air in cylinder
		Purging with O_2 in cylinder
		Purging with N_2 for 15 min and kept in BOD bottle
		Fenton process

Scenario P

Determination of effect of organo-ferric complex on Fe^{3+} solubility and crystallization in FBR. This scenario consisted of 2 parts. The first part studied under constant organo-ferric complex concentration without Fenton's reagent in FBR (Table 3.16), the type and concentration of carboxylic acids being used simulated from the

conditions found during the oxidation of 1 mM of 2,6-DMA. The second part aimed to investigate under the dynamic condition in the fluidized-bed Fenton process (Table 3.17).

Table 3.16 Conditions for the effect of organo-ferric complex on Fe^{3+} solubility/crystallization in FBR.

Fe^{3+} (mM)	Formic acid (mM)	Acetic acid (mM)	Oxalic acid (mM)	pH	CS (g/l)
1	2.0	0.5	2.0	3	230.77
	-	-	-		

Table 3.17 Conditions for the effect of organo-ferric complex on Fe^{3+} solubility/crystallization under dynamic state in fluidized-bed Fenton process.

2,6-DMA (mM)	AN (mM)	Fe^{2+} (mM)	H_2O_2 (mM)	pH	CS (g/l)	Operating Mode
0.1	0.1	1	20	3	230.77	fully FBR
						1-hr pre-CMR+FBR
1	1					fully FBR
						1-hr pre-CMR+FBR

Scenario Q

Determination of the reusability of iron-coated CS for iron crystallization with the conditions as shown in Table 3.18. This part aimed to investigate the capability of CS to serve as the fluidized medium for iron crystallization.

Table 3.18 Conditions for the reusability of iron-coated CS for iron crystallization.

Fe^{2+} (mM)	H_2O_2 (mM)	pH	CS (230.77 g/l)
1	20	3	Cycle 1st – Cycle 5th
2	40		Cycle 6th – Cycle 101st

Scenario R

Determination of the catalytic ability of iron-coated CS in comparison with the goethite in Fenton reaction with the conditions as shown in Table 3.19. Since iron oxide can serve as a catalyst in Fenton process, this study part aimed to determined the catalytic activity of the iron-coated CS obtained from the fluidized-bed Fenton process and compared with the commercial goethite. The test was performed in a batch mode due to the cost limitation of expensive goethite.

Table 3.19 Experimental scenarios for the catalytic ability of iron-coated construction sand on the oxidation of 2,6-DMA and AN.

2,6-DMA (mM)	AN (mM)	H_2O_2 (mM)	pH	Catalyst
1	1	20	3	75 g/l iron-coated CS
				0.075 g/l goethite
				0.75 g/l goethite
				1.0 g/l goethite
				7.5 g/l goethite
				75 g/l goethite

3.4 Analytical Methods

3.4.1 Measurement of Aromatic Compounds

After raising the pH by 0.1 N NaOH addition and filtered by cellulose acetate membranes with 0.22 μm pore size to separate precipitated iron, the sample was analyzed for residual organic compounds and its intermediates by using a GC-17A gas chromatograph equipped with a flame ionization detector and HP-5 capillary column (Hewlett-Packard) with 0.53-mm in inside diameter and 15-m length. Exactly 1.0 μl of sample was injected into the injection port. The column temperature was initially set at 85°C for 3 minutes, then increased by 65°C per minute to 200°C and maintained at this temperature for the final 5 minutes. Injector and detector temperatures were set at 250 and 280°C, respectively. *o*-toluidine was used as the internal standard. Chromatogram of all aromatic compounds used in this study is shown in Figure 3.3 and the standard curves are shown in Appendix B.

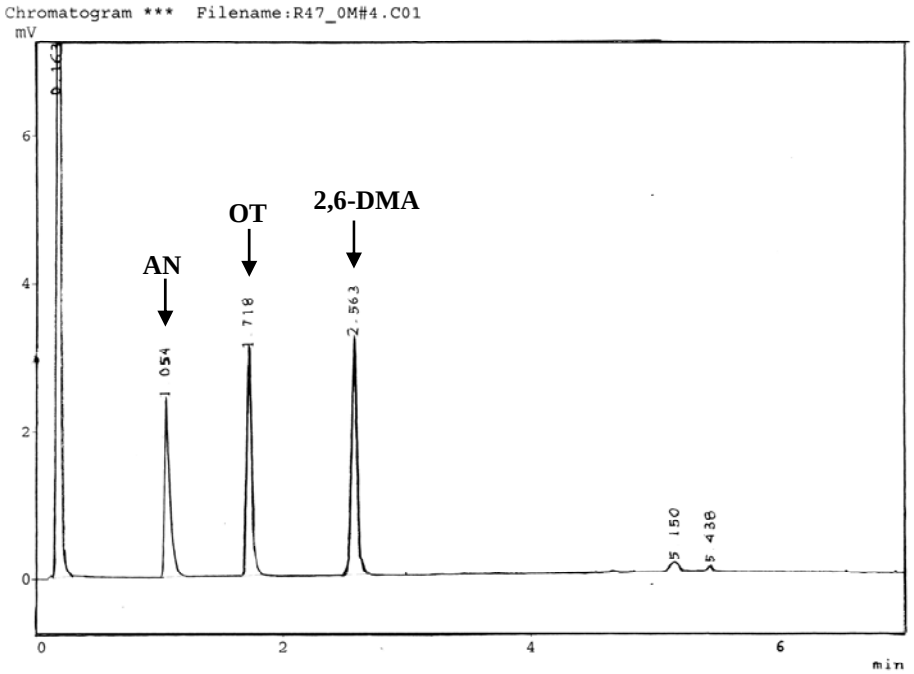

Figure 3.3 Gas chromatography chromatogram.

3.4.2 Measurement of Iron

Concentration of iron species, Fe^{2+}, soluble and total iron, were performed immediately after sampling without alkaline addition in order to prevent the precipitation of $Fe(OH)_2$. For ferrous analysis, the sample was analyzed by light absorbance measurement at 510 nm after being complexed with 1,10-phenanthroline using UV-vis spetophotometer (Genesys 20, ThermoSpectronic, USA) following the Standard Methods (APHA, 1992). The DI water mixed with the sample without phenanthroline was used as a blank for every sample. For total and soluble iron analysis, the samples were digested by concentrated hydrochloric acid (HCl) and hydroxylamine as the reductant to transform Fe^{3+} to Fe^{2+}. Then, the samples were formed a colored complex with 1,10-phenanthroline following to the ferrous analysis.

3.4.3 Measurement of Hydrogen Peroxide Residual

Similar to Fe^{2+} analysis, the sample was analyzed for H_2O_2 immediately after sampling. The concentration of hydrogen peroxide residual was determined by standard iodometric method in which the potassium iodide and sodium thiosulfate were used as the reactant and titrant, respectively, as described in Appendix C.

3.4.4 Measurement of Total Organic Carbon

Mineralization of the effluent was determined by a mean of total organic carbon using SHIMADZU TOC-V_{CPH} (Japan). Before the analysis, the Fenton reaction was stopped by 6 N NaOH at the ratio of 1:10 (20 ml NaOH to 200 ml sample), and then the solution was filtered with 0.22-μm microfilter to separate iron sludge from the solution.

3.4.5 Identification and Measurement of Carboxylic Intermediates

Carboxylic acids were determined by the Ion Chromatograph (SHIMADSU) equipped with SCL-10A VP system controller, DGU-$20A_3$ degasser, LC-20AD VP liquid chromatograph, CTO-20A column oven, CDD-10A VP conductivity detector,

Shim-pack IC-GA3 guard column and Shim-pack IC-A3 analytical column (4.6 mm ϕ×15 cm). The mobile phase was 8.0 mM p-hydroxybenzoic acid and 3.2 mM bis(2-hydroxyethyl)iminotris(hydroxymethyl)methane. The flow rate and temperature were set at 1.2 ml min^{-1} and 40 °C, respectively. Exactly 10 μl of the alkaline sample after NaOH addition was injected into the injecting port.

3.4.6 Identification of Aromatic Intermediates

To identify the aromatic intermediates from 2,6-DMA oxidation by $OH^{\bullet}$, 4 ml of the sample after stopping Fenton reaction was injected into an extraction tube containing 2 ml of n-hexane. The tube was then shaken by hand 100 times, followed by 15 minutes of sonication, and then centrifuged at 4,000 rpm for 5 minutes. The upper-layer of n-hexane was withdrawn as much as possible into a 5-ml analyzing tube. The remaining mixture in the extraction tube was then re-extracted twice more following the same procedure. At the third extraction, the upper-layer of n-hexane was pulled out and filled the analyzing tube up to the 5-ml mark. A small amount of anhydrous Na_2SO_4 was added to remove moisture before GC analysis. One μl of the extraction solvent into the Agilent Technologies 6890N Network GC System equipped with a J&W DB-5MS capillary column (0.25 mm × 30 m) and connected with the 5973 Network Mass Selective Detector. The GC temperature program was as follows: 40°C for 2 min, followed by a 15 °C min^{-1} ramp to 280 °C, then hold for 5 min.

3.4.7 Solid Characterization

Iron oxide coated media were characterized for their surface properties, including specific surface area, pore volume, and pore size, and iron oxide species by BET surface analyzer (Autosorb-1 from Quantachrome) and XRD analyzer (D8 Discover from Bruker AXS.), respectively.

CHAPTER IV
RESULTS AND DISCUSSION

4.1 Kinetics of 2,6-Dimethyl-aniline Degradation

4.1.1 Experimental Control

4.1.1.1 2,6-Dimethyl-aniline, n,n-Dimethyl-aniline and Aniline Oxidation by H_2O_2 and Volatilization

This experimental part (Scenario A) aimed to determine the oxidation of 2,6-dimethyl-aniline (2,6-DMA), n,n-dimethyl-aniline (n,n-DMA) and aniline (AN) by H_2O_2 as well as their volatilization. The results demonstrated that H_2O_2 did not have any significant impact on degradation of these three compounds as shown in Figure 4.1 (raw data are shown in Appendix D). In addition, volatilization of these three compounds could be neglected within the experimental period. From these results, it believed that the target compound (2,6-DMA) and the reference compounds could not be degraded effectively and rapidly without an involvement of hydroxyl radicals under the studied conditions.

4.1.1.2 o-Toluidine Oxidation by H_2O_2

In this study, *o*-toluidine (OT) was used as the internal standard for gas chromatograph analysis to obtain accurate concentrations of the compounds. As a result, it is necessary to assure that *o*-toluidine would not be degraded under the conditions in GC vial in which the pH was adjusted to 11 to stop Fenton reaction and the sample was diluted 10 times (Scenario B). Figure 4.2 exhibits that *o*-toluidine concentration was not significantly decreased in the presence of H_2O_2, so it means that *o*-toluidine can serve very well as the internal standard.

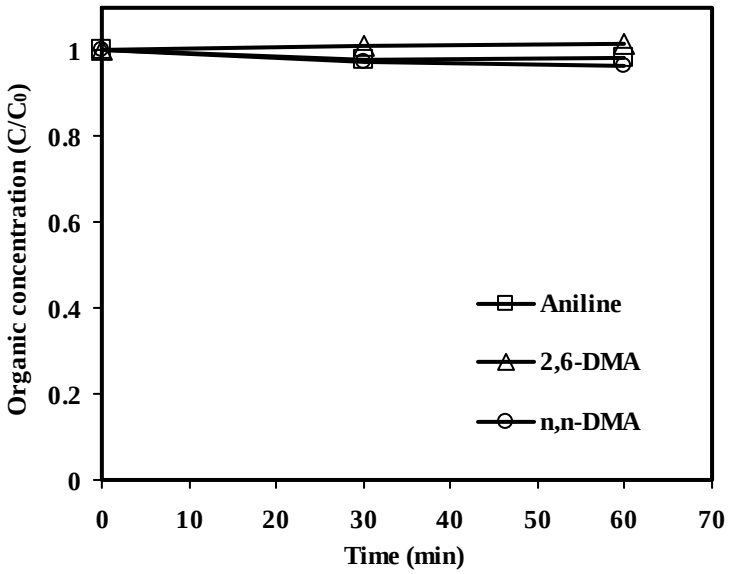

Figure 4.1 Control experiment for direct H_2O_2 oxidation and volatilization with the initial conditions as follows: 1 mM of 2,6-DMA, n,n-DMA and AN, 20 mM of H_2O_2 at pH 3 and 25°C.

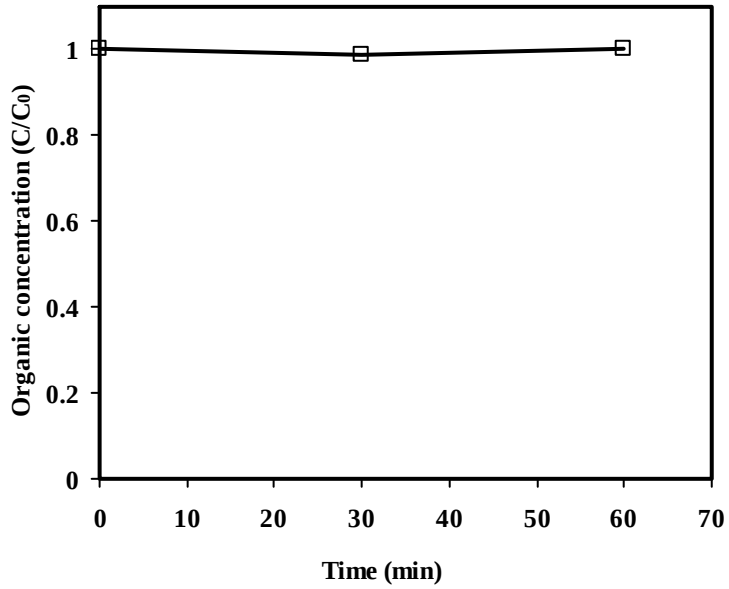

Figure 4.2 Control experiment for direct H_2O_2 oxidation of the internal standard (OT) with the initial conditions as follows: 0.1 mM of OT, 2 mM of H_2O_2 and pH 11.

4.1.2 Verification of Competitive Kinetics Technique

A preliminary study was conducted to verify the accuracy of this competitive kinetics technique by monitoring the degradation rate of aniline with the rate constant with $OH^{\bullet}$ of 4.8×10^{9} $M^{-1}sec^{-1}$ in the presence of n,n-DMA of which its second-order rate constant with $OH^{\bullet}$ is also known (2.9×10^{9} $M^{-1}sec^{-1}$) as shown in Scenario C. Data repeatability and reliability were also conducted as shown in Figure 4.3 as an example case in which the Fenton experiment was carried out in triplicate. It can be seen from the figure that the data obtained from three different runs with similar conditions were almost the same; hence, verifying the consistency of experimental set up and procedure. Considering on the aniline and n,n-DMA removal efficiencies from Figure 4.3(a), it can been seen that aniline was removed faster than n,n-DMA because aniline molecular structure was simpler than n,n-DMA which has a dimethylamino group attached to a phenyl group. This is in agreement with the reported rate constants where the second-order rate constant with $OH^{\bullet}$ of aniline was greater than n,n-DMA. Figure 4.3(b) is the plot between $\ln([n,n\text{-DMA}]/[n,n\text{-DMA}]_0)$ versus $\ln([AN]/[AN]_0)$ shows a linear relationship and the slope will represent the ratio of the rate constants between aniline and n,n-DMA. The average slope of 0.65 was obtained which was very close to the theoretical value of 0.60; hence, this competitive kinetics technique employed in this research is valid.

4.1.3 Intrinsic Rate Constant of 2,6-Dimethyl-aniline with Hydroxyl Radical

4.1.3.1 Batch Study in the Absence of Media

The intrinsic rate constant of 2,6-DMA was determined by using the similar procedure in a batch reactor similar to the case of technique verification, Data repeatability was repeatedly obtained as shown in Figure 4.4 as an example case. Figure 4.4(a) showed that the removal efficiency of aniline was slower than 2,6-DMA. It can expected that the second order rate constant of 2,6-DMA with $OH^{\bullet}$ will

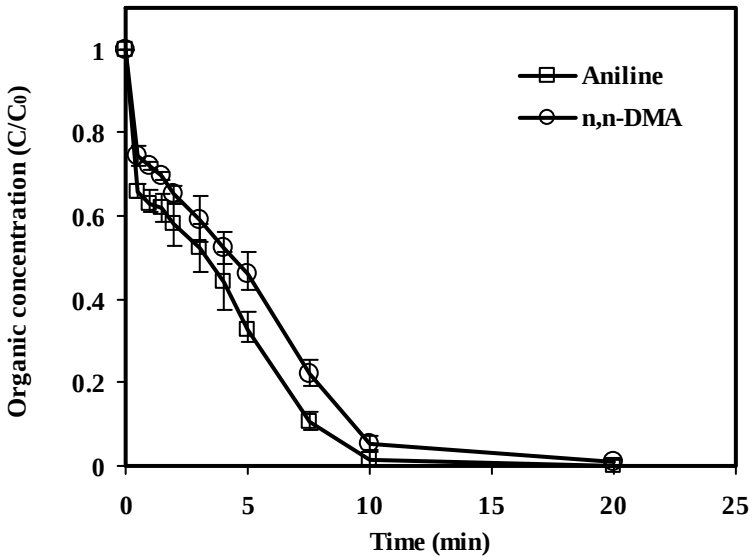

(a) Profile of AN and n,n-DMA

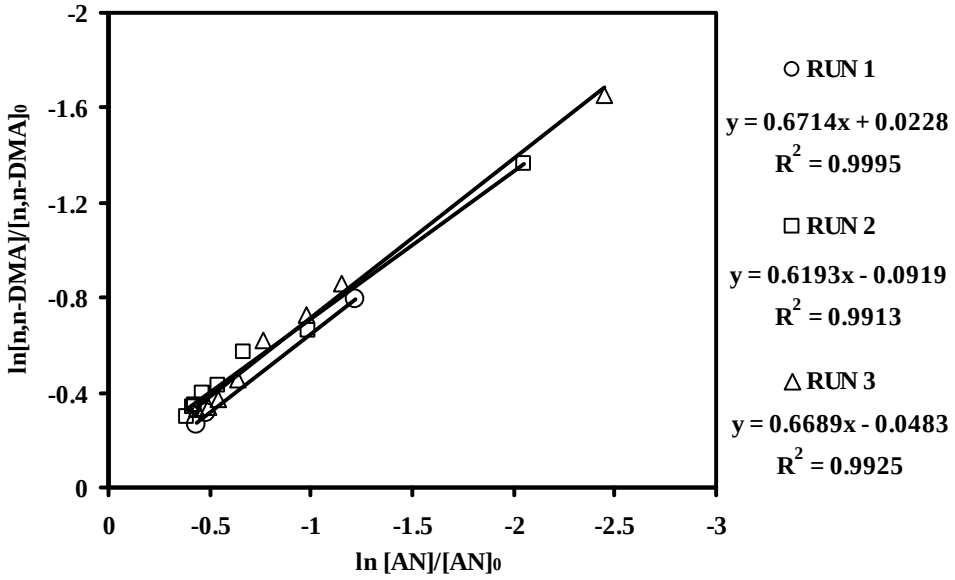

(b) Relationship between ln([n,n-DMA]/[n,n-DMA]$_0$) versus ln([AN]/[AN]$_0$)

Figure 4.3 Verification of competitive technique with the initial conditions as follows: 1 mM of AN, 1 mM of n,n-DMA, 1 mM of Fe^{2+}, 20 mM of H_2O_2 at pH 3 and 25°C.

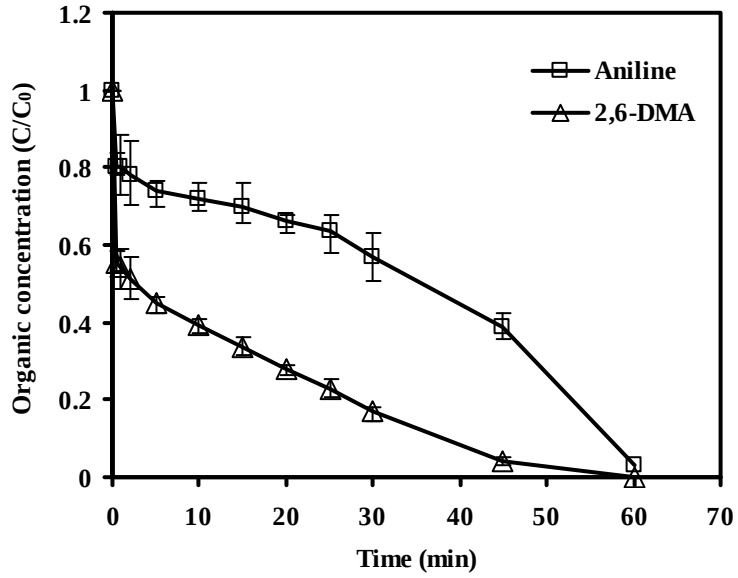

(a) Profile of AN and 2,6-DMA

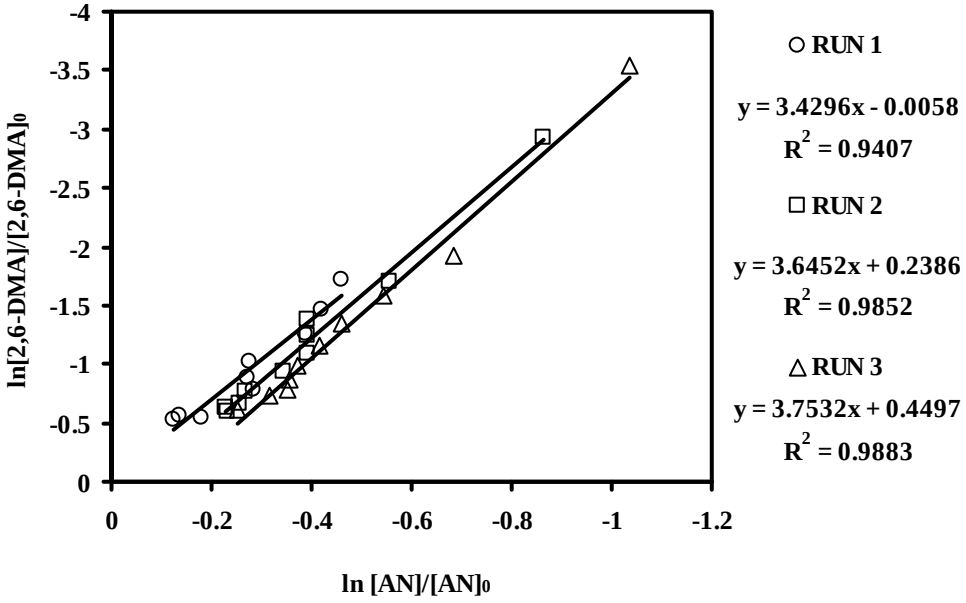

(b) Relationship between ln([2,6-DMA]/[n2,6-DMA]$_0$) versus ln([AN]/[AN]$_0$)

Figure 4.4 Intrinsic rate constant determination of 2,6-DMA in batch mode with the initial conditions as follows: 1 mM of AN, 1 mM of 2,6-DMA, 1 mM of Fe^{2+}, 20 mM of H_2O_2 at pH 3 and 25°C.

be greater than aniline. Following the experimental triplications from Figure 4.4(b), the results showed that the ratios of the rate constant between 2,6-DMA and aniline by the Fenton process under the condition of 1 mM of 2,6-DMA, 1 mM of aniline, 1 mM of Fe^{2+}, 20 mM of H_2O_2, pH 3, and 25°C were quite steady with an average of 3.61. The rate constants were estimated to be in the range of 1.65×10^{10} to 1.80×10^{10} $M^{-1}sec^{-1}$ as shown in Table 4.1. Furthermore, under other conditions as described in Scenario D, the rate constants between 2,6-DMA and $OH^{\bullet}$ in the Fenton reaction were found to be quite steady between 1.59×10^{10} and 1.80×10^{10} M^{-1} sec^{-1} as summarized in Table 4.1 (graphical determinations are shown in Appendix E). By averaging the values in Table 4.1, the second-order intrinsic rate constant between 2,6-DMA and $OH^{\bullet}$ obtained from the batch study without media was 1.71×10^{10} $M^{-1}sec^{-1}$.

4.1.3.2 Batch Study in the Presence of Media

In this section, the intrinsic rate constant of 2,6-DMA with $OH^{\bullet}$ was determined in a silica-suspension batch reactor to simulate a fluidized-bed reactor (Scenario E). Figure 4.5(a) shows the time profiles of aniline and 2,6-DMA in the presence of SiO_2. As compared to ordinary Fenton process without SiO_2 (Figure 4.4a), it can be seen that both removal rate and efficiency in the presence of SiO_2 were significantly lower. This is possibly due to the limitation of Fe^{2+} in the presence of SiO_2 suspension as a result from surface complexation which should be similar to the condition which occurs in the fluidized-bed Fenton reactor. Certain portion of added Fe^{2+} was adsorbed onto the surface of SiO_2; hence, reduced the amount of free Fe^{2+} to catalyze the decomposition of H_2O_2 to generate the powerful $OH^{\bullet}$. As a result, the disappearance rates of aniline and 2,6-DMA were decelerated as compared to in the absence of SiO_2. Nonetheless, the results showed that the ratio of the rate constants between 2,6-DMA and aniline obtained from the SiO_2-suspension reactor which simulating the fluidized-bed Fenton reactor of 3.34 (Figure 4.5(b)) which is corresponding to the value of the rate constant of 1.6×10^{10} M^{-1} sec^{-1} (Table 4.1) was comparable to the results from previous part.

Table 4.1 Intrinsic rate constants of 2,6-DMA obtained from various experimental conditions.

Operating Condition	**AN (mM)**	**2,6-DMA (mM)**	**Fe^{2+} (mM)**	**H_2O_2 (mM)**	**Media (g/l)**	**k ($M^{-1}sec^{-1}$)**
Batch without media	1	1	1	20	-	1.65×10^{10}
	1	1	1	20	-	1.75×10^{10}
	1	1	1	20	-	1.80×10^{10}
	1	0.5	1	20	-	1.73×10^{10}
	0.5	1	1	20	-	1.59×10^{10}
	0.5	0.5	1	20	-	1.59×10^{10}
	1	1	1.5	30	-	1.74×10^{10}
	1	1	2	40	-	1.77×10^{10}
	1	1	1	30	-	1.76×10^{10}
	average					1.71×10^{10}
Batch with media	1	1	1	20	37.04 (SiO_2)	1.60×10^{10}
Batch in fluidized-bed Reactor	1	1	1	20	230.77 (CS)	1.67×10^{10}
	1	1	1	20	230.77 (CS)	1.75×10^{10}
	average					1.71×10^{10}
Continuous without media	1	1	1	20	-	1.70×10^{10}
	1	1	1	20	-	1.71×10^{10}
	average					1.71×10^{10}
Overall average						1.70×10^{10}

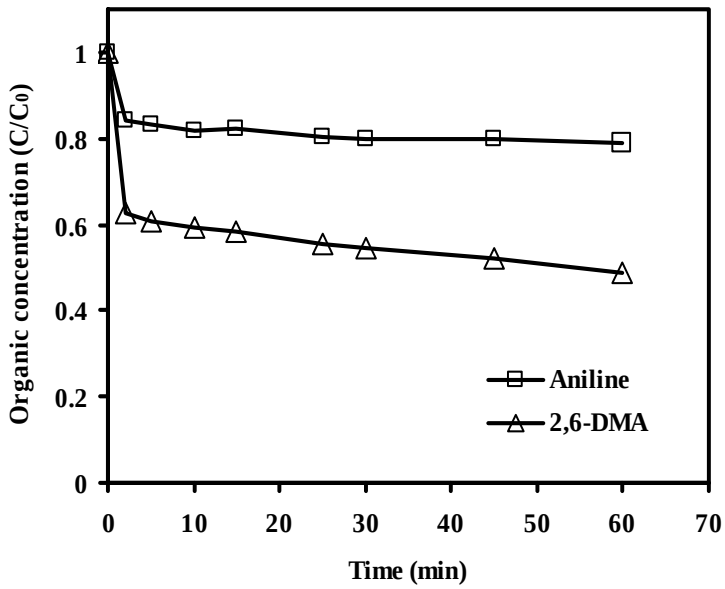

(a) Profile of AN and 2,6-DMA

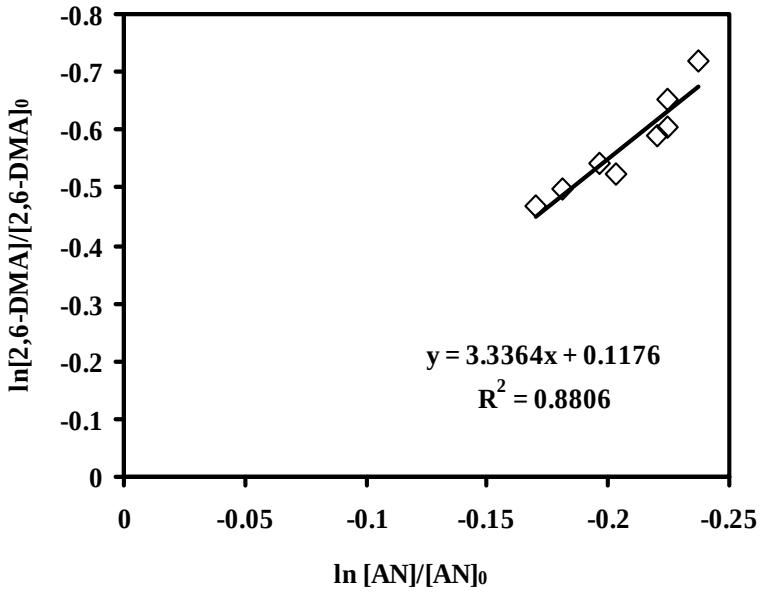

(b) Relationship between ln([2,6-DMA]/[n2,6-DMA]$_0$) versus ln([AN]/[AN]$_0$)

Figure 4.5 Intrinsic rate constant determination between 2,6-DMA and $OH^{\bullet}$ in a SiO_2-suspension reactor with following conditions: 1 mM of AN, 1 mM of 2,6-DMA, 1 mM of Fe^{2+}, 20 mM of H_2O_2, 37.04 g/l of SiO_2 at pH 3 and 25°C.

4.1.3.3 Batch Study in the Fluidized-bed Reactor

In this experiment, the second-order rate constants of 2,6-DMA with $OH^{\bullet}$ was determined in the real fluidized-bed Fenton process (Scenario F). From Figure 4.6(a), the data repeatability of the fluidized-bed Fenton process was also confirmed. It can be seen that the data obtained from two different runs with similar conditions were almost the same; thus, it can verify the consistency of experimental set up and procedure. The outcomes for the slopes of Figure 4.6(b) found that the average rate constant was 1.71×10^{10} M^{-1} sec^{-1} (Table 4.1) which was very close to the results from previous two cases. This could verify the reliability of the rate constant obtained in this study.

4.1.3.4 Continuous Study in the Absence of Media

The continuous study was also carried out to examine the intrinsic rate constant of 2,6-DMA (Scenario G). From Figure 4.7, the repeatability of the continuous study was also assured. It can been seen from the figure that the data obtained from two different runs with similar conditions under the steady state were almost the same; hence, verified the consistency of experimental set up and procedure. Moreover, the oxidation of aniline was slower than 2,6-DMA similar to the batch study. The concentrations of aniline and 2,6-DMA reached the equilibrium within 30 minutes. It means that within the experimental period for 2.5 hours, both of these compounds were quite steady. The second-order intrinsic rate constant from this continuous experiment could be determined by following Eq. 2.28 and found to be with the average of 1.71×10^{10} $M^{-1}sec^{-1}$ as shown in Table 4.1. In addition, since the influent flow rates were also known, the concentrations of $OH^{\bullet}$ at the steady state could be estimated and were found to be in the range of 4.85×10^{-10} to 6.82×10^{10} mM. Due to its high reactivity and short lifetime the concentration of $OH^{\bullet}$ in aqueous solution can be expected as very low depending on the presence of reactants, scavengers, organic compounds, and environmental conditions.

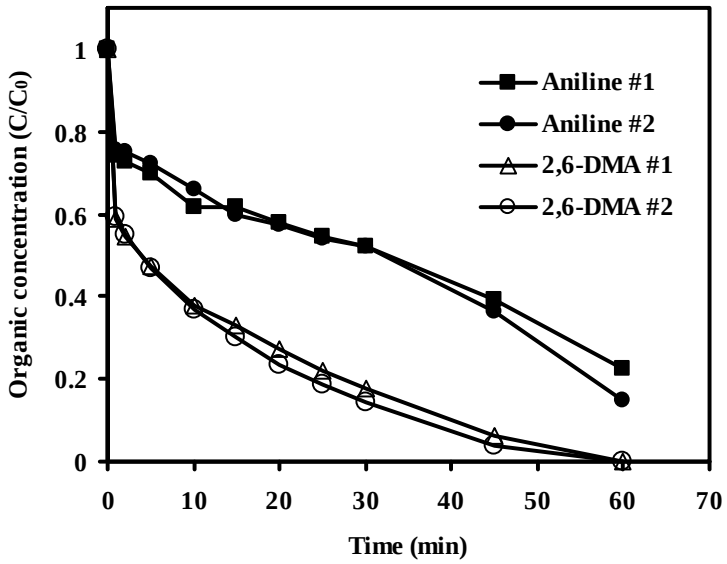

(a) Profile of AN and 2,6-DMA

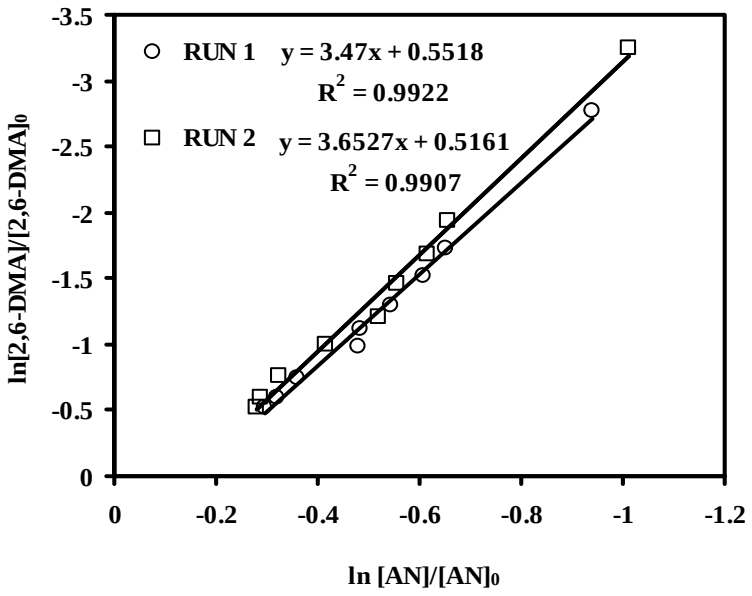

(b) Relationship between ln([2,6-DMA]/[n2,6-DMA]$_0$) versus ln([AN]/[AN]$_0$)

Figure 4.6 Instrinsic rate constant determination between 2,6-DMA and $OH^{\bullet}$ in a batch fluidized-bed reactor with following conditions: 1 mM of AN, 1 mM of 2,6-DMA, 1 mM of Fe^{2+}, 20 mM of H_2O_2, 230.77 g/l of CS at pH 3 and 25°C.

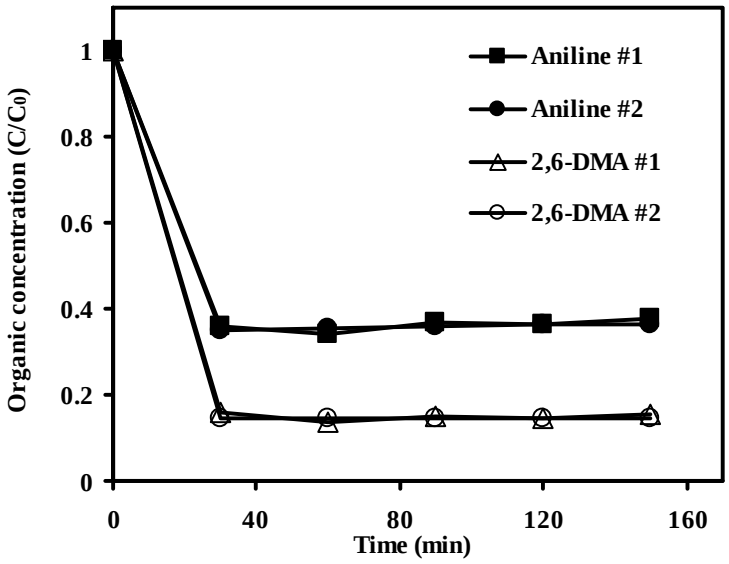

Figure 4.7 Time-profile of 2,6-DMA and AN in continuous mode with the initial conditions as follows: 1 mM of AN, 1 mM of 2,6-DMA, 1 mM of Fe^{2+}, 20 mM of H_2O_2 at pH 3 and 25°C.

4.1.3.5 Overall Rate Constant and Confidence Interval

Average intrinsic second-order rate constant between 2,6-DMA and $OH^{\bullet}$ from 14 runs was 1.70×10^{10} M^{-1} sec^{-1} as shown in Table 4.1. An attempt has been made to determine the confidence interval for this rate constant mean. By assuming that the measured data were normally distributed and the population variance was unknown, the confidence intervals had to be estimated by using the "t-distribution" instead of the "standard normal distribution" since the data size was less than 30 (Daniel, 1991). The calculation result revealed that the average and 95 percent confidence interval of the intrinsic second-order rate constant between 2,6-DMA and $OH^{\bullet}$ was $1.70\pm0.04\times10^{10}$ M^{-1} sec^{-1}.

4.1.4 Effect of Fenton's Reagent on Organic Degradation

Concentrations of the Fenton's reagent, Fe^{2+} and H_2O_2, have a major impact on Fenton reaction not only because they generate the $OH^{\bullet}$ but also act as the scavengers for $OH^{\bullet}$. It is interesting to investigate the effect of Fenton's reagent on

the degradation of 2,6-DMA and AN (using the data obtained from Scenario D). Figure 4.8 shows the degradation profiles of 2,6-DMA and AN concurrently present in the Fenton process. It can be seen that when the Fe^{2+}:H_2O_2 ratio was kept constant at 1:20, the disappearance rate of both target compounds increased as the concentration of Fenton's reagent increased. This implies that, for the 2,6-DMA and AN solution at 1 mM each, the amounts of Fe^{2+} and H_2O_2 being added in this study were still under

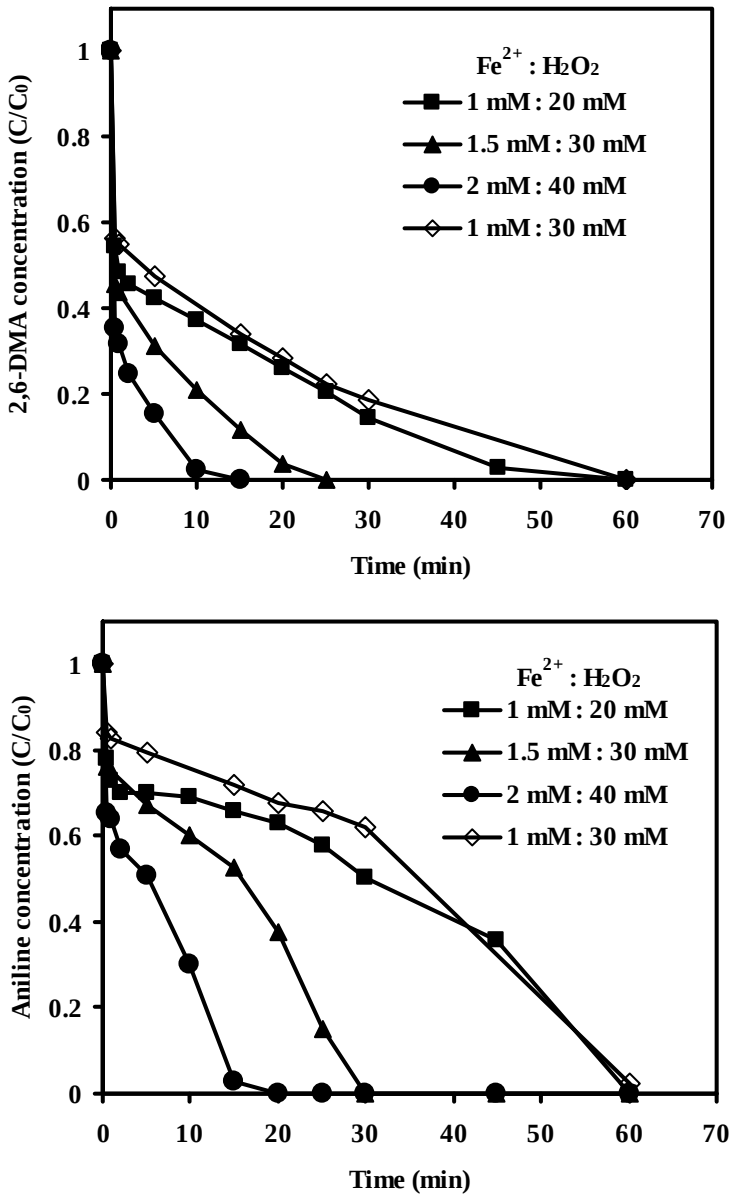

Figure 4.8 Effect of Fenton's reagent on the degradation of 2,6-DMA and AN in a batch mode without media with the initial conditions as follows: 1 mM of AN, 1 mM of 2,6-DMA at pH 3 and 25°C.

the optimum doses; hence, scavenging effect from Fe^{2+} and H_2O_2 was minimal. Decreasing the Fe^{2+}:H_2O_2 ratio from 1 mM : 20 mM to 1 mM : 30 mM did not provide any significant impact on the degradation process indicating that H_2O_2 was not the limiting recipe under the studied conditions; however, increasing the Fe^{2+}:H_2O_2 ratio from 1 mM : 30 mM to 1.5 mM : 30 mM notably accelerated the oxidation rate. This indicates that Fe^{2+} was the principal variable in this case.

4.1.5 Degradation Intermediates and Pathway

The mechanism of 2,6-DMA oxidation by $OH^{\bullet}$ was also investigated in this study (Scenario H). The concentrations of 2,6-DMA and Fenton's reagent were increased 10 times in order to raise the intermediate concentrations to a level that could be accurately identified by the GC/MS and IC. In addition, several extra experiments were also performed using the identified aromatic intermediates as the target compounds to identify their respective oxidation products in order to cross-check the results. The aromatic intermediates found with 80% matching quality or greater were 2,6-DMN, 2,6-DMP, 2,6-DMB, 2,6-dimethyl-hydroquinone (2,6-DMH), 2,6-dimethyl-nitrophenol, and 2,6-dimethyl-3-hydroxy-benzoquinone as shown in Table 4.2. According to the MSDS, only 2,6-DMP is more toxic than the mother compound, 2,6-DMA; nonetheless, its toxicity could be neglected as will be discussed later. This indicated that the methyl group on the aromatic ring was less sensitive to

Table 4.2. Identified aromatic intermediates of 2,6-DMA oxidation by $OH^{\bullet}$.

Retention Time (min)	Chemical formula	Q[a] (%)
8.000	$C_8H_8O_2$ (2,6-dimethyl-benzoquinone)	83
8.097	$C_8H_{10}O$ (2,6-dimethyl-phenol)	97
8.943	$C_8H_9NO_2$ (2,6-dimethyl-nitrobenzene)	98
9.046	$C_8H_8O_3$ (2,6-dimethyl-3-hydroxy-p-benzoquinone)	80
10.046	$C_8H_{10}O_2$ (2,6-dimethyl-hydroquinone)	81
10.674	$C_8H_9NO_3$ (2,6-dimethyl-nitrophenol)	90

[a]Q is the matching quality when compared with the mass spectrum in the Wiley7n database.

$OH^{\bullet}$ attack than amine- and nitro-functional groups. In addition to the aromatic intermediates, several carboxylic acids were also detected; including maleic, lactic, oxalic, acetic, and formic acids. The pathway of 2,6-DMA oxidation by $OH^{\bullet}$ is proposed as shown in Figure 4.9. The proposed mechanism is quite similar to those of aniline oxidation by $OH^{\bullet}$ either in the Fenton processes (Brillas et al., 1998) or in the catalytic ozonation (Sauleda and Brillas, 2001) or by oxygen in the wet air oxidation (Oliviero et al., 2003). This is understandable since the methyl group on the aromatic ring of 2,6-DMA was not susceptible to $OH^{\bullet}$ attack as mentioned previously; therefore, $OH^{\bullet}$ would attack other sites around the benzene ring of 2,6-DMA (either at the amine or hydrogen positions) as if it was AN. In addition, several identified species obtained from this study were also in agreement with Skoumal et al. (2008) who studied the oxidation of chloroxylenol by electrochemical advanced oxidation processes. They found $OH^{\bullet}$ attacked at the chlorine position to form 2,6-DMH, which was further oxidized to 2,6-DMB and several carboxylic acids similar to the observation in this study. Moreover, the ring-cleavage C-3 or lower compounds identified in this work were corresponding very well with the reaction network for the catalytic wet air oxidation of maleic acid proposed by Oliviero et al. (2001).

The time profiles of the major products are illustrated in Figure 4.10(a), which reveals that the concentrations of the aromatic intermediates were very low (i.e., less than 0.015 mM) even though 80% of 10 mM 2,6-DMA have been already transformed. This indicates that the aromatic ring was rapidly ruptured to form open-chain products. Hence, the toxicity impact of these aromatic intermediates could be neglected since 2,6-DMP which is more toxic than 2,6-DMA was accumulated at the very low concentrations of around 0.014 mM or less and disappeared rapidly when the oxidation process proceeded. Acetic and formic acids, which are the most successive organic products prior to conversion to CO_2, were accumulated in the solution. This implies that under the studied conditions within 60 minutes of reaction time, 2,6-DMA could not be completely mineralized to CO_2. This is in agreement with the total organic carbon profile as shown in Figure 4.10(b) in which only 35% of initial organic carbon was converted to CO_2. Considering the carbon balance at the end of the reaction period, it can be seen that approximately 70% of the organic carbon could be quantified from the identified intermediates.

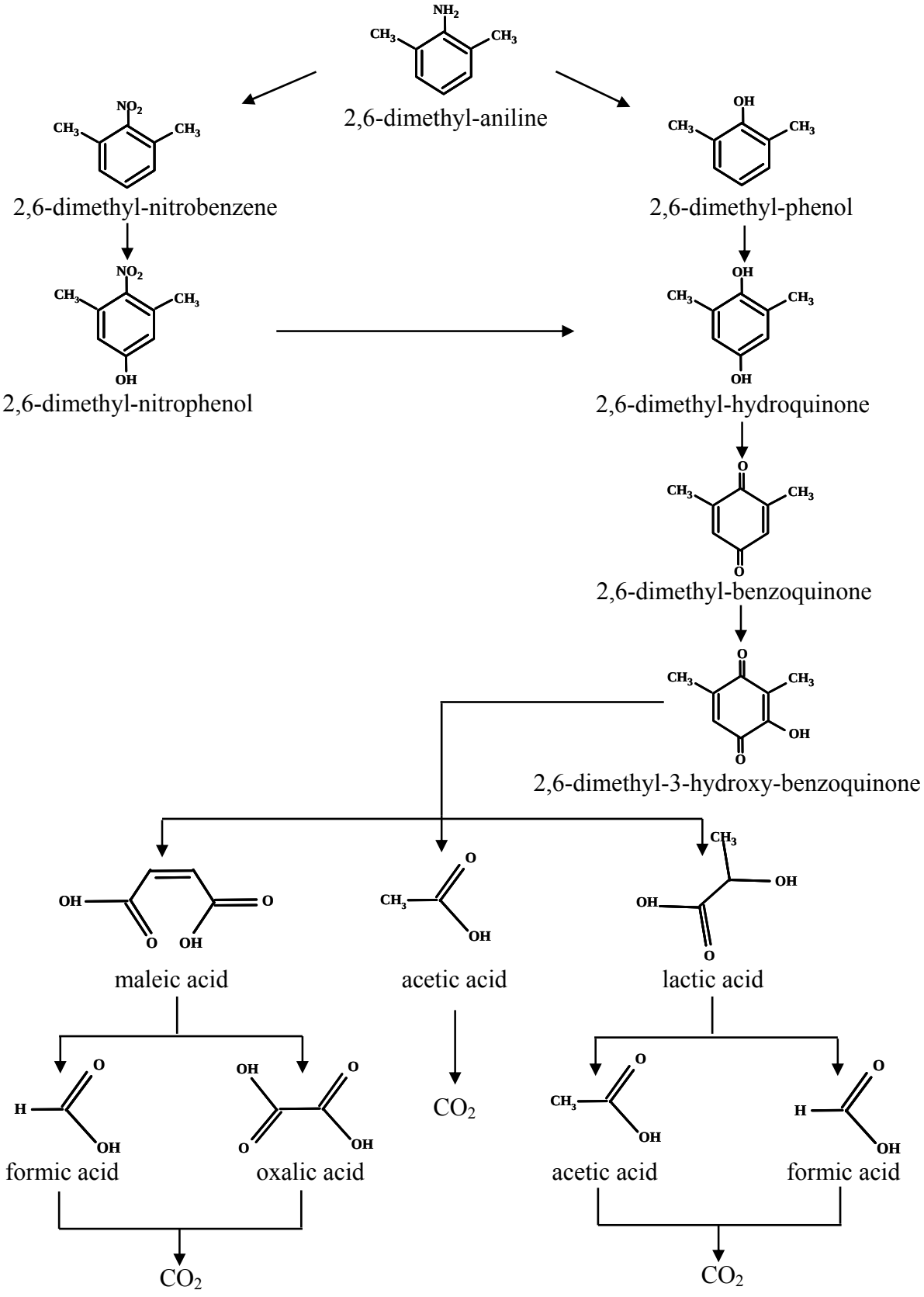

Figure 4.9 Proposed reaction pathway for the mineralization of 2,6-DMA by $OH^{\bullet}$.

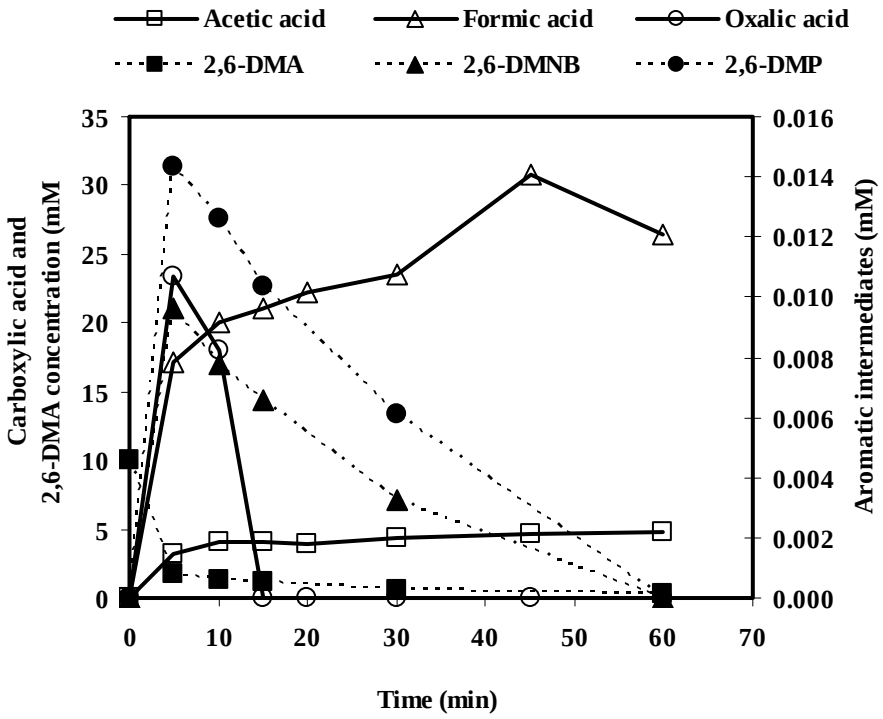

(a) Concentration profile

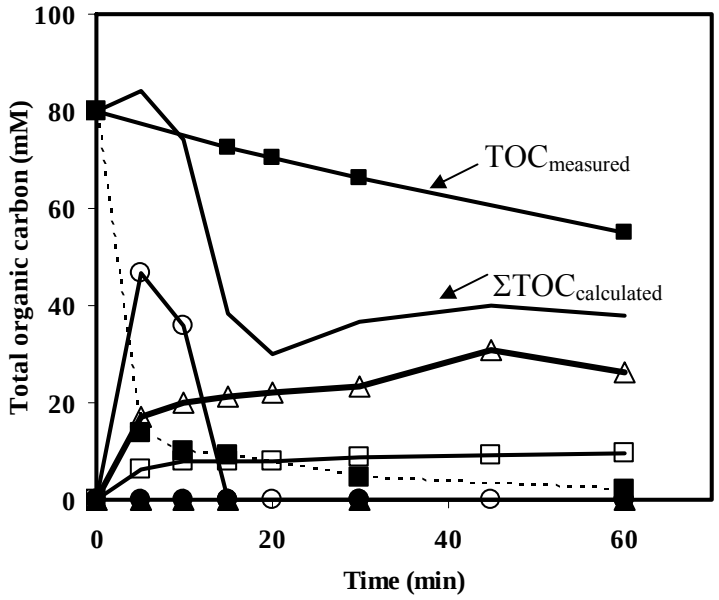

(b) Total organic carbon profile

Figure 4.10 Intermediate products and TOC profiles of 10 mM of 2,6-DMA degradation by Fenton reaction with 10 mM of Fe^{2+} and 200 mM of H_2O_2 at pH 3 and 25 °C.

4.2 Iron Crystallization

4.2.1 Iron Solubility

In this section, the aqueous solubility of Fe^{2+} and Fe^{3+} which are the major iron species in water was determined within the pH range of 2 and 12 with the conditions mentioned in Scenarios I and J. Figure 4.11(a) shows that Fe^{2+} dissolved very well in water when the pH was less than 5 but became less soluble as the pH increased toward pH 12. The precipitation was expected to be in the form of $Fe(OH)_2$.

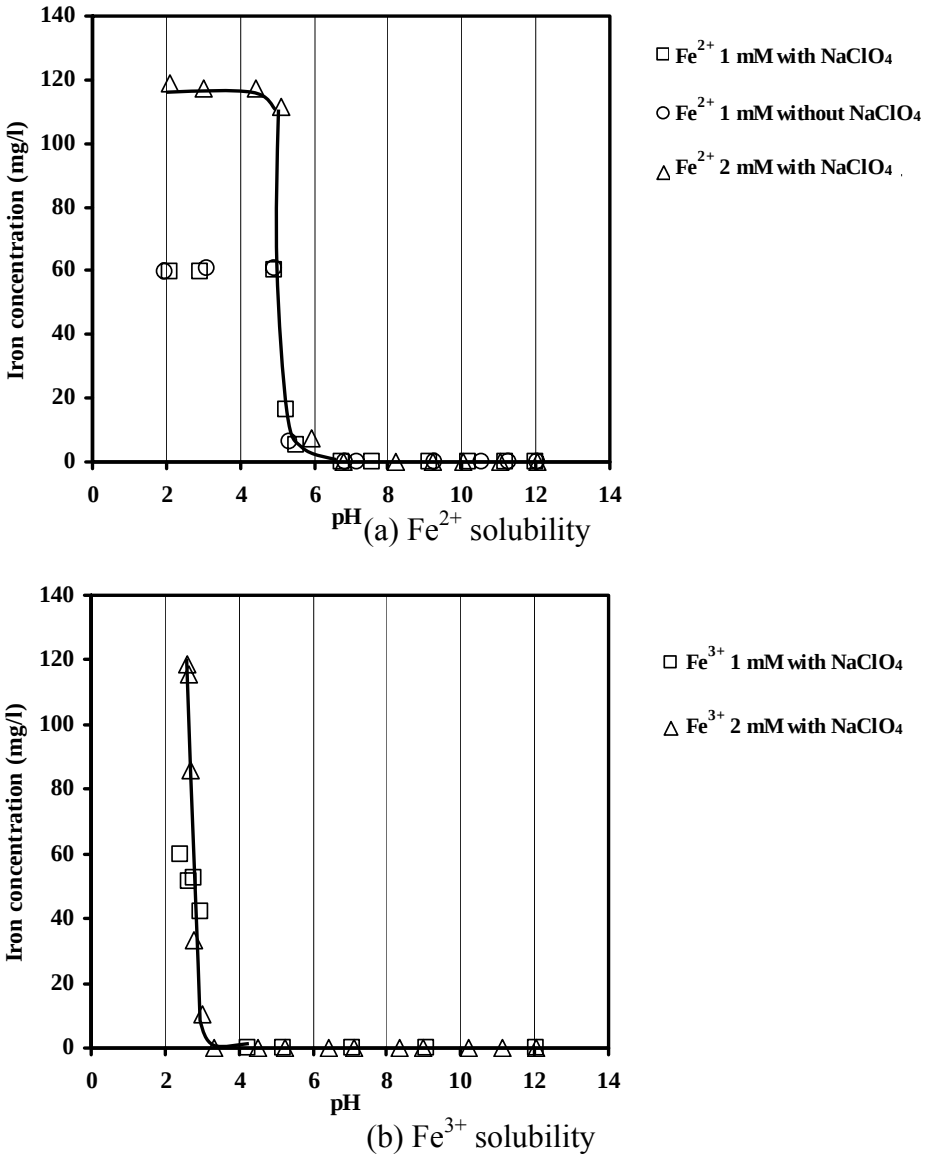

Figure 4.11 Effect of ionic strength and pH on iron solubility at 25°C.

On the other hand, Fe^{3+} which was the product from Fe^{2+} oxidation by H_2O_2 in Fenton reaction was much less soluble than Fe^{2+}, i.e., only 10 mg/l dissolved at pH 3 and became lessen as the pH increased as shown in Figure 4.11(b). These results suggest the Fe^{3+} should continuously precipitate out in the form of $Fe(OH)_3$ during the Fenton reaction at pH greater than 3 since the concentration of Fe^{2+} being used was typically higher than 10 mg/l. These results are in agreement with the theoretical principle as shown in Figure 4.12. The lines which representing the concentrations of various ferric-hydroxo complexes as a function of pH are calculated based on theoretical principle of ferric-hydroxo complexes and ferric hydroxide precipitation at 25°C in ideal solution (neglecting the ionic strength). Details for the calculation are shown in Appendix F. The points were the solubility data observed from the experiments. The difference might be due to the effect of ionic strength in the real solution. The data at pH greater than 3 could not be detected accurately because they were lower than the detection limit of the Phenanthroline method.

In order to ensure that the solid ferric phase precipitated out was $Fe(OH)_3$ rather than other ferric oxide species, a test was performed in the absence of oxygen gas by purging with nitrogen gas during the dissolution and placing into the BOD bottle (Scenario O). The results in Figure 4.13 show that the solubility of Fe^{3+} gradually decreased with time and the soluble Fe^{3+} was approaching the value

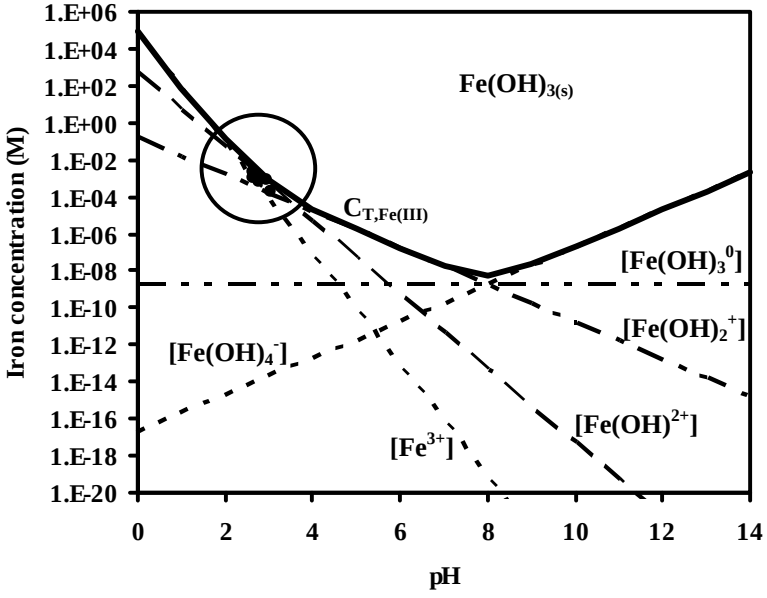

Figure 4.12 Theoretical Fe^{3+} solubility in an ideal solution.

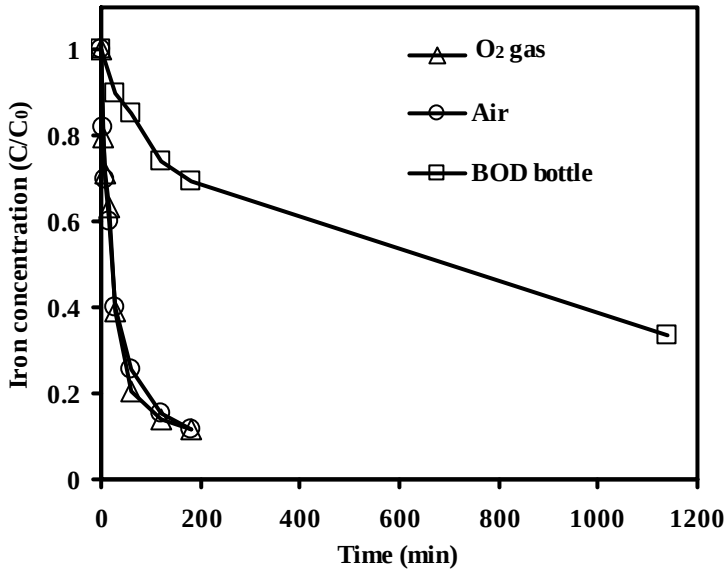

Figure 4.13 Ferric precipitation under different dissolved oxygen levels and turbulence condition (purging with O_2 and air versus stagnant condition in BOD bottle) with the initial conditions as follows: 1 mM of Fe^{3+} at pH 3 and 25°C.

obtained from the solubility test under O_2 gas and air purging (Scenario O) indicating that oxygen did not directly involve in the precipitation process. These iron precipitates should have a potential to crystallize onto the solid particles existing in the fluidized bed reactor under proper environments. Nonetheless, it is important to note that the physical appearance of ferric precipitates at acidic pH was significantly different from those precipitated at neutral pH. At low pH, the solids were dark yellow with discrete particle appearance whereas were orange to red with agglomerate puffy-floc appearance at neutral pH (See Figure A.7). The difference in crystalline structure/color might be due to the pH dependency of the crystalline formation rate. At low pH, the OH^- concentration is very low, resulting in a slower crystallization rate than at high pH where OH^- is dominated. It is very interesting to observe that the color of iron particles in the solution at pH 3 in the BOD bottle gradually changed from dark yellow to orange and red similar to those of pH 7 at the end of 19 hours. This observation supports the statement that the color of the $Fe(OH)_3$ precipitates depends largely on the ripening or aging period of the crystals. According to Stumm and Morgan (1996), there is a metastable zone within which the crystal formation/growth is possible at a lower saturation ratio on a solid surface than in

solution. The crystallization can occur without the concomitant nucleation stage if the solution is seeded with crystallites or foreign particles which could provide their surfaces for nucleation or so called “heterogeneous nucleation”. These differences in solid properties also impacted the crystallization onto fluidized-bed media as will be discussed later.

It is important to note that the iron solutions prepared at pH 2 to 12 would significantly have different ionic strength due to acid/alkaline addition for pH adjustment. The difference in ionic strength might affect the solubility of iron due to activity dissimilarity. As a result, another test (Scenario I) was conducted by buffering the ionic strength of the solutions at different pH with 0.1 M of $NaClO_4$. Figure 4.11(a) shows that the effect of ionic strength on ferrous solubility. Between pH 5.4 and 5.8, the ionic strengths of Fe^{2+} solution with and without $NaClO_4$ were approximately 2.0×10^{-6} (mainly from SO_4^{2-}) and 1.0×10^{-1} M (mainly from Na^+ and ClO_4^-), respectively. It can be seen that the effect was diminutive and could be neglected even though the ionic strengths of these solutions were almost 50 times different. This was possible due to the accuracy of the phenanthroline method at very low Fe^{2+} concentration; i.e., the remaining Fe^{2+} concentration might be lower than the detectable limit for 1 cm light path. Nonetheless, the ionic strength of the solution was buffered by 0.1 M $NaClO_4$ in the case of Fe^{3+} solubility test.

4.2.2 $Fe(OH)_3$ Crystallization in Fluidized-bed Reactor

In this part (from Scenario K), Fe^{3+} was precipitated out in the form of $Fe(OH)_3$ at pH 7 in the absence of H_2O_2 to simulate the neutralization condition after Fenton treatment. Under this condition, the concentration product of Fe^{3+} and OH^- was much higher than the solubility product of $Fe(OH)_3$ implying a supersaturated solution. It was very interesting to found that $Fe(OH)_3$ very poorly crystallized onto the fluidized media including SiO_2, Al_2O_3, and CS as shown in Figure 4.14. It is believed that the formation of $Fe(OH)_3$ at pH 7 is very rapid; hence, the mechanism mainly followed the homogeneous crystallization rather than the heterogeneous crystallization. $Fe(OH)_3$ cluster or nucleus was rapidly formed from the supersaturated solution and serving as nuclei for further material deposition to

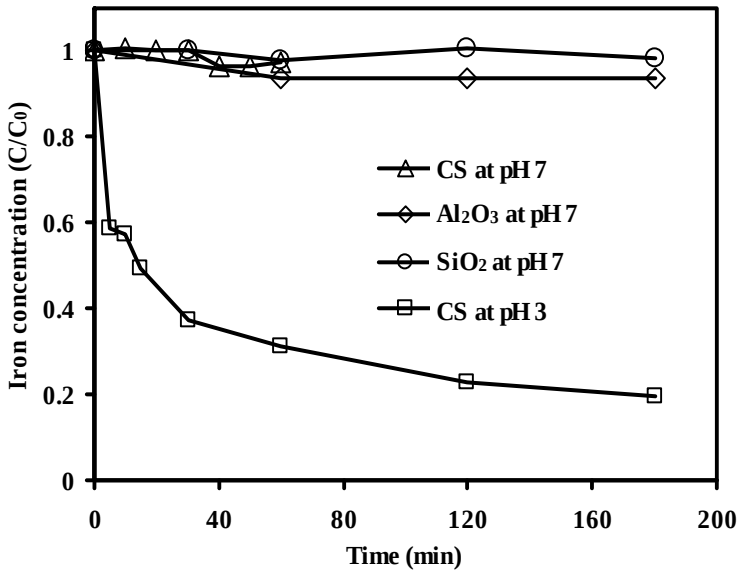

Figure 4.14 Effect of pH and fluidized-bed material on total iron removal with the initial conditions as follows: 1 mM of Fe^{3+}, 230.77 g/l of media at 25 °C.

form crystallites which sequentially ripening to form crystals. The role of fluidized-bed media was minute by the overwhelmingly nucleus formation. In other word, the $Fe(OH)_3$ crystals could be effectively formed and grown by themselves without foreign solids. This suggests that crystallization of iron in fluidized-bed Fenton process could not performed rapidly and effectively after neutralization. In order to verify this hypothesis, Fe^{3+} solution at pH 3 was circulated in the FBR with construction sands under the same operating conditions. The result revealed that iron could efficiently crystallize onto the sand surface with the removal efficiency of 78% in 3 hours. At pH 3, the OH^- concentration was 10^4 times lower than at pH 7; hence, the precipitation occurred within the metastable zone where foreign particles could effectively stimulate the crystallization by providing their surface for heterogeneous nucleation.

4.2.3 $Fe(OH)_3$ Crystallization in Fluidized-bed Fenton Process

From previous section, it was found that Fe^{3+} could effectively crystallize onto the sand surface at pH 3. This section investigated into more details by simulating the real fluidized-bed Fenton process (Scenario L). Fe^{2+} and H_2O_2 were added

simultaneously into the FBR with either CS or SiO_2 serving as the fluidized materials at pH 3. In this scenario, the experiment with CS was duplicated to determine the reliability and repeatability of the experimental setup and procedure. It can be seen from Figure 4.15 that these two duplicated runs provided very close results which implied that the experimental setup and procedure were reliable and accurate. Regarding on the type of fluidized material, it was found that the iron crystallization onto the CS was faster than onto the SiO_2 even though the iron removal efficiencies at 180 minutes were comparable. This may be due to the impurity on the CS surface and/or surface property of the CS. To verify this hypothesis, CS with different size distribution, i.e., passing sieve #30 but retained on sieve #40 (0.42 mm < ϕ < 059 mm) versus passing sieve #30 (ϕ < 059 mm), were tested and the results were shown in Figure 4.15. It can be seen that the iron crystallization rate and efficiency of both sets were comparable indicating that the size of CS did not have any significant impact on iron crystallization under the studied conditions. It is well documented that most of Fe^{2+} is simultaneously transformed to Fe^{3+} after the initiation of the Fenton reaction. Data from this study confirmed with this statement as shown in the Table D.30, i.e., Fe^{2+} disappeared instantly within the first 5 minutes to form Fe^{3+}. Most of

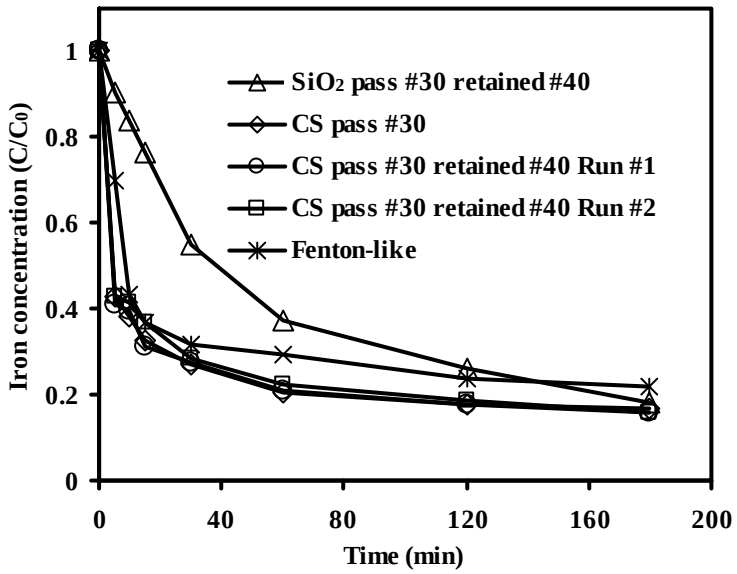

Figure 4.15 Total iron removal in the fluidized-bed Fenton process with various solid materials and sizes with the initial condition as follows: 1 mM of Fe^{2+} or Fe^{3+}, 20 mM of H_2O_2, 230.77 g/l of media at pH 3 and 25 °C.

Fe^{3+} being formed precipitated out and sequentially crystallized onto the CS surface leaving only a small portion of soluble Fe^{3+} in the solution as representing by the soluble iron concentration. It is also interesting to observe that iron reduction in the Fenton-like process with 1 mM Fe^{3+} and similar H_2O_2 concentration was comparable to those of Fenton process as shown in Figure 4.15. This implies that H_2O_2 did not play a major role on iron crystallization, instead the species of iron and its precipitation/crystallization environment primarily controlled the crystallization process.

4.2.4 Effect of $Fe(OH)_3$ Crystallites

To better understand the crystallization mechanism occurred in the fluidized-bed Fenton process, a set of experiment was performed. Fenton reaction was allowed to proceed in a completely mixed reactor (CMR) in the absence of sand for 60 minutes before switching to the fluidized-bed reactor using CS as the media (Scenario M). By doing this, significant amount of $Fe(OH)_3$ crystallites should be formed prior to contact with sand whereas in real fluidized-bed reactor, the $Fe(OH)_3$ nuclei were formed and simultaneously contact with sand. The results for 1 mM of Fe^{2+} and 20 mM of H_2O_2 were shown in Figure 4.16(a) indicating that the crystallization rate was faster in the real fluidized-bed reactor than in the 1-hr pre-CMR+FBR run although the iron removal efficiencies were comparable. As the iron content increased from 1 mM to 2 and 3 mM (Scenario N), the crystallization rate in the 1-hr pre-CMR+FBR mode became worsen and worsen, respectively, when compared to those of real FBR mode as shown in Figures 4.16(b) and 4.16(c). This is because the formation of the crystallites and crystals became ripened and ripened as the iron concentration increased resulting in more homogeneous crystallization than heterogeneous pathway. This implies that newly formed nuclei could adsorb and crystallize onto the sand surface more rapidly and effectively than the matured crystallites. To determine the impact of ripening time on crystallization, another experiment was performed in the CMR for 5 minutes before switching to the fluidized-bed reactor and the results are shown in Figure 4.16(c). As compared to the 1-hr pre-CMR+FBR, it was found that

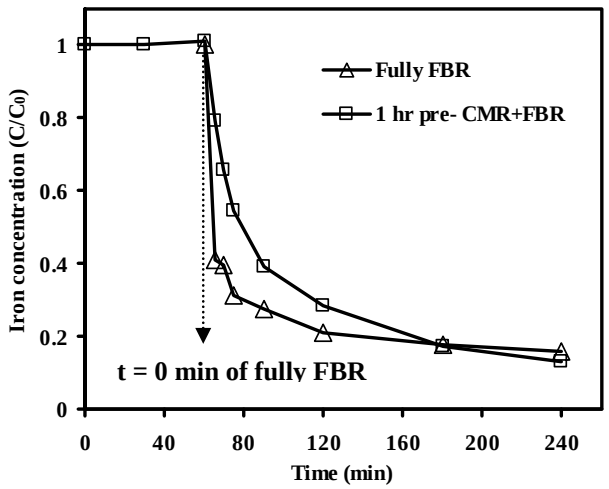

(a) Fe^{2+} 1 mM +H_2O_2 20 mM

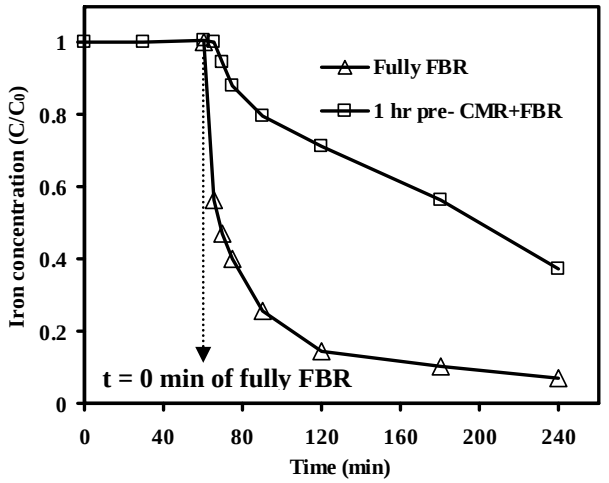

(b) Fe^{2+} 2 mM +H_2O_2 40 mM

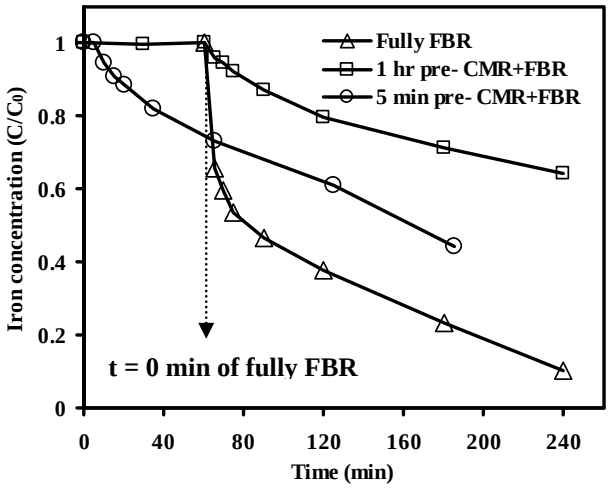

(c) Fe^{2+} 3 mM +H_2O_2 60 mM

Figure 4.16 Comparison between fully FBR and pre-CMR+FBR operations on total iron removal with the initial conditions as follows: 230.77 g/l of CS at pH 3 and 25°C.

the crystallization rates were comparable indicating that the ripening step happened very fast and should mainly depend on iron concentration. The results from this part suggest that for crystallization optimization in field practice, the crystallization should begin as soon as possible in the fluidized-bed reactor.

4.2.5 Effect of Iron Concentration

As mentioned earlier, the crystallization onto the sand surface or heterogeneous crystallization will occur primarily within the metastable zone. Thus, to optimize the iron removal performance, a low saturation ratio on a solid surface has to be maintained. Therefore, it can be expected that when the iron content increases, the solution would move toward intense supersaturated condition since the concentration product would be much higher than the solubility product of the concerned solid phase. The results of this part (Scenario N) are summarized in Figure 4.17. It can be seen that total iron remaining at 180 minutes was quite constant regardless on initial iron concentration. This observation is understandable since the solubility of $Fe(OH)_3$ was mainly controlled by the solution pH. Since the pH was maintained constantly at 3.0, the soluble iron should also be constant at the equilibrium as governed by the solubility product. In addition, the soluble irons at 30 minutes of all three runs were almost the same regardless on initial iron concentration. This implies that the rate of crystal growth increased as the initial iron increased from 1 mM to 2 and 3 mM, respectively. This observation was opposite to those in the study of pH effect even though both scenarios increased the degree of supersaturation of the $Fe(OH)_3$, i.e., increased Fe^{3+} and OH^- concentration, respectively. This is because in this part the iron concentration was increased only 3 times as compared to an increase of 10^4 times in OH^- concentration when pH increased from 3 to 7. In addition, according to the solubility product formula, OH^- concentration has the power of three whereas the Fe^{3+} has only the power of one; hence, the influence of OH^- concentration is much more drastic than those of Fe^{3+}. The phenomenon happened in the FBR was similar to those in the case of 1-hr pre-CMR before FBR (Scenario N) as shown in Figure 4.18. The soluble irons at 30 minutes for all three

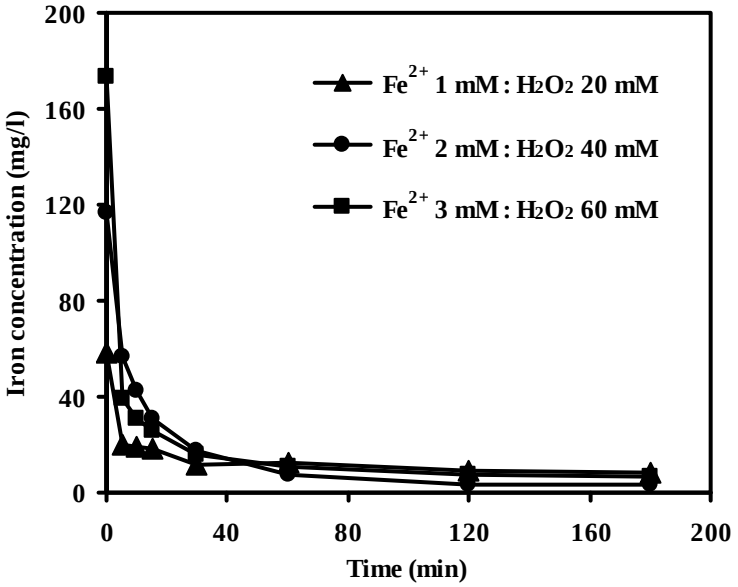

(a) Soluble iron

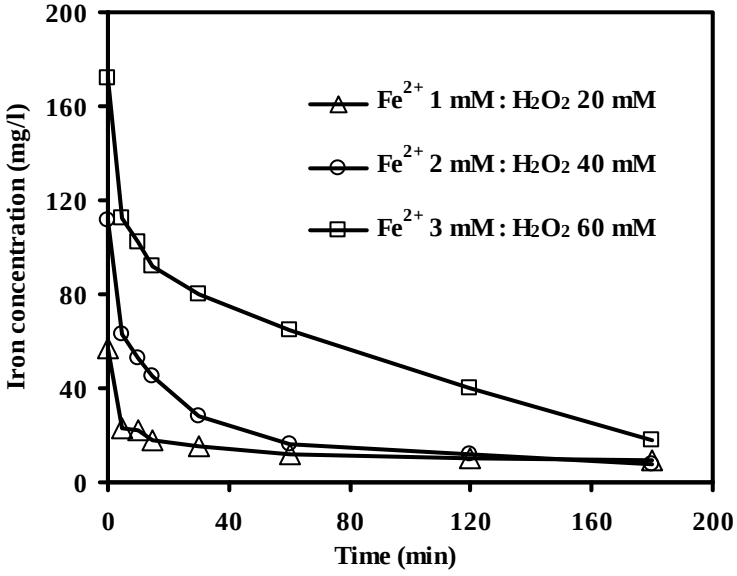

(b) Total iron

Figure 4.17 Effect of Fe^{2+} concentration on iron removal in the fluidized-bed Fenton process under constant Fe^{2+}:H_2O_2 ratio scenario with the initial conditions as follows: 230.77 g/l of CS at pH 3 and 25°C.

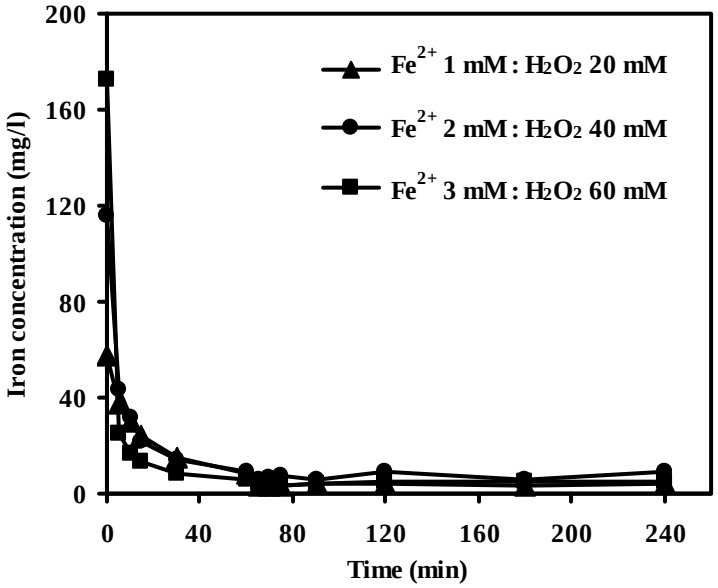

(a) Soluble iron

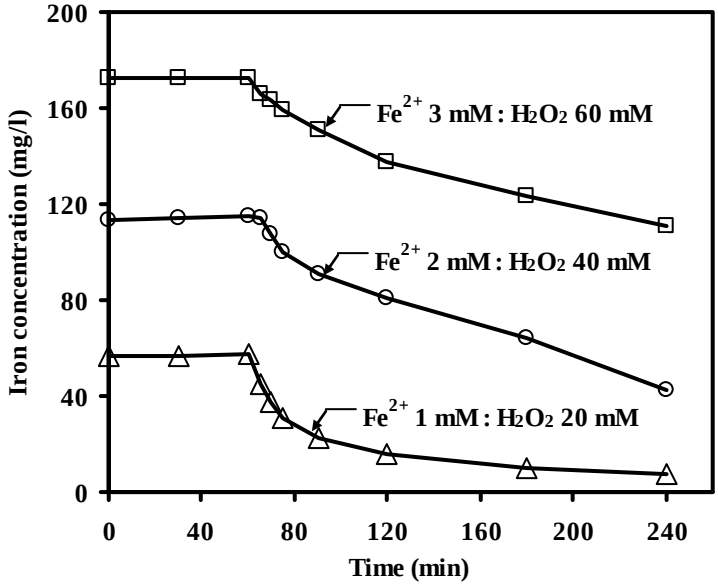

(b) Total iron

Figure 4.18 Effect of Fe^{2+} concentration on iron removal in the 1-hr pre-CMR+FBR under constant Fe^{2+}:H_2O_2 ratio scenario with the initial conditions as follows: 230.77 g/l of CS at pH 3 and 25°C.

initial iron concentrations were comparable indicating that the rate of crystal growth also increased with iron concentration.

4.2.6 Effect of Turbulence

After the nucleation process (i.e., the initial formation of solid nuclei), spontaneous growth of crystal will occur. The attachment of a molecule/nucleus to another nucleus to form a solid lattice which includes the transportation of materials to the surface of these nuclei and surface deposition will become very important and should follow the mechanism of solid-solution interface at the molecular level. To understand the mechanism of iron crystallization, a set of experiment was performed. Ferric solution at 1 mM was prepared at pH 3 and vigorously purging with either air or O_2 (Scenario O). The results show that soluble iron decreased at the same pace for both conditions as shown in Figure 4.19. In addition, the reduction of soluble iron in

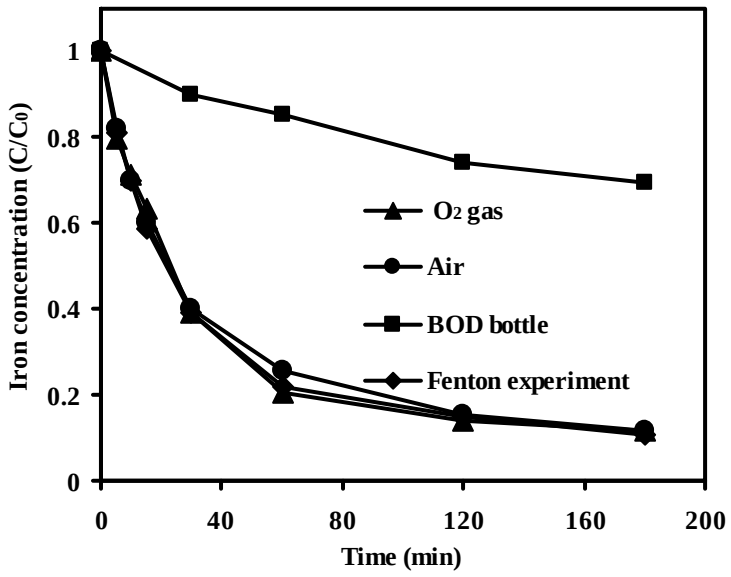

Figure 4.19 Ferric precipitation under turbulence condition by purging with O_2 and air, and stagnant condition in BOD bottle (replotted of Figure 4.13 for 180 minutes) with the initial conditions as follows: 1 mM of Fe^{3+} at pH 3 and 25°C as compare to those in Fenton experiment with the initial conditions as follows: 1 mM of Fe^{2+}, 20 mM of H_2O_2 at pH 3 and 25°C.

the Fenton experiment performed in a beaker with sufficient mixing with Fe^{2+} concentration of 1 mM also followed the similar pattern. It is important to note that Fe^{2+} should be rapidly transformed to Fe^{3+} by Fenton reaction (measured residual Fe^{2+} was negligible). However, if in the stagnant environment where no mixing was provided (1 mM Fe^{3+} solution in the BOD bottles and sacrificed one bottle per sampling), the soluble iron decreased very slowly as seen in Figure 4.19. These results indicated that when the mixing was sufficiently provided, the agglomeration of nuclei resulting in the crystal growth was similar regardless on mixing type and the oxygen gas did not chemically involved in the process. It is interesting to observe that the iron profiles in Figure 4.19 did not show a linear relationship implying that the crystallization process was not controlled by surface reaction as mentioned in Section 2.6.3. Further analysis to verify the effect of molecular transport on the crystal growth by constructing a relationship between iron concentration and the square root of time (plot of C vs $t^{1/2}$) was shown in Figure 4.20(a). It can be seen that only the data from the BOD-bottle experiment under a stagnant condition had a linear relationship. This indicates that the molecular/nucleus diffusion step controlled the crystallization process in this case whereas was not the rate-limiting step under the turbulence condition (either in the O_2-supplied, air-supplied, or Fenton experiment). This was understandable since the mixing would homogenize the iron oxide molecules in the solution and eliminate the concentration gradient at the molecular/nucleus level. To determine the real mechanism other than the molecular/nucleus diffusion and surface reaction which controlling the crystallization process under turbulence condition, another plot of the reciprocal iron with time following the second-order kinetics (plot of 1/C vs time) was constructed as shown in Figure 4.20(b) and found to have the linear relationship for all cases. Hence, the crystallization was controlled by the transport/ collision of the crystallites/ crystals in the mixture via colloidal behavior. In addition, the crystallization should be controlled by orthokinetic flocculation in the case of turbulence environment whereas by perikinetic flocculation in the case of stagnant environment. This conclusion was in agreement with previous observation that the molecule/ nucleus transport was also the rate-controlled step under the stagnant environment. This is because the perikinetic flocculation will become more predominant as the size of colloids is smaller.

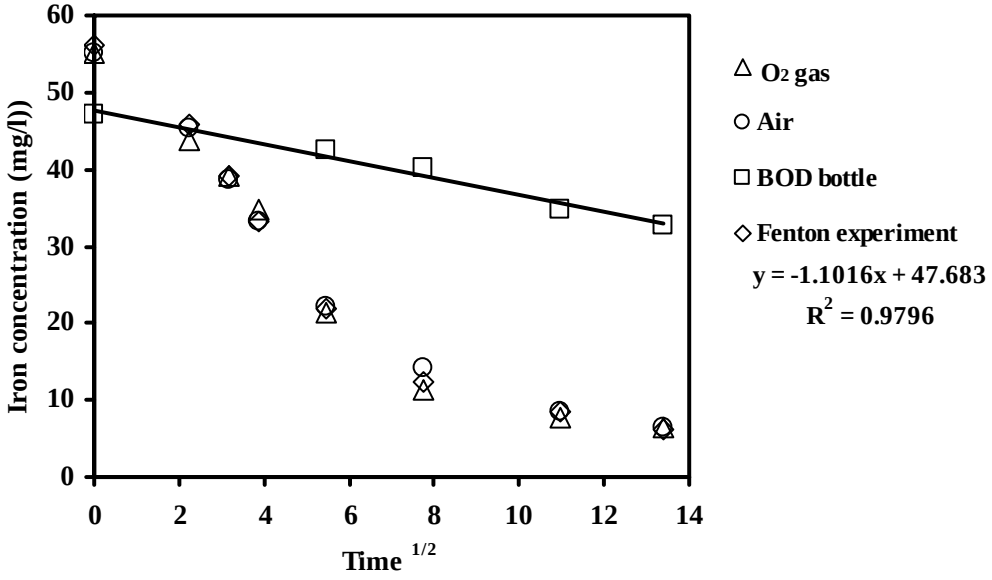

(a) Molecular transport control

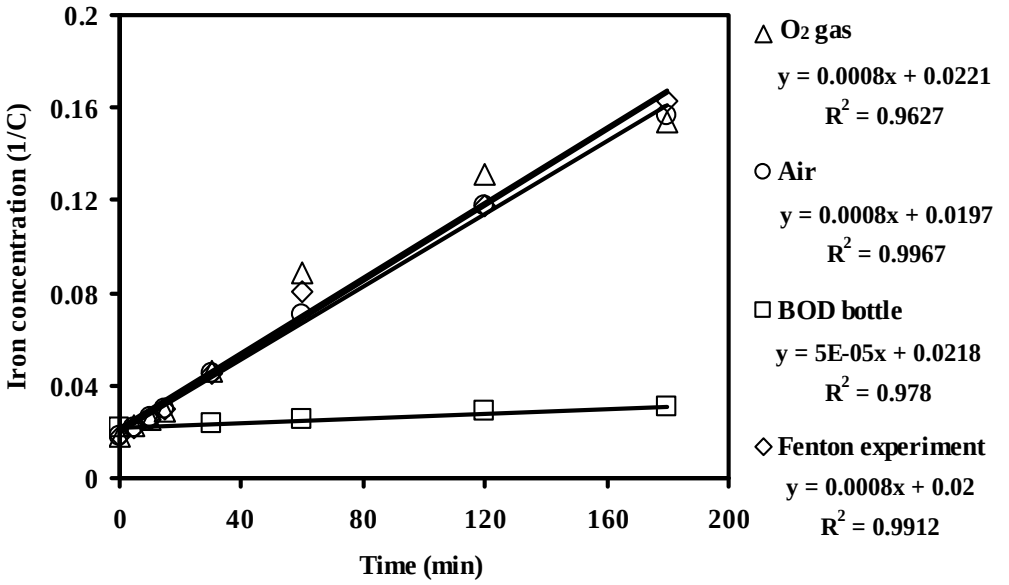

(b) Crystallite transport control

Figure 4.20 Determination of the rate-limiting step controlling the crystallization process.

4.2.7 Effect of Organic Compounds

Some organic intermediates from $OH^{\bullet}$ oxidation such as oxalic acid can significantly form complex with ferric ion. These ferro-organic complexes will increase the solubility of iron in the system and sequentially deteriorate the iron crystallization process. To verify the effect of ferro-organic complexes on iron crystallization, oxalic, acetic, and formic acids which have been identified as the intermediates from 2,6-DMA oxidation in Section 4.1.5 were added into the Fe^{3+} solution at pH 3 to determine Fe^{3+} solubility (Scenario P). The data as shown in Figure 4.21 indicating that the solubility of Fe^{3+} significantly increased in the presence of volatile fatty acids and as a result the crystallization of iron on the CS became minimal. The results from this part supported with the hypothesis mentioned above. In addition, the experiments under true fluidized-bed Fenton process also confirmed with this observation. Figure 4.22 shows that iron removal was the best in the absence of organic matters followed by in the presence of 0.1 and 1.0 mM of both 2,6-DMA and AN, respectively. It is very interesting to observe a re-emerging of total iron in the experiment with 1.0 mM organics, i.e., total iron decreased considerably in

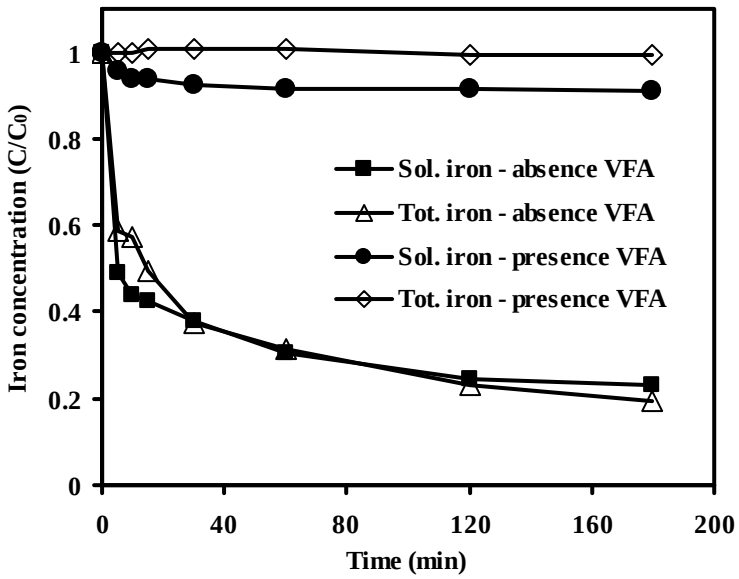

Figure 4.21 Effect of organo-ferric complex on iron crystallization in FBR with the initial conditions as follows: 1 mM of Fe^{3+}, 230.77 g/l of CS at pH 3 and 25°C, VFA consisted of 2 mM of formic acid, 0.5 mM of acetic acid and 2 mM of oxalic acid.

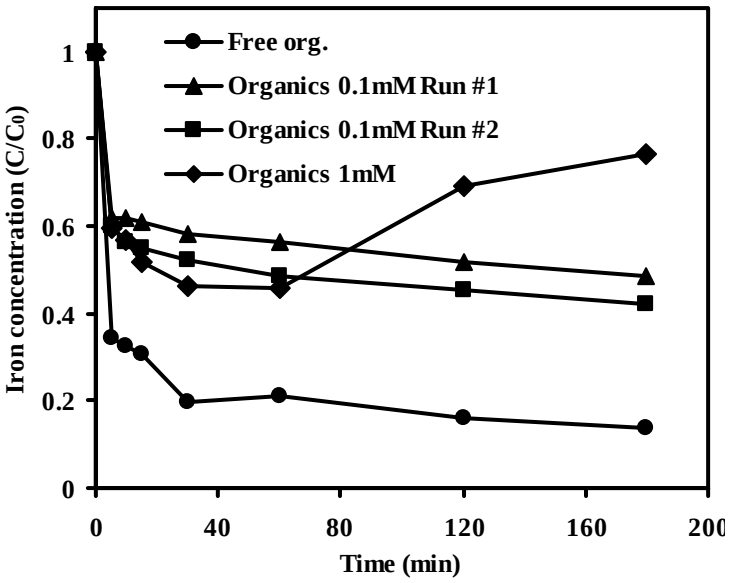

(a) Soluble iron

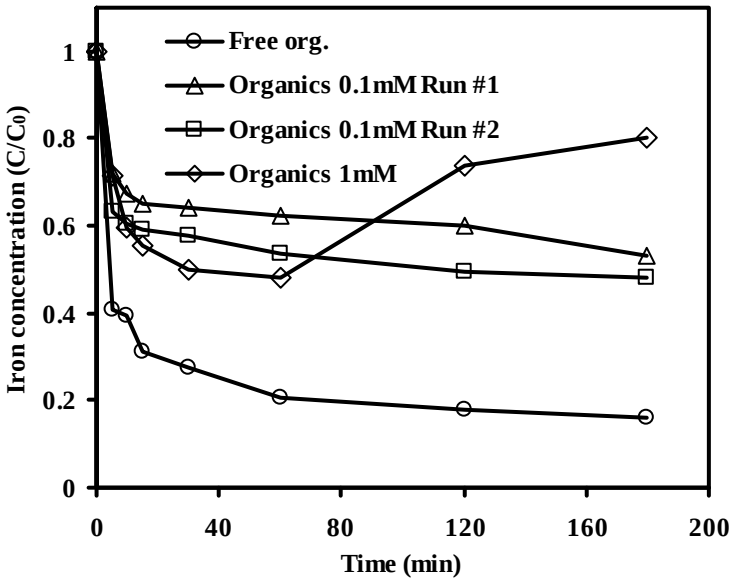

(b) Total iron

Figure 4.22 Effect of organo-ferric complex on iron crystallization in fluidized-bed Fenton process in the presence of 2,6-DMA and AN with the initial conditions as follows: 1 mM of Fe^{2+}, 20 mM of H_2O_2, 230.77 g/l of CS at pH 3 and 25°C.

the first 60 minutes but increased again afterward. This can be explained that after 60 minutes, the volatile fatty acids such as oxalic acid were generated which could form complex with ferric and increased the solubility of ferric in the solution. If the Fenton reaction was allowed to proceed for 1 hour before the FBR started (1-hr pre-CMR+FBR), it still observed the similar trend as in the case of FBR, i.e., the iron could be removed most efficiently in the absence of organics followed by 0.1 and 1.0 mM of both 2,6-DMA and AN, respectively. Another interesting point regarding on the effect of organics is the comparison between fully FBR and 1-hr pre-CMR+FBR as shown in Figures 4.23 and 4.24. These 2 runs were carried out under the same conditions except for the 1-hr pre-CMR+FBR allowed the Fenton reaction to proceed in a batch reactor for 1 hour before switching to FBR mode. In this manner, 2,6-DMA and AN were more completely transformed to several products including the ferric-complexable species. Hence, very limited iron was crystallized onto the sand surface. On the other hand, when the system was operated in fully FBR mode, it can be seen that total iron decreased in the first 60 minutes due to crystallization onto sand surface; however, as the reaction period proceeded, the ferric-complexable organics were formed and sequentially deteriorated the crystallization process. Observing from the trend, it can be expected that the total iron would continuously increased and eventually should be at the same level as in the case of 1-hr pre-CMR+FBR. The results from this part are very valuable for FBR operation. It implies that the removal of iron via crystallization will be promising if the Fenton reaction could remove most of the volatile fatty acids. Or in other word, iron removal will follow the organic removal efficiency. It also implies that fluidized-bed Fenton process is suitable for diluted wastewater or using for the polishing purpose. By this way, the process will be very effective for both pollutant and iron removals

4.2.8 Reusability of Iron-coated Construction Sand for Iron Crystallization

This part aimed to evaluate the capability of CS to serve as media for iron crystallization in the fluidized-bed Fenton process (Scenario Q). The iron crystallization was performed for 101 cycles and the results are shown in Figure 4.25.

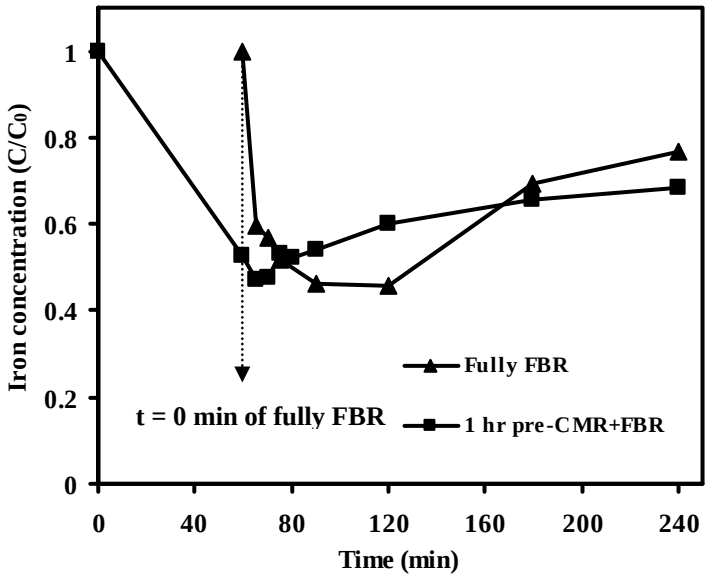

(a) Soluble iron

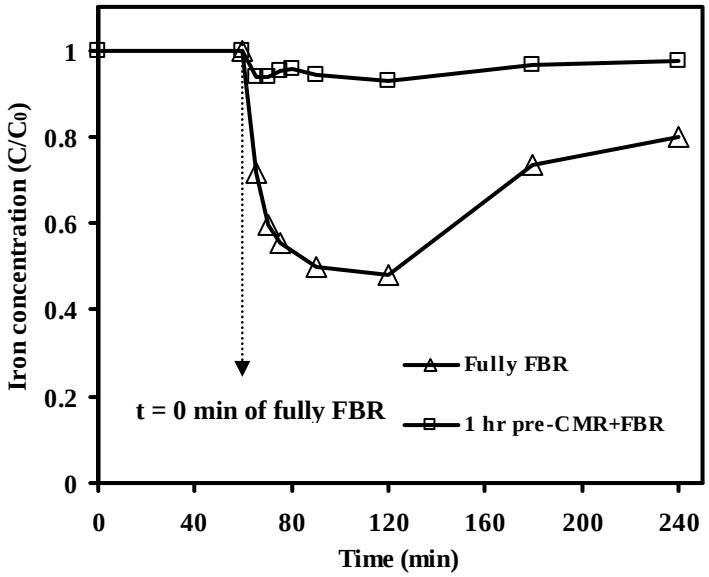

(b) Total iron

Figure 4.23 Effect of organo-ferric complex on iron crystallization of 1 mM of 2,6-DMA and 1 mM of AN with the initial conditions as follows:, 1 mM of Fe^{2+}, 20 mM of H_2O_2, 230.77 g/l of CS at pH 3 and 25°C.

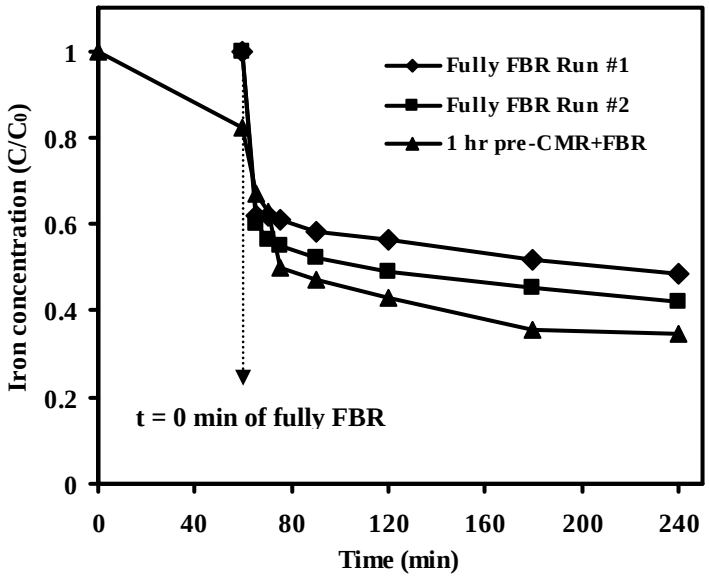

(a) Soluble iron

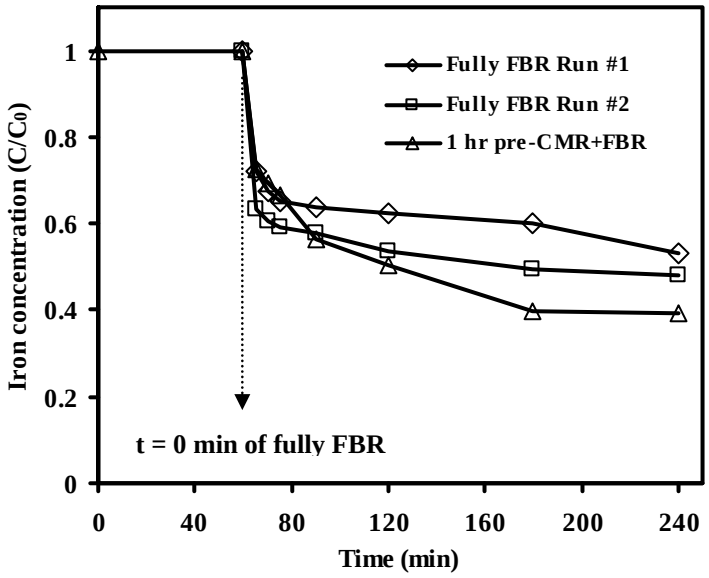

(b) Total iron

Figure 4.24 Effect of organo-ferric complex on iron crystallization of 0.1 mM of 2,6-DMA and 0.1 mM of AN with the initial conditions as follows: 1 mM of Fe^{2+}, 20 mM of H_2O_2, 230.77 g/l of CS at pH 3 and 25°C.

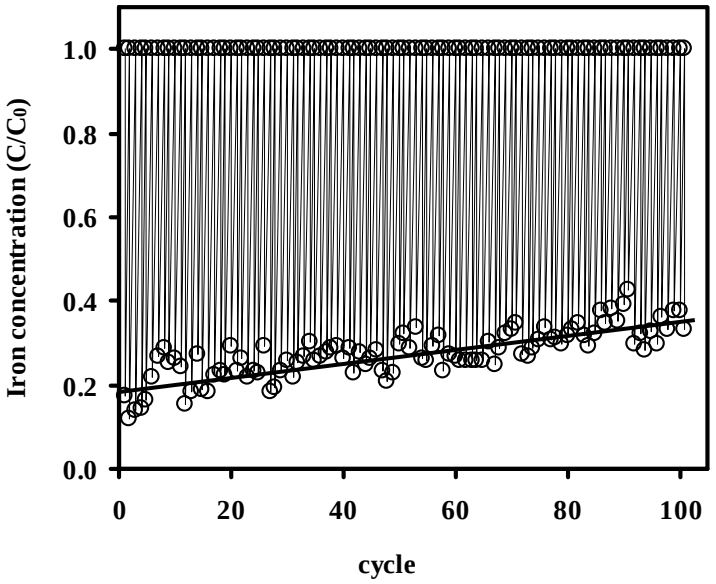

Figure 4.25 Reusability of iron-coated CS for iron crystallization with the initial conditions as follows: 230.77 g/l of CS, pH 3 at 25°C and 1 mM of Fe^{2+} and 20 mM of H_2O_2 for cycle 1 to 5 and 2 mM of Fe^{2+} and 40 mM of H_2O_2 for cycle 6 to 101.

It can be seen that the iron crystallization efficiency in 1 hour decreased gradually from 80% in the first cycle to 65% in the 101st cycle. This is believed to be due to the decreasing in the crystallization rate of iron crystallites onto the interaction sites on the iron-coated CS as the $Fe(OH)_3$ accumulating on the surface. Exhaustion of effective sites for crystallization was not believed to be the main cause because the reduction in iron still proceeded after 3 hours as shown in the profile plot of the 101st cycle as compared to the first cycle (Figure 4.26). It is very interesting to observe that the reduction of soluble iron in the 101st cycle was more rapid than those in the first cycle whereas the reduction of total iron turned to the opposite direction. This implies that the $Fe(OH)_3$ coated on the CS could somehow accelerate the formation of iron nuclei and crystallites; however, retard the crystallization rate of those crystallites onto the sand surface. The results from this part reveal that the iron crystallization performance in the real fluidized-bed Fenton reactor will be gradually deteriorated or decelerated with time. Hence, to maintain the high iron removal performance, it is wisely to continuously and constantly replace a portion of iron-coated CS in the FBR with the similar amount of fresh CS. To characterize the iron oxide coated on the CS surface, the 101st-cycle CS sample was analyzed by the XRD analyzer to determine

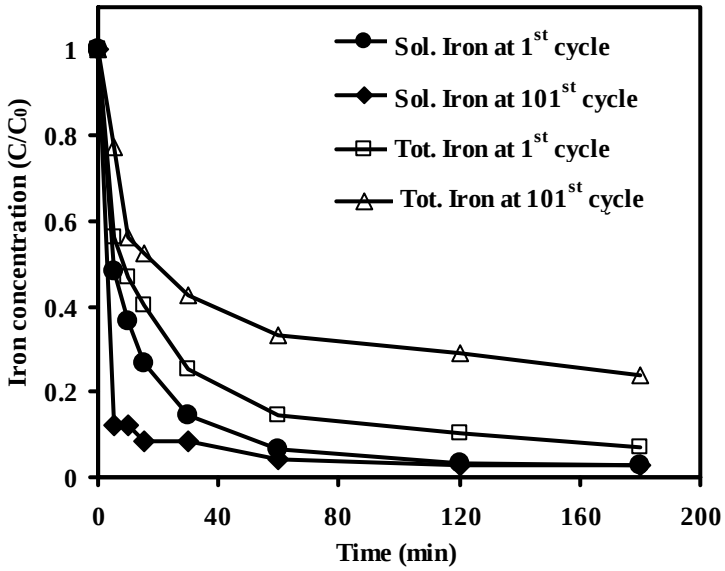

Figure 4.26 Comparison of iron profile between the 1st- and 101st –cycles with the initial conditions as follow: 2 mM of Fe^{2+}, 40 mM of H_2O_2, 230.77 g/l of CS at pH 3 and 25°C.

the iron oxide species coated on the surface. The result from XRD analysis as shown in Figure 4.27 revealed that only SiO_2 was detected. According to the calculation of iron removal from aqueous phase, the amount of iron coated on the CS surface should be more than 3.5% by weight and its catalytic activity was observed as will be discussed in the next part. Physical appearance between fresh CS and the 101st-cycle iron-coated CS was very distinguished from each other as shown in Figures A5 and A6, respectively. Despite of that, it can be expected that the iron oxide coated on the surface of CS should be $Fe(OH)_3$ since the results from the solubility study were consistent with the values calculated based on the presence of $Fe(OH)_3$ precipitates. In addition, Homanee (2005) characterized the iron oxide which crystallized on the SiO_2 in the fluidized-bed Fenton process at pH 6.5 within 5 hr and found to be $Fe(OH)_3$.

4.2.9 Catalytic Activity of Iron-coated Construction Sand

Iron oxides in various forms are believed to have catalytic activity which can stimulate H_2O_2 decomposition to generate $OH^{\bullet}$. The objective of this part was to

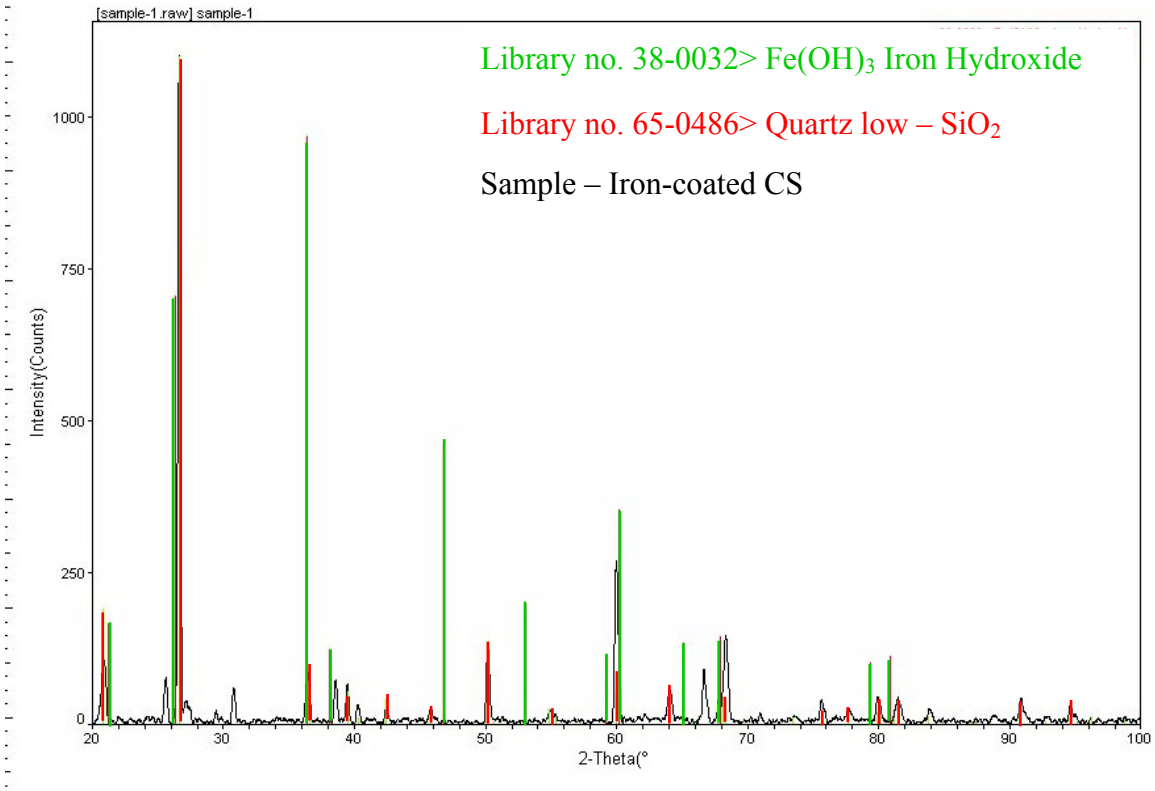

Figure 4.27 XRD analysis of the 101st-cycle iron-coated CS.

determine the catalytic activity of iron-coated CS and compare with those of commercial goethite (Scenario R). The results show that the 75 g of the 101st-cycle iron-coated CS had the catalytic activity approximately equivalent to 3 g of goethite in terms of AN and 2,6-DMA oxidations as shown in Figure 4.28. It is important to note that goethite had higher BET surface than iron-coated CS (8.63 versus 13.51 m^2/gm) which might affect the catalytic activity of these two iron oxides since the reactions involved surface interaction. In spite of surface difference, other factors such as iron oxide species should have more impact on the catalytic activity since the difference in surface area between these two iron oxides was only 1.6 time but the difference in reactivity was enormous, i.e., 75 g/l of iron-coated CS could remove only 30 and 40% of 1 mM of AN and 2,6-DMA, respectively, at 180 minutes whereas the same amount of goethite could completely remove both compounds in just 15 minutes. It was well documented that $Fe(OH)_3$ has much lower catalytic activity than goethite and this should be the main contribution to poorer performance of the 101st-cycle iron-coated CS as compared to goethite (α-FeOOH).

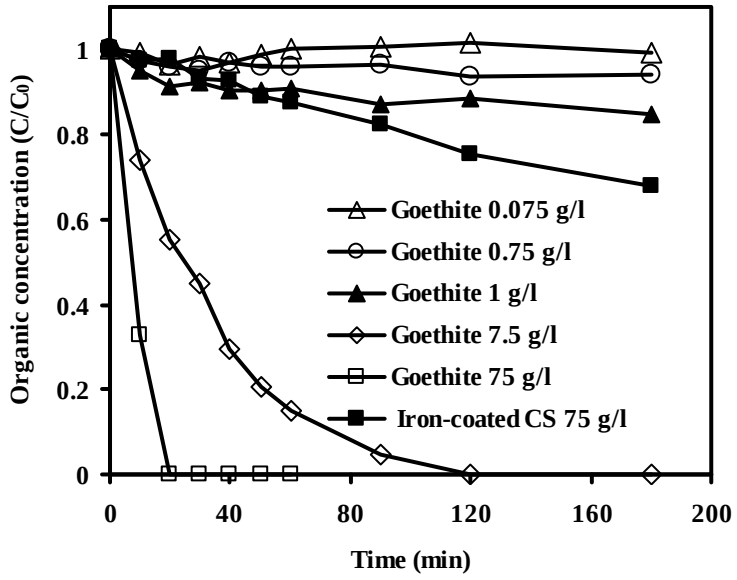

(a) Aniline

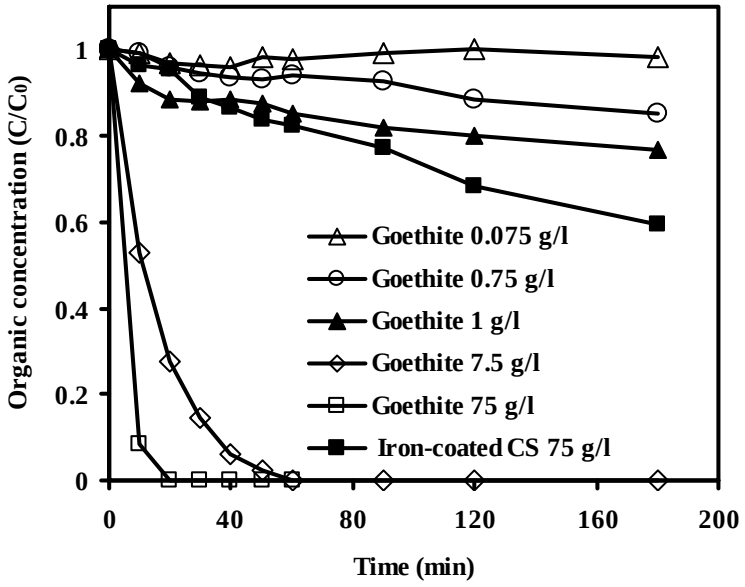

(b) 2,6-DMA

Figure 4.28 Catalytic activity of iron-coated CS on organic degradation in heterogeneous Fenton process as compare to commercial goethite with the initial conditions as follows: 1 mM of 2,6-DMA, 1 mM of AN, 20 mM of H_2O_2 at pH 3 and 25 °C.

Certain amounts of iron in the forms of Fe^{2+} and Fe^{3+} were leaching out into the mixture as shown in Figure 4.29 indicating that the reductive dissolution of iron oxide also happened in the mixture as suggested by Lu (2000). Nonetheless, further analysis for the determination of the rate constant between 2,6-DMA and $OH^{\bullet}$ by using competitive rate kinetics with AN as a reference compound as shown in Figure 4.30 (as an example plot) provided the slope, which is the ratio of $k_{2,6\text{-DMA}}$ to k_{AN}, of 1.2725. This value was significantly different from the average of 3.5462 obtained from previous part where Fe^{2+} was added as illustrated in Section 4.1. This indicates that the degradation mechanism of 2,6-DMA and AN in the heterogeneous Fenton reaction was different from those in homogeneous Fenton reaction. As proposed by Lin and Gurol (1998), the decomposition of H_2O_2 occurred at the iron oxide surface. Hence, the oxidation of 2,6-DMA and AN in the heterogeneous Fenton reaction might involve the surface reaction resulting in different apparent rate constant from those of homogeneous reaction.

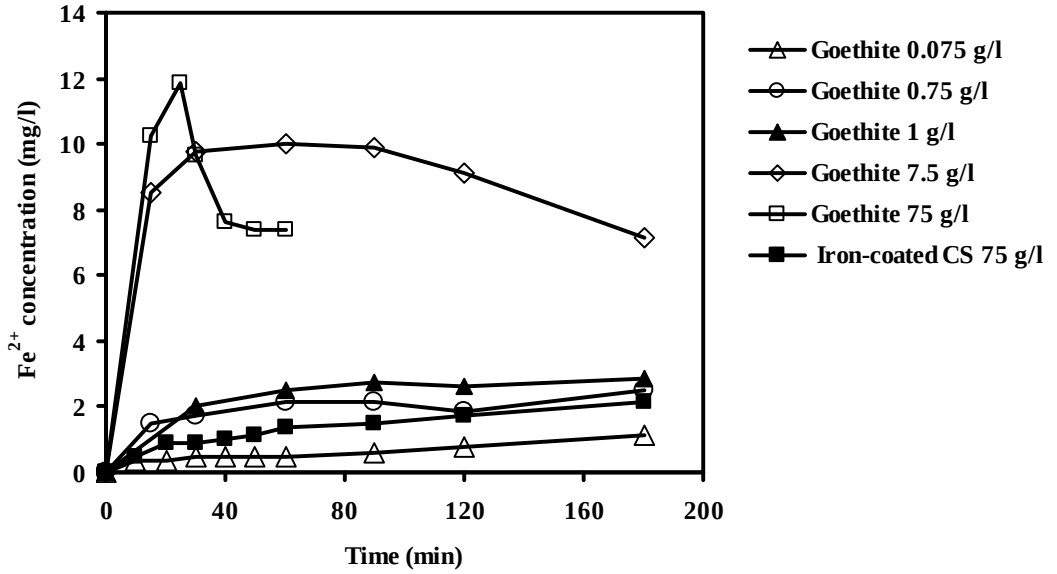

(a) Ferrous

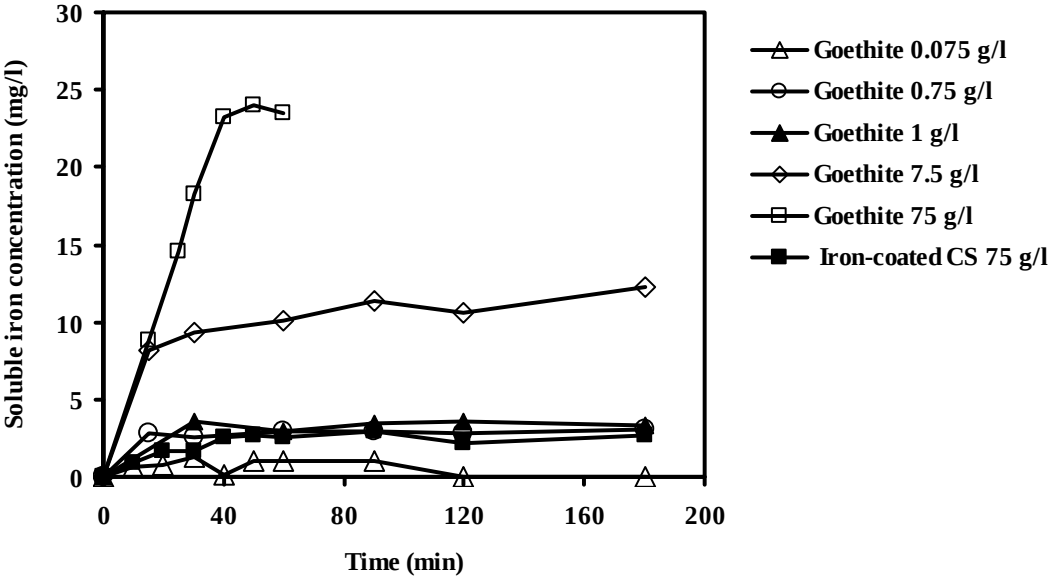

(b) Soluble iron

Figure 4.29 Iron leach ability of iron-coated CS and commercial goethite during the heterogeneous Fenton process with the initial conditions as follows: 1 mM of 2,6-DMA, 1 mM of AN, 20 mM of H_2O_2 at pH 3 and 25 °C.

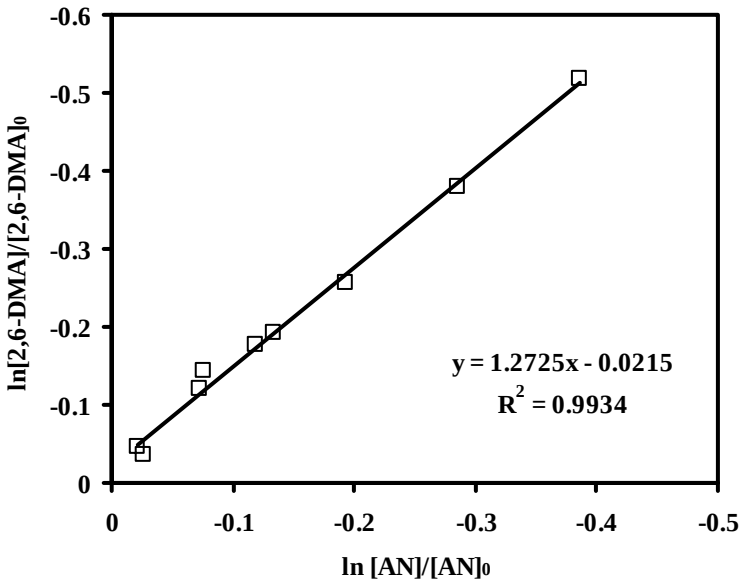

Figure 4.30 Relationship between ln([2,6-DMA]/[2,6-DMA]$_0$) versus ln([AN]/[AN]$_0$) using the data from the experiment with 75 g/l of 101st-cycle iron-coated CS with the initial conditions as follows: 1 mM of AN, 1 mM of 2,6-DMA, 20 mM of H_2O_2 at pH 3 and 25 °C.

CHAPTER V
CONCLUSIONS

5.1 Conclusions

5.1.1 Kinetics of 2,6-Dimethyl-aniline Degradation

The reaction between 2,6-DMA and OH• has been investigated by using Fenton reaction under various conditions, i.e., batch versus continuous operations, presence versus absence of solid media, and different Fenton's reagent. The following conclusions could be drawn from this part:

- Under the studied conditions, Fe^{2+} was the limiting reagent for organic oxidation.
- Competitive kinetics technique was proven to be an efficient and reliable method to determine the rate constant between organic compounds and hydroxyl radicals.
- Intrinsic 2^{nd}-order rate constants between 2,6-dimethyl-aniline and hydroxyl radicals under various conditions were in between 1.59×10^{10} and 1.80×10^{10} M^{-1} s^{-1} with an average and 95% confidence interval of $1.70\pm0.04\times10^{10}M^{-1}$ s^{-1}.
- Intermediates from 2,6-DMA oxidation by hydroxyl radicals were 2,6-dimethyl-nitrobenzene, 2,6-dimethy-phenol, 2,6-dimethyl-nitrophenol, 2,6-dimethyl-hydroquinone, 2,6-dimethyl-benzoquinone, 2,6-dimethyl-3-hydroxy-benzoquinone, maleic, lactic, oxalic, acetic, and formic acids. The degradation pathway of 2,6-DMA was also proposed in this study.

5.1.2 Iron Crystallization

Iron precipitation and crystallization mechanisms were thoroughly investigated which could provide a better understanding on iron removal in the

fluidized-bed Fenton process. The outcomes of this part could be concluded as follows:

- Solubility of ferric is much less than those of ferrous; hence, after the initiation of Fenton reaction, ferric from ferrous oxidation should precipitate out in the form of ferric hydroxide even in the acidic solution.
- Saturation degree is the major factor controlling the precipitation process. Solid phase will be formed via the homogeneous nucleation if the precipitation occurs in the labile zone; iron removal in the fluidized-bed Fenton reactor will be sequentially unimpressive because the crystallization rate of iron onto fluidized media is very slow. On the other hand, if the precipitation happens within the metastable zone, heterogeneous nucleation will become predominate and the removal of iron in the fluidized-bed Fenton reactor will be rapid and exceptional.
- Newly formed crystallite has higher affinity with the foreign solid surface than aging or ripening crystallites; hence, the crystallization should occur simultaneously with the Fenton reaction in the fluidized-bed reactor in order to obtain the highest iron removal rate.
- Under the studied conditions, the crystallization process was controlled by the transport step rather than the surface-interaction step. Rate of crystal growth under turbulent condition followed the 2^{nd}-order rate with respect to iron concentration (orthokinetic flocculation). In contrast, the growth rate under stagnant condition could be sufficiently explained by the transport mechanism both at the molecular and crystallite (perikinetic flocculation) levels.
- Presence of organic compounds/intermediates which can form complex with ferric such as oxalic acid will increase the solubility of ferric; hence, deteriorate the crystallization process. As a result, to obtain the significant iron removal in a full-scale fluidized-bed Fenton reactor, the oxidation reaction should proceed intensively toward complete mineralization.
- The rate of iron crystallization in the fluidized-bed Fenton reactor will gradually decrease with time; hence, to maintain the crystallization rate, a portion of coated-media has to be continuously replaced with fresh media.

- Catalytic activity of 75 g of the 101st-cycle iron-coated construction sands (>3.5% iron by weight) was approximately equivalent to 3 g of commercial goethite in term of aniline and 2,6-dimethyl-aniline degradation.

5.2 Recommendations for Further Studies

- Determine the rate constant of 2,6-dimethyl-aniline with hydroxyl radicals by using the competitive kinetics technique with different reference compounds and compare with the values obtained from this study.
- Determine the rate constant of 2,6-dimethyl-aniline with hydroxyl radicals by using other advanced oxidation processes such as TiO_2/UV, H_2O_2/UV and O_3/UV and compare with the values obtained from this study.
- Determine the effect of pH on the rate constant between 2,6-dimethyl-aniline and hydroxyl radicals and compare with the values obtained from this study.
- Determine the effect of temperature on the rate constant between 2,6-dimethyl-aniline and hydroxyl radicals via Arrhenius equation so that the rate constant can be applied in field practice for every required temperature.
- Investigate into more details on the factors affecting iron crystallization in the fluidized-bed Fenton process such as bed expansion, upflow velocity, pH, and temperature to obtain necessary information for scale up the fluidized-bed reactor for real application.
- Optimize the fluidized-bed Fenton process in term of organic and iron removals and compare the outcomes with the proposed mechanisms in this study.

REFERENCES

APHA (1992) Standard methods for the examination of water and wastewater, 18th Edition, American Public Health Association, Washington D.C.

Balci, B., Oturan, N., Cherrier, R. and Oturan, M.A. (2009) Degradation of atrazine in aqueous medium by electrocatalytically generated hydroxyl radicals. A kinetic and mechanistic study. Water Research 43: 1924-1934.

Baldrian, P., Merhautova, V., Gabriel, J., Nerud, F., Stopka, P., Hruby, M. And Benes, M.J. (2006) Decolorization of synthetic dyes by hydrogen peroxide with heterogeneous catalysis by mixed iron oxides. Applied Catalysis B: Environmental 66: 258–264

Brillas, E., Mur, E., Sauleda, R., Sanchez, L., Peral, J., Domenech, X. and Casadi J. (1998) Aniline mineralization by AOP's: anodic oxidation, photocatalysis, electro-Fenton and photoelectro-Fenton processes. Applied Catalysis B: Environmental 16(1): 31-42.

Buxton, G.V., Greenstock, C.L., Helman, W.P. and Ross, A.B. (1988) Critical review of rate constants for reactions of hydrated electrons, hydrogen atoms and hydroxyl radical ($^{\bullet}OH/^{\bullet}O^{-}$) in aqueous solution. Journal of Physical and Chemical Reference Data 17: 513-886.

Chen, G., Hoag, G.E., Chedda, P., Nadim, F., Woody, B.A. and Dobbs, G.M. (2001) The mechanism and applicability of in situ oxidation of trichloroethelene with Fenton's reagent. Journal of Hazardous Materials B87: 171-186.

Chou, S. and Huang, C. (1998) Application of a supported iron oxyhydroxide catalyst in oxidation of benzoic acid by hydrogen peroxide. Chemosphere 38(12): 2719-2731

Chou, S. and Huang, C. (1999) Effect of Fe^{2+} on catalytic oxidation in a fluidized bed reactor. Chemosphere 39, 2: 1997-2006.

Chou, S., Huang, C. and Huang, Y.H. (2001) Heterogeneous and homogeneous oxidation by supported γ-FeOOH in a fluidized-bed reactor: kinetic approach. Environmental Science and Technology 35: 1247-1251.

Chou, S., Huang, G.H., Liao, C.C., Hsu, S.F. and Huang, Y.H. (2003) Fenton family-advanced oxidation technologies for wastewater treatment. Asian Pacific Regional Conference on Practical Environmental Technologies, Tainan, Taiwan. (18-21 December 2003): (A2-17)-(A2-24).

Chou, S., Liao, C.C., Perng, S.H. and Chang, S.H. (2004) Factors influencing the preparation of supported iron oxide in fluidized-Bed crystallization. Chemosphere 54: 859-866.

Christopher, K.D., William, J.C. and T.David Waite. (2005) Fenton-Mediated oxidation in the presence and absence of oxygen. Environmental Science & Technology 39: 5052-5058.

Daniel, W.W. (1991) Biostatistics: A foundation for analysis in the health sciences. 5th-Edition, John Wiley & Sons, Inc., New York.

Dantas, T.L.P., Mendonca, V.P., Jose, H.J., Rodrigues, A.E. and Moreira, R.F.P.M. (2006) Treatment of textile wastewater by heterogeneous Fenton process using a new composite Fe_2O_3/carbon. Chemical Engineering Journal 118: 77–82

Einschlag, F. S. G., Carlos, L. And Capparelli, A. L. (2003) Conpetition kinetics using the UV/H_2O_2 process: a structure reactivity correlation for the rate constants of hydroxyl radicals toward nitroaromatic compounds. Chemosphere 53: 1-7.

Ewa, L.K. (1991) Degradation of aqueous nitrophenol and nitrobenzene by means of the Fenton reaction. Chemospere 22: 529-536.

Fenton, H.J.H. (1894) Oxidative properties of the H_2O_2/Fe^{2+} system and its application. Journal of Chemical Sources 65: 889-899.

Flores, Y., Flores, R. and Gallegos, A.A. (2008) Heterogeneous catalysis in the Fenton-type system reactive black 5/H_2O_2. Journal of Molecular Catalysis A: Chemical 281: 184–191

Glaze, W.H., Kang, J.W. and Chapin, D.H. (1987) The chemistry of water treatment processed involving ozone, hydrogen peroxide and ultraviolet radiation. Ozone Science & Engineering 9: 335-352.

Hoigné, J. (1998) Chemistry of aqueous ozone and transformation of pollutants by ozonation and advanced oxidation processes. Hutzinger, O. (Ed.). Handbook of Environmental Chemistry 5, Springer-Verlag, Berlin 5, pp. 83-141 (Part C).

Homanee, S. (2005) Iron pelletization with various seeding materials. Master's Thesis, Department of Environmental Management (Inter-Department), Graduate School, Chulalongkorn University.

Hsueh, C.L., Huang, Y.H., Wang, C.C. and Chen, C.Y. (2006) Photoassisted fenton degradation of nonbiodegradable azo-dye (Reactive Black 5) over a novel supported iron oxide catalyst at neutral pH. Journal of Molecular Catalysis A: Chemical 245: 78–86

Huang, C.P., Dong, C. and Tang, Z. (1993) Advanced chemical oxidation: its present role and potential future in hazardous waste treatment. Water Management 13: 361-377.

Huang, H.H., Lu, M.C. and Chen, J.N. (2001) Catalytic decomposition of hydrogen peroxide and 2-chlorophenol with iron oxides. Water Research 35(9): 2291-2299

IARC, Monographs on the Evaluation of Carcinogenic Risks to Humans, 57, 1993.

Kwon, B.G., Ryu, S. and Yoon, J. (2009) Determination of hydroxyl radical rate constant in a continuous flow system using competition kinetics. Journal of Industrial and Engineering Chemistry 15: 809-812.

Leitner, N.K.V. and Roshani, B. (2010) Kinetic of benzotriazole oxidation by ozone and hydroxyl radical. Water Research 44: 2058-2066.

Lin, S.S. and Gural, M.D. (1996) Heterogeneous catalytic oxidation of organic compounds by hydrogen peroxide. Water Science and Technology 34(9): 57-64.

Lin, S.S. and Gurol, M.D. (1998) Catalytic decomposition of hydrogen peroxide on iron oxide: kineics, mechanisms, and implications. Environmental Science and Technology 32: 1417-1423.

Lo, S.L. and Chen, T.Y. (1997) Adsorption of Se (IV) and Se (VI) on am iron coated sand from water. Journal of Chemosphere: 919-930.

Lunar, L., Sicilia, D., Rubio, S., Perez-Bendito, D. and Nickel, U. (2000) Degradation of photographic developers by Fenton's reagent: condition optimization and kinetics for metal oxidation. Water Research 34, 6: 1791-1802.

Lu, M.C. (2000) Oxidation of chlorophenols with hydrogen peroxide in the presence of goethite. Chemosphere 40: 125-130

Lu, M.C., Chen, J.N. and Chang, C.P. (1999) Oxidation of dichlorvos with hydrogen peroxide using ferrous ion as catalyst. Journal of Hazardous Materials B65: 277-288.

Lu, M.C., Chen, J.N. and Huang, H.H. (2002) Role of Goethite Dissolution in the oxidation of 2-chlorophenol with hydrogen peroxide. Chemosphere 46: 131-136

Masomboon, N., Ratanatamskul, C. and Lu, M.C. (2009) Chemical oxidation of 2,6-dimethylaniline in the Fenton process. Environmental Science and Technology 43: 8629-8634.

Masomboon, N., Ratanatamskul, C. and Lu, M.C. (2010) Chemical oxidation of 2,6-dimethylaniline by electrochemically generated Fenton's reagent. Journal of Hazardous Materials 176: 92-98.

Masten, S. and Davies, S. (1994) The use of ozonation to degrade organic contaminants in wastewater. Environmental Science and Technology 28: 180A-185A.

Mazellier, P., Busset, C., Delmont, A. and Laat, J.D. (2007) A comparison of fenuron degradation by hydroxyl and carbonate radicals in aqueous solution. Water Research 41: 4585-4594.

Morel F.M.M. and Hering J.G. (1993) Principles and applications of aquatic chemistry, John Wiley & Sons, Inc., New York.

Munter, R. (2001) Advanced oxidation processes-current status and prospects. Process Estinian Acadamic Science Chemistry 50(2): 59-80.

NTP, National Toxicology Program. Toxicology and Carcinogenesis Studies of 2,6-Xylidine (2,6-dimethyl-aniline) in Charles River CS Rats (Feed Studies), TR 278 U.S. Department of Health and Human Services, Public Health Service, (online) 1990. Available from: http://ntp.niehs.nih.gov/ntp/htdocs/LTrpts/tr278.pdf (accessed April 2009)

Oliviero, L., Barbier, Jr. J., Duprez, D., Wahyu, H., Ponton, J.W., Metcalfe, I.S. and Mantzavinos, D. (2001) Wet air oxidation of aqueous solutions of maleic acid over Ru/CeO_2 catalysts. Applied Catalysis B: Environmental 35(1): 1-1.

Oliviero, L., Wahyu, H., Barbier, Jr. J., Duprez, D., Ponton, J.W., Metcalfe, I.S. and Mantzavinos, D. (2003) Experimental and predictive approach for determining wet air oxidation reaction pathways in synthetic wastewaters. Chemical Engineering Research and Design 81(3): 384-392.

O'Melia, C.R., and Tiller, C.L. (1993) Physicochemical aggregation and deposition in aquatic environments. In Environmental Particles, Vol. 2, J. Buffle and H.P. van Leeuwen, Eds., Lewis, Boca Raton, FL.

Parsons, S. (2004) Advance oxidation processes for water and wastewater treatment, No.1, IWA Publishing, U.S.A. 130-145.

Peres, A.J., Heredia, D.J. and Dominguez, R.J. (2003) Integrated Fenton's Reagent Coagulation/Flocculation Process for the Treatment of cork processing wastewater. Journal of Hazardous Materials B107: 115-121.

Pignatello, J.J. (1992) Dark and photoassisted Fe^{3+}-catalyzed degradation of chlorophenoxy herbicides by hydrogen peroxide. Environmental Science and Technology 26: 944-951.

Prengle, H.W., Symos, M.J. and Bellhateche, D. (1978) H_2O_2/vis UV process for photo-oxidation of waterborne hazardous substances C_1-C_6 chlorinated hydrocarbons. Waste Management 16: 326-333.

Rodgers, J.D. and Bunce, N.J. (2001) Review paper, treatment methods for the remediation of nitroaromatic explosives. Water Research 35(9): 2101-2111.

Sauleda, R. and Brillas, E. (2001) Mineralization of aniline and 4-chlorophenol in acidic solution by ozonation catalyzed with Fe^{2+} and UVA light. Applied Catalysis B: Environmental 29(2): 135-145.

Skoumal, M., Arias, C., Cabot, P.L., Centellas, F., Garrido, J.A., Rodriguez, R.M. and Brillas, E. (2008) Mineralization of the biocide chloroxylenol by electrochemical advanced oxidation processes. Chemosphere 71: 1718-1729.

Spanggord, R.J., Yao, D. and Mill, T. (2000) Kinetics of aminodinitrotoluene oxidations with ozone and hydroxyl radical. Environmental Science and Technology 34: 450-454.

Shen, J.M., Chen, Z.L., Xu, Z.Z., Li, X.Y., Xu, B.B. and Qi, F. (2008) Kinetics and mechanism of degradation of p-chloronitrobenzene in water by ozonation. Journal of Hazardous Materials 152: 1325-1331.

Stumm, W. and Morgan, J.J. (1996) Aquatic chemistry: Chemical equilibria and rates in natural waters. 3rd Edition, John Wiley & Sons, Inc., New York.

Tai, C.Y. (1999) Crystal growth kinetics of two-step growth process in liquid fluidized-bed crystallizer. Journal of Crystal Growth 206: 109-108.

Tchobanoglous, G., Burton, F.L. and Stensel, H.D. (2003) Wastewater engineering treatment and reuse. 4th edition. New York: McGraw-Hill.

Ting, W.P., Lu, M.C. and Huang, Y.H. (2009) Kinetics of 2,6-dimethylaniline degradation by electro-Fenton process. Journal of Hazardous Materials 161: 1484-1490.

Zelmanov, G. and Semiat, R. (2008) Iron(3) oxide-based nanoparticles as catalysts in advanced organic aqueous oxidation. Water Research 42: 492 – 498.

APPENDIX A: 執行國際合作出差報告

一、緣由

本案與外國合作計畫，選定之目標污染物均為含苯環之化合物，計畫執行期間，對方派博士生及碩士生前來台灣共同參與研究，但是經費由對方支付。藉由學生互訪共同參與研究，提升雙方英語能力。在論文發表方面，除國際期刊外，也各自在自己的國家共同具名發表，增加雙方合作的能見度。

二、工作內容

（一） 98 年 3 月 5 日

本年度共訪問泰國兩次，每次停留兩天參與討論，聽取研究進度及報告，也為共同指導之研究生主持論文口試。 3 月 5 日為共同指導碩士學生論文口試日期，論文題目如下。 口試委員共有五位，最後一致通過該生之學位論文。

1. Removal of aniline by electro-Fenton process (student: Sermpong Sairiam)
2. Comparison of *o*-toluidine degradation by fresh carriers and iron oxide catalyst in a fluidized bed reactor (student: Pumis Thuptimdang)

（二） 98 年 3 月 28 日

再度前往泰國參與研究進度簡報，並與新接受之學生討論未來研究論文內容，每位學生先與指導教授 Jin Anotai 先行初步擬定研究方向，本人拜訪當天早上，再逐一簡報為來可能之研究內容，討論並確認研究方向與預期目標，下午到實驗室確認現場操作。隔天為兩位博士生口試，論文內容如附件一及附件二

102

附件一

Thesis Title: Kinetics of Aniline Degradation and Iron Crystallization in Fluidized-bed Fenton Process

Student: Nonglak Boonrattanakij **ID:** 5087809220
Program: Ph.D.
Credit: 36
Advisor: Assoc. Professor Jin Anotai, Ph.D.
Co-advisor: Professor Ming-Chun Lu, Ph.D.

---

1) Introduction

Aniline has been used widely as a chemical intermediate to produce many products such as polyurethane foam, agricultural chemicals, synthetic dyes, antioxidants, herbicides, pharmaceutical products, and explosives (US EPA, 1985). Aniline contaminated wastewaters from these manufacturers can pose adverse impacts in receiving waters due to its biorefractory and highly toxic properties (Brillas and Casado, 2002). Aniline has also been found in at least 59 of the 1,585 National Priorities List sites identified by the US EPA (ATSDA, 2002). In Thailand, aniline has been classified as a toxic hazardous chemical by Ministry of Industry which required a special control, treatment, and disposal (MOI, 2540). As a result, appropriate and effective treatment technologies are needed to purify or clean up these contaminated wastewaters.

Advanced oxidation processes (AOPs) are one of the possible alternatives which can provide the destruction of refractory and hazardous organic compounds including aniline. Hydroxyl radicals ($OH^{\bullet}$) generated in the AOPs are extremely reactive, short lived and unselective transient species which can readily oxidize organic/inorganic pollutant in water and wastewater and convert them into simple, relatively harmless substances. A number of methods can lead to the generation of $OH^{\bullet}$ including H_2O_2/UV, O_3/H_2O_2, O_3/UV, TiO_2/UV, and Fenton's family which is of interest in this research.

Fenton process is normally initiated by the addition of ferrous (Fe^{2+}) and hydrogen peroxide (H_2O_2) which are called "Fenton's reagent". The conventional Fenton process is typically simple and effective, and requires no highly capital investment. Nonetheless, it has one serious disadvantage considering on the production of an enormous amount of ferric hydroxide sludge which requires further separation and disposal. The use of fluidized-bed reactor can overcome or lessen this problem. Ferric ions result from Fenton reaction can precipitate and crystallize onto the carriers' surface; hence, significantly reduces the formation of iron puffy sludge (Chou and Huang, 1999). In addition, it was also found that these crystallized iron oxides could catalyze the decomposition of H_2O_2 to generate $OH^{\bullet}$ which enhancing the removal of pollutant (Lin and Gurol, 1998).

Although the oxidation of aniline by $OH^{\bullet}$ has been investigated previously by several studies (Brillas and Casado, 2002; Sauleda and Brillas, 2001; Brillas et al., 1998; Anotai et al.,

2006), no intrinsic kinetic rate constant of the reaction between aniline and $OH^{\bullet}$ has been reported. This constant is very important and useful scientific and engineering information and is deserved to be investigated. As a result, this research project will focus on the determination of the second-order rate constant between aniline and $OH^{\bullet}$. In addition, this research will also characterize the iron crystallization onto the carriers in a fluidized-bed reactor in order to provide a better understanding on iron removal from Fenton process which is valuable to field practice.

2) Objectives

1. To determine the intrinsic rate constant between aniline and hydroxyl radicals in ordinary and fluidized-bed Fenton processes.
2. To characterize iron precipitation and crystallization onto the carriers in fluidized-bed Fenton process.

3) Hypotheses

1. Oxidation of aniline by hydroxyl radicals is a second-order reaction.
2. Aniline decomposition by ordinary and fluidized-bed Fenton processes depends on system pH and chemical dosages.
3. Metal oxide can effectively serve as a medium for iron crystallization in fluidized-bed Fenton process.
4. Aniline and its intermediates have an effect on iron crystallization in fluidized-bed Fenton process.

4) Theoretical Background

Properties of aniline **(USEPA, 1985; ASTDR, 2002)**

Aniline ($C_6H_5NH_2$) is an organic compound consisting of a benzene ring and an amino group. The chemical structure of aniline is shown in Figure 1. Aniline is a clear to slightly yellow liquid and is moderately soluble in water but mixes readily with most organic solvents. Aniline ignites readily, burning with a large smoky flame. It possesses a somewhat pleasant vinous odour and a burning aromatic taste; it is a highly acrid poison. It is used to manufacture many products including polyurethane foam, agricultural chemicals, synthetic dyes, antioxidants, stabilizers for rubber industry, herbicides, varnishes, and explosives. Aniline can be toxic if ingested, inhaled, or by skin contact. Aniline damages hemoglobin, a protein that normally transports oxygen in the blood, so that oxygen cannot be transported to cells and tissues causing them to lack oxygen for their metabolisms. This condition is known as "methemoglobinemia". Dizziness, headaches, irregular heart beat, convulsions, coma, and death may also occur resulting from an acute exposure to high aniline dosage. Direct contact with aniline can also produce skin and eye irritation. Long-term exposure to lower levels of aniline may cause symptoms similar to those experienced in acute high-level exposure. Aniline is released into the environmental primarily from industrial uses. Aniline has been found in industrial wastewater and leachates from disposal sites.

104

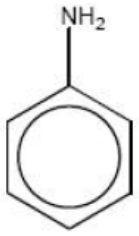

Figure 1. Structure of aniline.

Chemistry of Fenton's reagent

Fenton process and its modified versions are being increasingly used in the treatment of contaminated water and soil. The conventional "dark" Fenton process involves the use of an oxidizing agent (usually H_2O_2) and a catalyst (usually Fe^{2+}) to generate highly reactive $OH^{\bullet}$. Once the Fenton's reagent is combined together, its sequential reactions are very complicated but well specified as shown in Eqs. (1) to (12) (Pignatello, 1992; Lu et al., 1999; Chen et al., 2001).

$$Fe^{2+} + H_2O_2 \rightarrow Fe^{3+} + {}^{\bullet}OH + OH^- \quad k_1 = 76\ M^{-1}s^{-1} \quad (1)$$

$$H_2O_2 \leftrightarrow HO_2^- + H^+ \quad K_2 = 1.59\times10^{-12}\ M \quad (2)$$

$$Fe^{3+} + H_2O_2 \rightarrow Fe^{2+} + HO_2^{\bullet} \quad k_3 = 0.02\ M^{-1}s^{-1} \quad (3)$$

$$HO_2^{\bullet} \leftrightarrow O_2^{\bullet-} + H^+ \quad K_4 = 1.6\times10^{-5}\ M \quad (4)$$

$$Fe^{2+} + {}^{\bullet}OH \rightarrow Fe^{3+} + OH^- \quad k_5 = 4.3\times10^{6}\ M^{-1}s^{-1} \quad (5)$$

$$Fe^{2+} + O_2^{\bullet-} \rightarrow Fe^{3+} + O_2^- \quad k_6 = 1\times10^{7}\ M^{-1}s^{-1} \quad (6)$$

$$Fe^{2+} + HO_2^{\bullet} \rightarrow Fe^{3+} + HO_2 \quad k_7 = 1.2\times10^{6}\ M^{-1}s^{-1} \quad (7)$$

$$H_2O_2 + {}^{\bullet}OH \rightarrow HO_2^{\bullet} + H_2O \quad k_8 = 2.7\times10^{7}\ M^{-1}s^{-1} \quad (8)$$

$$HO_2^{\bullet} + HO_2^{\bullet} \rightarrow H_2O_2 + O_2 \quad k_9 = 8.3\times10^{5}\ M^{-1}s^{-1} \quad (9)$$

$$^{\bullet}OH + {}^{\bullet}OH \rightarrow H_2O_2 \quad k_{10} = 5.3\times10^{9}\ M^{-1}s^{-1} \quad (10)$$

$$RH + {}^{\bullet}OH \rightarrow RH^{\bullet} + OH^- \rightarrow \rightarrow \rightarrow \text{products or } CO_2 + H_2O \quad (11)$$

$$Fe^{3+} + 3OH^- \rightarrow Fe(OH)_{3(s)} \quad K_{sp} = 4\times10^{-38} \quad (12)$$

Although Fe^{2+} is acting as a catalyst in the Fenton reaction series, it can be seen that the consumption rate of Fe^{2+} in Eq. (1) is almost 3,800 times faster than the regeneration rate of Fe^{2+} from Fe^{3+} in Eq. (3). As a result, the pollutant degradation in Fenton process typically proceeds in two sequential steps. In the first step, the pollutant disappears rapidly under sufficient Fe^{2+} leading to the $OH^{\bullet}$ excessive environment whereas, in the slower second step, the oxidation rate of the pollutant is controlled by Eq. (3) which is known as "Fenton-like process" (Lunar et al., 2000). After treatment with Fenton process, the mixture will be neutralized to comply with the effluent standard and the ferric hydroxide will precipitate out as illustrated in Eq. (12). This ferric hydroxide sludge will cause a burden for further separation and disposal which is a major drawback for ordinary Fenton process.

Fluidized-bed Fenton Process

As mentioned previously, the major disadvantage of Fenton process is the production of a substantial amount of iron precipitation. To overcome and/or ease this problem, the fluidized-bed reactor (FBR) is one of the possible alternatives. In FBR, several important processes occur simultaneously including: a) Homogeneous chemical oxidation (H_2O_2/Fe^{2+}); b) Heterogeneous chemical oxidation (H_2O_2/ iron oxide); c) Fluidized-bed crystallization; d) Reductive dissolution of iron oxides. The ferric hydrolysis product of Fenton's reaction can crystallize and grow on the surface of the carriers; hence, decreasing the precipitation in puffy ferric hydroxide form (Chou et al., 1999). At the same time, the synthesized ferric oxide can also serve as a catalyst for hydrogen peroxide decomposition in a heterogeneous oxidation (Chou et al., 2001)

Rate constant determination

In this research, the intrinsic second-order rate constant of the reaction between aniline and $OH^{\bullet}$ will be determined by using a technique of competitive kinetics between aniline and an organic probe in the presence of $OH^{\bullet}$. This organic probe has to have the intrinsic rate constant with $OH^{\bullet}$ reported (Buxton et al., 1988). Nonetheless, the competitive kinetics as will be described later is a very useful and simple tool to estimate the unknown rate constant of a compound without any complexity in experimental setup and equipments. It is well established that $OH^{\bullet}$ will react with any compound in a second-order manner; hence, the rate laws can be written as follows:

$$\frac{d[AN]}{dt} = -k_1[AN][OH^{\bullet}] \quad (13)$$

$$\frac{d[P]}{dt} = -k_P[P][OH^{\bullet}] \quad (14)$$

$$\frac{d[S_i]}{dt} = -k_{S_i}[S_i][OH^{\bullet}] \quad (15)$$

where "P" is the organic probe and "S_i" is intermediate scavenger

At the initial stage where the competition reactions from the intermediates from the oxidation of aniline and organic probe are minimal, Eq (15) can be neglected; hence:

$$\frac{Eq(12)}{Eq(13)} = \frac{\left(\frac{d[AN]}{dt}\right)_{initial}}{\left(\frac{d[P]}{dt}\right)_{initial}} = \frac{-k_1[AN][OH^{\bullet}]}{-k_P[P][OH^{\bullet}]} = \frac{k_1[AN]}{k_P[P]}$$

$$\frac{d[AN]}{dt}, \frac{d[P]}{dt}, [AN], k_P, [P] \text{ are known } \rightarrow k_1 \text{ can be determined}$$

However, this organic probe should have a comparable rate with $OH^{\bullet}$ to aniline in order to be able to obtain accurate initial rates for both compounds at the same time. In this study, several aromatic compounds with known rate constants such as benzene and benzoic acid will be tested for their potential to serve as an organic probe.

106

5) Literature Reviews

Degradation of aniline by advanced oxidation processes

Sun et al. (2007) determined the appearance kinetic rate constant (k_{ap}) for *p*-nitroaniline (PNA) degradation at different conditions by Fenton process including the role of pH, Fenton's reagent, PNA concentration and temperature. The results demonstrated that the oxidation of PNA increased rapidly only at the pH value of 3.0. The k_{ap} of PNA oxidation increased with increasing the dosage of Fenton's reagent and the temperature. However, the oxidation reaction was inhibited at the higher level of H_2O_2 and decreased with the increasing of initial PNA concentration.

Anotai et al. (2006) investigated the degradation of aniline at pH 2 by Fenton and electro-Fenton processes. The experiments showed that electro-Fenton process was superior to ordinary Fenton process with the current impacts of 1.2 to 3.1 for removal efficiency and 1.2 to 5.8 for degradation rate depending on initial Fe^{2+} concentration. With current application, aniline degradation rate seems to be autonomous from Fenton's reagent concentrations and approaching a half order with respect to aniline. Furthermore, the delay of current supply at the initial stage could save up to one-third of the total energy required by the ordinary electro-Fenton process.

Li et al. (2003) investigated the degradation of aniline solution in alkaline medium of pH 11.0 by electrocatalytic oxidation using an electrochemical reactor containing a SnO_2-Sb_2O_3-PtO anode and a Ti cathode. The results showed that electrocatalytic oxidation was a high efficiency process for aniline degradation. A possible mechanism involving $OH^{\bullet}$ reaction with aniline was proposed. The first reaction step was the hydroxylation of the aromatic ring to yield dianiline, 4-anilino phenol and azobenzol, which further oxidized by $OH^{\bullet}$ to yield phenylsuccinic acid. All intermediates formed initially were finally decomposed by $OH^{\bullet}$ to form CO_2 and H_2O.

Sarasa et al. (2002) ozonated aqueous solution of aniline and *p*-chloroaniline to investigate the reaction and oxidation by-product. The main examined aromatic by-products were nitrobenzene and azobenzene when the experiment was performed at acidic pH. All the aromatic by-products found were less toxic than the raw materials.

Sauleda et al. (2001) investigated on the mineralization of aniline and 4-chlorophenol in acidic solution by ozonation catalyzed with Fe^{2+} and UVA light. The initial mineralization rate was enhanced as more oxidizing hydroxyl radical being produced in the medium by the catalyzed ozonation. Each initial pollutant was degraded at the similar rate in all processes. *p*-Benzoquinone and nitrobenzene were identified as intermediates of aniline oxidation. Nitrate ion attained maximum production under UVA irradiation, indicating that the generation of nitrobenzene from selective attack of O_3 on the amino group of aniline was a photocatalysis reaction.

Utset et al. (2000) studied on the consumption of oxygen during the degradation of aniline by Fenton and photo-Fenton reaction. This study examined the effects of aniline, Fenton's reagent concentrations, pH, temperature, and O_2 flow rate on the ratio of $O_{2,consumed}$ to H_2O_2. The experimental results indicated that this replacement took place in a variable extent, but the presence

of H_2O_2 was necessary along the reaction.

Removal of organic compound in heterogeneous catalysis by hydrogen peroxide

Zelmanov and Semiat (2008) investigated the catalytic behavior of iron-based nano-catalysts for ethylene glycol and phenol treatment in the advanced oxidation processes. The results showed that the Fenton-like reaction using iron (III) oxide-based nano-catalysts in the presence of H_2O_2 could degrade both substances efficiently.

Flores et al. (2008) demonstrated that H_2O_2 could be activated in the presence of a heterogeneous catalyst (Fe^{3+}-containing ashes) to become a powerful oxidant. Fe^{3+} was immobilized by leaching test which indicated that more of the 99 wt.% of the iron ion still stayed in the solid catalysts and the presence of H_2O_2 did not alter this relation. It is concluded that radical species (HO_2•) are formed when H_2O_2 was activated by the immobilized Fe^{3+}. The results show that it was possible to oxidize reactive black 5 dye using a stoichiometric amount of H_2O_2. After 2 hours of treatment, reactive solutions were effectively decolorized and 80% of the original COD was removed.

Dantas et al. (2006) evaluated the use of new composites as the adsorbents and/or heterogeneous catalysts for Fenton process to treat textile wastewater. The efficiency of the process was explored as a function of the experimental parameters: pH, H_2O_2 concentration and iron oxides content. The composites with high iron oxides content could effectively adsorb the contaminants in textile wastewater, and the adsorptive capacity increased with the iron concentration. These solids were also used as the heterogeneous Fenton catalysts and were effective at pH 3.0 with a consumption of H_2O_2 lower than those required by the homogeneous Fenton process.

Baldrian et al. (2006) used the heterogeneous catalysts based on magnetic mixed iron oxides to decolorized several synthetic dyes. All the catalysts could catalyze H_2O_2 to yield highly reactive hydroxyl radicals which able to decolorize the synthetic dyes effectively. The most effective catalyst was $FeO.Fe_2O_3$ which provided more than 90% decolorization. The fastest decomposition proceeded during the first hour of the reaction. In addition to dye decolorization, all the catalysts also caused a significant decrease of COD. These catalysts were active in the pH range of 2–10 depending on their structures and able to perform sequential catalytic cycles with low metal leaching.

Christopher et al. (2005) studied Fenton-mediated oxidation in the presence and absence of oxygen. The experiment showed that the oxidation of formic acid occurred under a variety of experiment conditions by Fenton's process. The intermediate generated during formic acid oxidation was observed to increase oxidation efficiency, especially at high initial organic concentrations, by contributing in the redox cycling of iron. In the presence of oxygen, however, such improvement was attenuated through competition for the organic intermediates.

Lu et al. (2002) investigated how surface dissolution of goethite affected 2-chlorophenol oxidation in the goethite/H_2O_2 process. The results show that ligand and reductant could enhance the dissolution rate of goethite which was a surface-controlled mechanism. Furthermore, the result

108

from this study indicated that 2-chlorophenol could be effectively degraded by Fenton-liked reaction using the goethite as a catalyst at acidic pH. The extent of 2-chlorophenol degradation increased with increasing goethite dosage which providing more surface sites for the reductive dissolution.

Iron crystallization in fluidized-bed Fenton reactor (FBR)

Hsueh et al. (2006) used a novel supported iron oxide, prepared in a fluidized-bed reactor (FBR), as a catalyst for the heterogeneous photoassisted Fenton degradation of azo-dye Reactive Black 5 (RB5). This catalyst was much cheaper than Nafion-based catalysts, and could markedly accelerate the degradation of RB5 under irradiation by UVA (λ = 365 nm). The effects of the molar concentration of H_2O_2, the pH of the solution and the catalyst loading on the degradation of RB5 were elucidated. A simplified mechanism of RB5 decomposition which was consistent with the experimental findings for a solution with a pH of up to 7.0 was proposed. About 70% decolorization was measured and 45% of the total organic carbon was eliminated on the surface of the iron oxide at pH 7.0 after 480 minutes in the presence of 0.055 mM RB5, 5.0 g iron oxide/L, 29.4 mM H_2O_2, under 15W UVA.

Chou et al. (2004) determined the effect of operational pH, superficial velocity, specific iron loading, and influent H_2O_2 concentration on the crystallization efficiency of FeOOH. The results demonstrated that all these parameters were found to significantly influence the crystallization efficiency. Two types of FeOOH catalysts were synthesized: FeOOH I was prepared at pH 3.5, and FeOOH II was formed by aging FeOOH I at pH 13. The crystalline property significantly affects the performance of catalytic oxidation of benzoic acid.

Chou et al. (2004) applied a novel supported iron oxyhydroxide (FeOOH) catalyst to treat benzoic acid by H_2O_2 using a fluidized-bed crystallization reactor. Four operating variables, including pH, specific iron loading, H_2O_2/Fe^{2+} ratio, and superficial velocity, have been demonstrated to affect the crystallization efficiency. The crystallization reached the maximum between pH 3.0 and 4.0. When the specific iron loading increased, crystallization decreased gradually and proportionally. The crystallization increased with increasing H_2O_2 /Fe^{2+} ratio, and then attained a plateau. The superficial velocity must be maintained higher than 30 m/hr to avoid the aggregation of suspension solids and formation of flocs that retained in the reactor.

Chou et al. (2001) applied a novel supported γ-FeOOH catalyst to oxidize benzoic acid (BA) in a circulating fluidized-bed reactor (CFBR) by H_2O_2 and to determine the effects of homogeneous and heterogeneous catalysis. They found that the degradation rate of H_2O_2 was proportional to its concentration and the BA decomposition depended on both BA concentration and H_2O_2. Conclusively, although heterogeneous catalysis contributed primarily to the oxidation of BA at pH 4.4-7.0, the homogeneous catalysis was of increasing importance below pH 4.4.

6) Scopes of the study

1. Using lab scale reactors and synthetic wastewater.
2. For the fluidized-bed Fenton process, the carriers will be either iron oxide, aluminum oxide, or construction sand.
3. Working at room temperature and operating in a batch mode.

7) Methodology

Materials

- Demineralized water will be used for all solution preparation.
- Aniline, hydrogen peroxide, ferrous sulfate heptahydrated, and all other chemicals will be reagent grade.
- Iron oxide or construction sand or aluminum oxide will be sieved to obtain the appropriate and uniform size.

Fluidized-bed Reactor

- 1.35-litre glass-cylinder reactor with an inlet, outlet, and a recirculation pump as shown in Figure 2 will be used.
- The reactor will be covered, if necessary, to protect any interference from sunlight.

Analytical Methods

- Measurement of aniline and the organic probe using GC/ FID.
- Analysis of total organic carbon using TOC analyzer.
- Analysis of total iron concentration using AAs or ICP.
- Analysis of ferrous using phenanthroline method (APHA, 1992).
- Measurements of H_2O_2 using standard iodometric method.
- Analysis of carrier's surface property using EDS, SEM, and XRD.
- Other water characteristics following the procedures as described in the Standard Methods (APHA, 1992).

Experimental Outline

A. Investigation of point of zero charge of the selected carriers

B. Investigation of the degradation of aniline

-Determination on effect of carrier, H_2O_2, Fe^{2+} and pH on the degradation of aniline using an organic probe which already has a second-order rate constant with $OH^{\bullet}$ (for example benzene, butyl chloride, benzoic acid etc.).

-Comparison of the removal efficiency in Fenton and fluidized-bed Fenton process.

C. Investigation of iron crystallization

-Determination on the effect of H_2O_2, pH, upflow velocity and iron species on the crystallization process.

-Characterization of iron crystallization during the fluidized-bed Fenton process.

Experimental Procedures

A. Point of zero charge of the carriers

-Predetermined amounts of the carriers will be added into several flasks containing either deionized water or experimental solution to obtain 0, 0.2, 0.4,

0.6, 1.2, 2.4, 5, 10, 20, 30, 40, and 50 g/l.

B. Investigation of the degradation of aniline

-Amount of Fenton's reagent and carrier, pH, upflow velocity will be varied within the appropriate range for each factor.

-Major experimental procedures are described in Figure 3.

C. Investigation of iron crystallization

-Ferric and ferrous solutions at required concentrations will be used to determine the iron phase in aqueous solution and crystallization behavior in the presence of a medium.

-Similar Fenton's reagent as in earlier test will be used to determine the phase of iron in aqueous solution, crystallization behavior in the presence of a medium, and effect of H_2O_2, pH, upflow velocity on the crystallization process.

-Iron-coated medium will be analyzed for its surface properties and iron species coated on the medium surface.

References

Anotai, J.; Lu, M.C. and Chewpreecha, P. (2006) Kinetics of aniline degradation by Fenton and electro-Fenton processes. Water Research 40: 1841-1847.

APHA (1992) Standard methods for the examination of water and wastewater, 18th Edition, American Public Health Association, Washington D.C.

ASDA (2002) Managing hazardous materials incidents, Vol. III – Medical management guidelines for acute chemical exposures: aniline, U.S. Department of Health and Human Services, Public Health Service, Atlanta, GA. Available from: http://www. Atsda.cdc.gov

Baldrian, P.; Merhautova, V.; Gabriel, J.; Nerud, F.; Stopka, P.; Hruby, M. And Benes, M.J. (2006) Decolorization of synthetic dyes by hydrogen peroxide with heterogeneous catalysis by mixed iron oxides. Applied Catalysis B: Environmental 66: 258–264

Brillas, E.; Mur, E.; Sauleda, R.; Sanchez, L.; Peral, J.; Domenech, X. and Casado, J. (1998) Aniline mineralization by AOP's: anodic oxidation, photocatalysis, electro-Fenton and photoelectron-Fenton processes. Applied Catalysis B Environmental 16: 31-42.

Brillas, E. and Casado, J. (2002) Aniline degradation by electro-Fenton and peroxi-coagulation processes using a flow reactor for wastewater treatment. Chemosphere 47: 241-248.

Buxton, G.V.; Greenstock, C.L.; Helman, W.P. and Ross, A.B. (1988) Critical review of rate constants for reactions of hydrated electrons, hydrogen atoms and hydroxyl radical ($^{\bullet}OH/^{\bullet}O^{-}$) in aqueous solution. Journal of Physical and Chemical Reference Data 17: 513-886.

Chen G., Hoag G.E., Chedda P., Nadim F., Woody B.A. and Dobbs G.M. (2001) The mechanism and applicability of in situ oxidation of trichloroethelene with

Fenton's reagent. Journal of Hazardous Materials B87: 171-186.

Chou, S.S. and Huang, C. (1999) Effect of Fe^{2+} on catalytic oxidation in a fluidized bed reactor. Chemosphere 39, 2: 1997-2006.

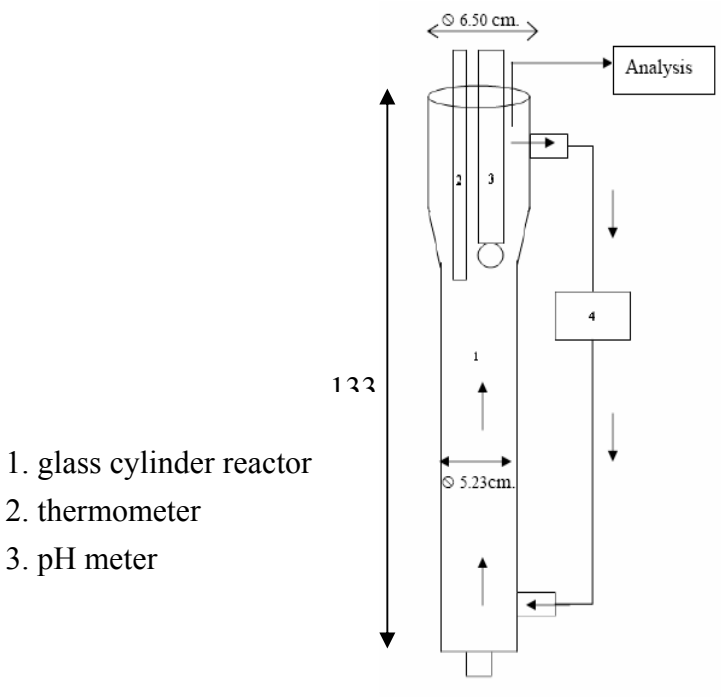

Figure 2. Fluidized-bed reactor (FBR)

112

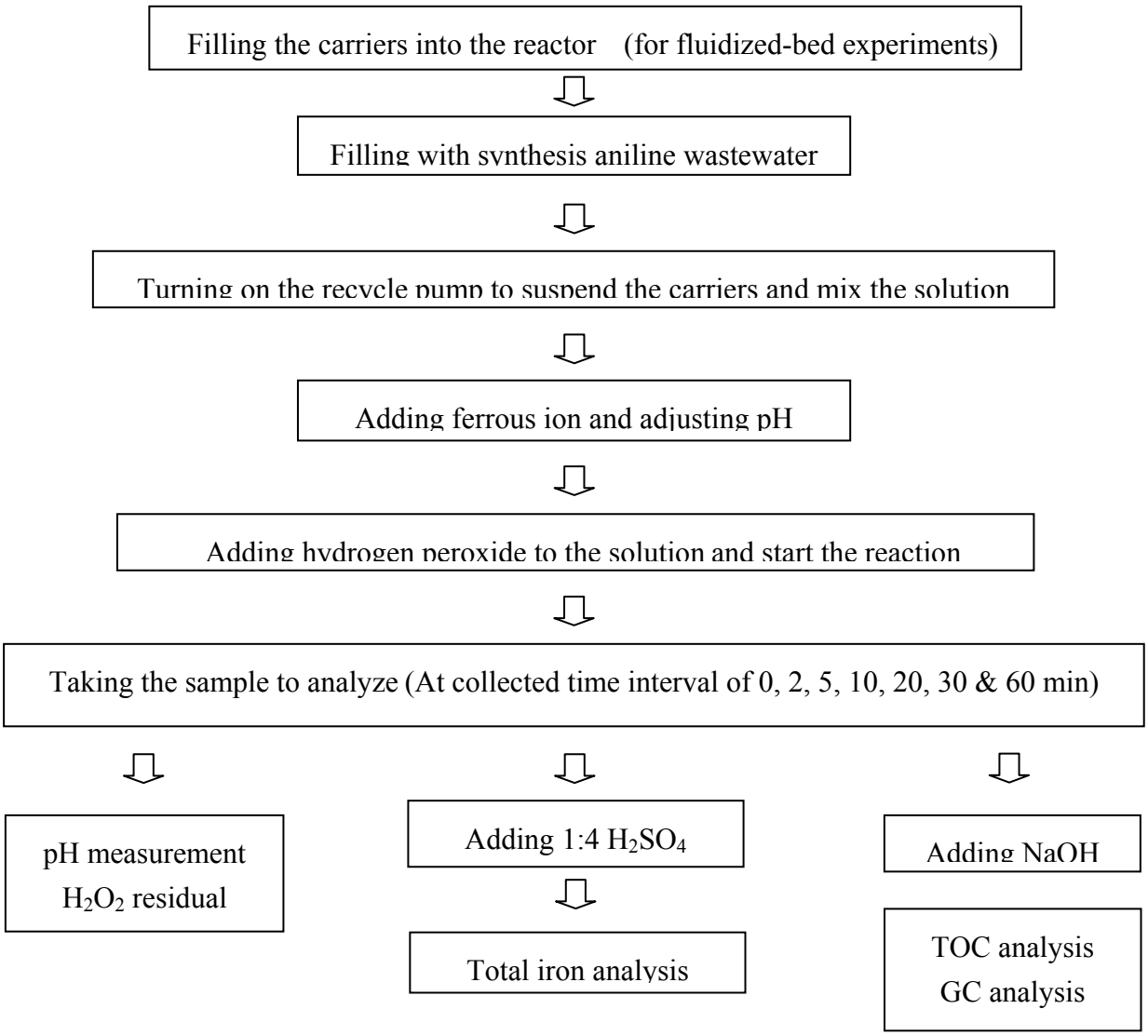

Figure 3. Experiment for Fenton and fluidized-bed Fenton process

Chou, S.; Huang, C. and Huang, Y.H. (2001) Heterogeneous and homogeneous oxidation by supported γ-FeOOH in a fluidized-bed reactor: kinetic approach. Environmental Science and Technology 35: 1247-1251.

Chou, S.; Liao, C.C.; Perng, S.H. and Chang, S.H. (2004) Factors influencing the preparation of supported iron oxide in fluidized-Bed crystallization. Chemosphere 54: 859-866.

Christopher, K.D.; William, J.C. and T.David Waite. (2005) Fenton-Mediated oxidation in the presence and absence of oxygen. Environmental Science & Technology 39: 5052-5058.

Dantas, T.L.P.; Mendonca, V.P.; Jose, H.J.; Rodrigues, A.E. and Moreira, R.F.P.M. (2006) Treatment of textile wastewater by heterogeneous Fenton process using a new composite Fe_2O_3/carbon. Chemical Engineering Journal 118: 77–82

Flores, Y.; Flores, R. and Gallegos, A.A. (2008) Heterogeneous catalysis in the Fenton-type system reactive black 5/H_2O_2. Journal of Molecular Catalysis A: Chemical

281: 184–191

Hsueh, C.L.; Huang, Y.H.; Wang, C.C. and Chen, C.Y. (2006) Photoassisted fenton degradation of nonbiodegradable azo-dye (Reactive Black 5) over a novel supported iron oxide catalyst at neutral pH. Journal of Molecular Catalysis A: Chemical 245: 78–86

Lin, S.S. and Gurol, M.D. (1998) Catalytic decomposition of hydrogen peroxide on iron oxide: kineics, mechanisms, and implications. Environmental Science andTechnology 32: 1417-1423.

Lu, M.C.; Chen, J.N. and Chang, C.P. (1999) Oxidation of dichlorvos with hydrogen peroxide using ferrous ion as catalyst. Journal of Hazardous Materials, B65: 277-288.

Lu, M.C.; Chen, J.N. and Huang, H.H. (2002) Role of Goethite Dissolution in the oxidation of 2-chlorophenol with hydrogen peroxide. Chemosphere 46: 131-136

Lunar, L.; Sicilia, D.; Rubio, S.; Perez-Bendito, D. and Nickel, U. (2000) Degradation of photographic developers by Fenton's reagent: condition optimization and kinetics for metal oxidation. Water Research 34, 6: 1791-1802.

MOI. (1992) The Hazardous Substances Act B.E. 2535, Ministry of Industry.

Pignatello, J.J. (1992) Dark and photoassisted Fe^{3+}-catalyzed degradation of chlorophenoxy herbicides by hydrogen peroxide. Environmental Science and Technology 26: 944-951.

Sarasa, J.; Corte, S.; Ormad, P.; Gracia, R. and Ovelleiro, J.L. (2002) Study of the aromatic by-products from ozonation of anilines in aqueous solution. Water Research 36: 3035-3044.

Sauleda, R. and Brillas, E. (2001) Mineralization of aniline and 4-chlorophenol in acidic solution by ozonation catalyzed with Fe^{2+} and UVA light, Applied Catalysis B: Environmental 29: 135-145.

Sun, J.H.; Sun, S.P.; Fan, M.H.; Gua, H.Q.; Qiao, L.P. and Sun, R.X. (2007) A kinetic study on the degradation of p-nitroaniline by Fenton oxidation process. Journal of Hazardous Materials 148: 172-177.

USEPA. (1985) Health and environmental effects profile for aniline. Environmental Criteria and Assessment Office, Office of Health and Environmental Assessment, Office of Research and Development, Cincinnati, OH. Available from: http://www.epa.gov/iris/subst/0350.html

Utset, B.; Garcia, J.; Casado, J.; Domenech, X. and Peral, J. (2000) Replacement of H_2O_2 by O_2 in Fenton and Photo-Fenton Reactions. Chemosphere 41: 1187-1192.

Zelmanov, G. and Semiat, R. (2008) Iron(3) oxide-based nanoparticles as catalysts in advanced organic aqueous oxidation. Water Research 42: 49

114

附件二

Thesis Title: Photoacatalytic Characteristics of Titanium Dioxide Doped with Various Elements under Visible-Light Activation

Student: Ms. Thapanan Putta **ID**: 5087805720

Program: National Center of Excellence for Environmental and Hazardous Waste Management (NCE-EHWM), Chulalongkorn University.

Credit Point: 36

Thesis Advisor: Assoc. Prof. Dr. Jin Anotai

Thesis Co-advisor: Prof. Dr. Ming-Chun Lu

Objectives:

The main objective of this study is to synthesize TiO_2 doping with various elements which can be activated by the visible-light region by using the sol-gel process. The specific objectives of this study are:

1. To study the photocatalytic activity of TiO_2 doping with various elements by using 2-chlorophenol as an organic probe.
2. To studies the optical and structural properties of TiO_2 doping with elements by using BET, TEM, XRD and XPS methods.

Hypothesis:

Doping can expand the photocatalytic activity of TiO_2 down to the visible light region.

Theoretical background:

Titanium Dioxide

Titanium dioxide, also known as titanium (IV) oxide or titania, is the naturally occurring oxide of titanium with the chemical formula "TiO_2". Normally, TiO_2 crystallizations have three polymorphic forms which are anatase, rutile, and brookite as shown in Figure 1.

TiO_2 is the most widely-used white pigment because of its brightness and very high refractive index. When deposited as a thin film, its refractive index and color make it an excellent reflective optical coating for dielectric mirrors and some gemstones. TiO_2 is also an effective opacifier in powder form, where it is employed as a pigment to provide whiteness and opacity to products such as paints, coatings, plastics, papers, inks, foods, medicines (i.e. pills and tablets) as well as most toothpaste. In cosmetic and skin care products, TiO_2 is used both as a pigment and a thickener. This TiO_2 pigment is used extensively in plastics and other applications for its UV resistant properties where it acts as a UV absorber, efficiently transforming destructive UV light energy into heat.

In the environmental applications, TiO_2 is the most preferable photocatalyst because of its physical and chemical stability and non-toxicity.

Photocatalytic process

Photocatalytic process is one process of advance oxidation processes (AOPs). These AOPs are very useful for the degradation of nonbiodegradable organic or toxic pollutants. Moreover, they are much more efficient than the conventional techniques such as coagulation, precipitation, adsorption on activated carbon in that the AOPs can lead to

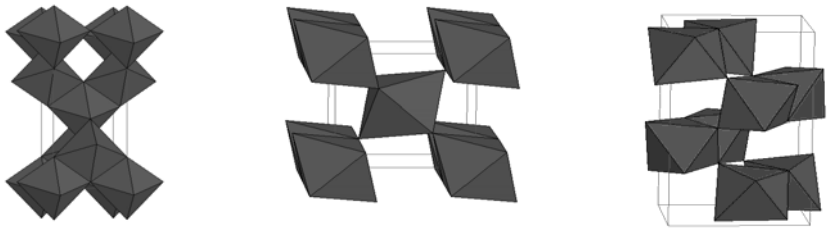

a) anatase **b) rutile**

c) brookite

Figure 1 crystallize form of TiO_2 [1].

the complete mineralization and can also dechlorinate the halogenous compounds.

Photocatalysis of TiO_2

Photocatalysis over a semiconductor oxide such as TiO_2 is initiated when TiO_2 absorbs ultraviolet (UV) radiation from sunlight or illuminated light source (fluorescent lamps), it will produce pairs of electrons and holes. The electron of the valence band of TiO_2 becomes excited when illuminated by light. The excess energy of this excited electron promoted the electron to transfer to the conduction band of TiO_2 creating the negative-electron (e^-) and positive-hole (h^+) pair. This stage is referred as the semiconductor's "photo-excitation" state. The energy difference between the valence band and the conduction band is known as the "Band Gap". Wavelength (λ) of the light necessary for photo-excitation of TiO_2 is 380 nm which is equivalent to 3.2 eV. The positive-hole of TiO_2 breaks apart the water molecule to form hydrogen gas and hydroxyl radical ($^{\bullet}OH$). The negative-electron reacts with oxygen molecule to form super oxide anion (O_2^-). These 2 powerful oxidizing agents will then disintegrate and rearrange the structure of the organic pollutants and convert them into CO_2 and H_2O. The overall process is illustrated in the Figure 2.

Photocatalysis of doping TiO_2

Recently, TiO_2 has been utilized as a photocatalyst for environmental remediation such as air-purification, deodorizing, sterilization, self-cleaning and water treatment. However, it is facing with two major limits in real practice. Firstly, TiO_2 requires UV of the wavelength shorter than 380 nm, whose energy exceeds the band gap of 3.2 eV of the anatase crystalline phase; hence, utilizing only a very small fraction of sunlight. Secondly, TiO_2 has a high recombination rate of

116

electron-hole pairs because it has wide band gap energy. The mechanism of TiO_2 photocatalysis mainly depends on the semiconductor interfacial redox reactions of electrons and holes. The efficiency of TiO_2 photocatalysis is low for its application because the photogenerated electron-hole pairs recombine rapidly after excitation leading to low charge carrier transfer rate on semiconductor surface.

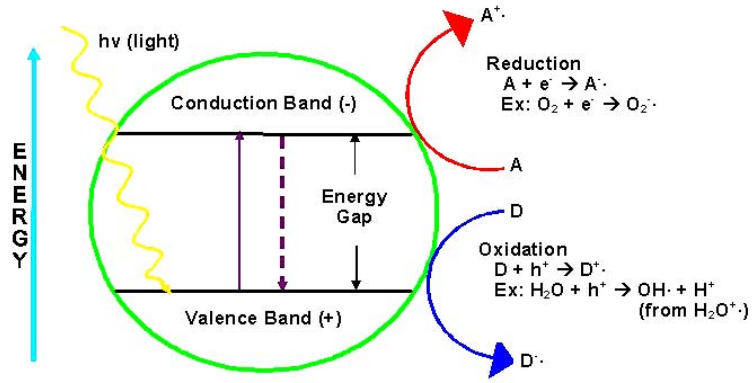

Figure 2 Schematic of photocatalytic process [2].

Three approaches have been made to reduce recombination of photogenerated electrons-holes and extend the light absorption of TiO_2 down to the visible region. The first is to introduce defects into the TiO_2 lattice by doping with transition metal ions. The second approach is to couple TiO_2 with other semiconductors in order to enhance the charge separation in the photocarriers generation process. The third possibility is to modify TiO_2 by surface deposition of noble metal.

Langmuir-Hinshelwood expression [3, 4]

Langmuir-Hinshelwood expression is one of kinetic model that used to analyze the heterogeneous photocatalytic oxidation [5, 6] on the assumption of no competition with reaction byproducts. The photocatalytic oxidation of 2-chlorophenol over TiO_2 complies with the following equation:

$$r = -\frac{d[2CP]}{dt} = \frac{k_r K[2CP]}{1+K[2CP]} \qquad (1)$$

Where "r" is the reaction rate for the oxidation of 2-chlorophenol ($M.min^{-1}$), "k_r" is the specific reaction rate constant for the oxidation of 2-chlorophenol ($M.min^{-1}$), "K" is the equilibrium adsorption constant of 2-chlorophenol (M^{-1}), and "[2CP]" is the concentration of 2-chlorophenol (M). This equation is a linear line when plotted between inverse initial rate and initial concentration as shown in equation 2.

$$\frac{1}{r} = \frac{1}{k_r} + \frac{1}{k_r K}\frac{1}{C} \qquad (2)$$

The constants, k_r and K, can be obtained from the intercept and slope of the line formed when "1/rate" is plotted against "1/C". The integrated form of equation 1 is shown in equation 3.

$$t = \frac{1}{k_r K} \ln\left(\frac{C}{C_0}\right) + \frac{1}{k_r}(C_0 - C) \qquad (3)$$

Where "C_0" is the initial concentration of 2-chlorophenol. When plot between "$t_{1/2}^*$" and initial concentration of 2-chlorophenol should be linear line as in the following equation:

$$t_{1/2}^* = \frac{0.5C_0}{k_r} + \frac{\ln 2}{k_r K} \qquad (4)$$

Where "$t_{1/2}^*$" is the half-life based on the initial rate (no effect of intermediate).

Sol-gel process

The sol-gel process is a flexible solution process for making ceramic and glass materials. In general, the sol-gel process involves the transition of a system from a liquid "sol" (mostly colloidal) into a solid "gel" phase. Applying the sol-gel process, it is possible to fabricate ceramic or glass materials in a wide variety of forms: ultrafine or spherical shaped powders, thin film coatings, ceramic fibers, microporous inorganic membranes, monolithic ceramics and glasses, or extremely porous aerogel materials.

The sol-gel process begins with the starting materials used in the preparation of the "sol" which are usually inorganic metal salts or metal organic compounds such as metal

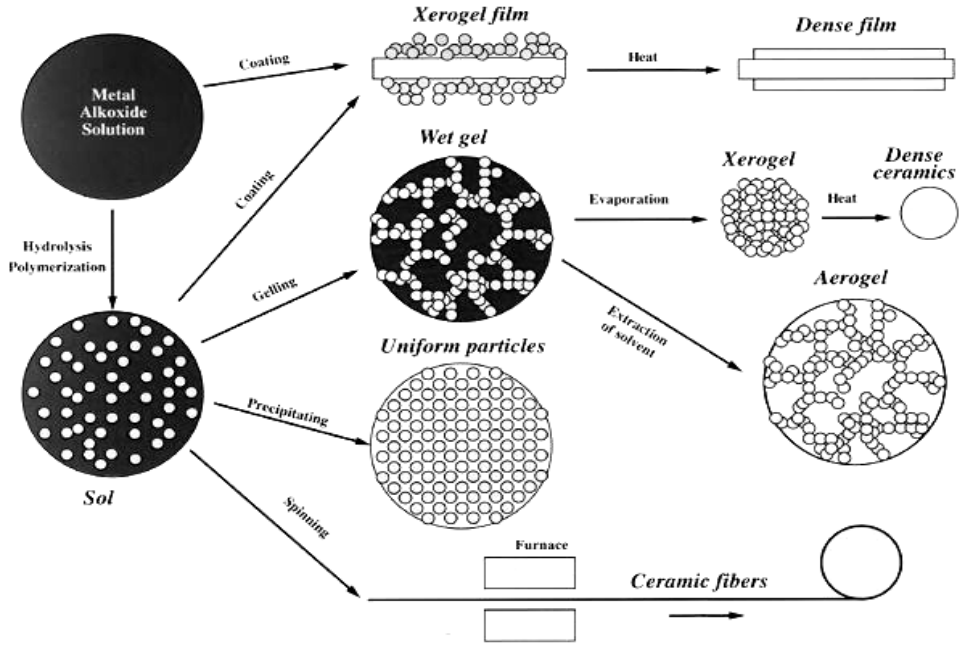

Figure 3 mechanism of sol-gel process [7].

118

alkoxides. In a typical sol-gel process, the precursor is subjected to a series of hydrolysis and polymeration reactions to form a colloidal suspension, or a “sol”. Further processing of the “sol” enables one to make ceramic materials in different forms. Thin films can be produced on a piece of substrate by spin-coating or dip-coating. When the “sol” is casted into a mold, a wet “gel” will form. With further drying and heat-treatment, the “gel” is converted into dense ceramic or glass articles. If the liquid in a wet “gel” is removed under a supercritical condition, a highly porous and extremely low density material called “aerogel” is obtained. As the viscosity of a “sol” is adjusted into a proper viscosity range, ceramic fibers can be drawn from the “sol”. Ultra-fine and uniform ceramic powders are formed by precipitation, spray pyrolysis, or emulsion techniques. Figure 3 shows the mechanism of sol-gel process.

2-Chlorophenol or ortho-Chlorophenol

2-chlorophenol is a benzene that is substituted with hydroxyl group (-OH) in first position and covalently bonded chlorine atoms in second or ortho position. 2-chlorophenol is produced by electrophilic halogenation of phenol with chlorine. It has a medicinal smell and is a slightly acidic liquid. According to the Notification of the Ministry of Industry No. 6 (1997), 2-chlorophenol is classified as a toxic hazardous waste and the industrial effluent standard for 2-chlorophenol is less than 1 mg/L. 2-Chlorophenol has been used as a biocide and disinfection and is also used as an intermediate in chemical industry. There are toxic for a wide range of organisms. 2-Chlorophenol is also used to preserve wood. It is used as an intermediate in the production of pesticides, dyestuffs and preservative. This chemical compound has an appearance as a light amber liquid at room temperature. 2-Chlorophenol is toxic to plants, fish and invertebrates. It spills have resulted in fish kills. Exposure to large quantities of 2-chlorophenol impairs algae reproduction and primary production. Biodegradation in soils is lightly to be reasonably rapid (day-weeks) and it binds moderately with soil/sediment particles, however for significant spills to land, leaching to groundwater may be possible. Bioaccumulation of 2-chlorophenol appears to be moderate. Explosive exposure to 2-chlorophenol can effect if swallowed, inhaled, or absorbed through the skin. 2-Chlorophenol may cause long-term adverse effects in the aquatic environment.

It may cause eye and skin damage, respiratory tract irritation, central nervous system effects, liver and kidney gastrointestinal system damage. The molecular structure and MSDS are shown in Figure 4 and Table 1 below.

2-Chlorophenol in wastewater

2-Chlorophenol represents an important water pollutant and has been named as the priority pollutant by the USEPA. The stability of the C–Cl bond in halo-hydrocarbons is responsible for their toxicity and persistence in the biological environment. The main entry routes of 2-chlorophenol to the aquatic environment are discharges from plants manufacturing it, or from plants those employ it as an intermediate in the production of higher chlorinated phenols or

phenoxy herbicides. Indirect sources include discharges from pulp and paper mills as by-products of chlorine-based bleaching, the release from manufacturing industries are significant with accidental spillage being negligible, as a result of disinfection of sewage and industrial wastewater with chlorine and from slow microbial breakdown of herbicides during post-application period. The compound is also used as a solvent for extracting sulfur and nitrogen compounds from coal.

2-Chlorophenol is very toxic and poorly biodegradable. A wastewater stream containing 2-chlorophenol over 200 mg/l may not be treated effectively by direct biological methods [8]. There are many researches studied on the oxidation of 2-chlorophenol under photocatalytic, electrocatalytic, and Fenton oxidation. It has been observed that the types and distribution of intermediates depended on the experimental conditions. Thus, catechol and cyclopentadienic acids were reported as major intermediates in photolysis, whereas phenol, hydroquinone, benzoquinone, chlorohydroquinone, and hydroxyhydroquinone were formed under photocatalytic conditions.

It is reported that higher pH discouraged the formation of aromatic intermediates. Moreover, when organochlorine compounds undergo oxidation, they may produce other organochlorine compounds that may be more toxic than the parent compound itself.

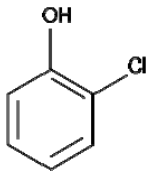

Figure 4 2-Chlorophenol molecular structure.

Table 1 MSDS of 2-Chlorophenol.

Name	2-Chlorophenol / 2-ydroxychlorobenzene/ *o*-Chlorophenol
CAS number	[95-57-8]
Molecular formula	C_6H_5ClO
Molar mass	128.56 g/mol
Appearance	Light amber, liquid
Density	1.262 g/cm³, liquid
Melting point	8 °C /(46.40°F)
Boiling point	173.0 - 175.0 °C
Solubility in water	Slightly Soluble (20-25°C)

Literature reviews:

120

TiO_2 is one of the most preferable photocatalyst because of its optical and electronic properties, stability, low cost and non-toxicity, and can be applied in eliminating persistent organic pollutants in air or water. However, the wide spread technological applications of TiO_2 are impaired by its wide band gap (3.2 eV) which requires ultraviolet irradiation (wavelength <380nm) for photocatalytic activation [9]. Research efforts have been performed to synthesize specific TiO_2 that can be effectively activated by visible light, the main portion of solar light. It was initially reported that the doping of various transitional metal ions into TiO_2 could shift its optical absorption edge from UV into visible light range.

In 2005, Liu *et al*. [9] synthesized the visible-light responsive TiO_2-V_2O_5 photocatalyst by using a binary sol-gel and in-situ intercalation method. The photoactivity of the prepared catalyst under UV and visible light irradiation were evaluated by decolorization of methylene blue solution. The results showed that the composite catalyst displayed a homogeneous anatase phase, and the vanadium pentoxide species was highly dispersed in the TiO_2 phase. The composite catalyst responded to visible light because of the narrowed band gap.

Huang *et al*. [10] studied Pt/N-codoped TiO_2 nano tubes and its photocatalytic activity under visible light by photodegradation of Rhodamine B in an aqueous solution. It was confirmed that Pt/N-codoped TiO_2 nanotubes could be excited by visible light and the recombination rate of electron–hole pairs reduced significantly. The higher visible light activity was due to the codoping of nitrogen and platinum.

Ishibai *et al*., (2008) [11] synthesized TiO_2 photocatalyst with Pt-modification which was active to visible-light. The results showed that Pt on the surface of TiO_2 increased photocatalytic activity under visible light irradiation, depending on the calcination temperature. The temperature correlated with the light absorption properties of the Pt complex on TiO_2 nano-particles. It was found that TiO_2 surface structure played an important role in the formation of Ti–O–Pt bonds resulting in a large visible light absorbance and high photocatalytic activity under visible light irradiation.

F-doped TiO_2 film prepared in the low-temperature was studied by Xu *et al*. [12]. The photocatalytic activity was evaluated by decomposing X-3B under artificial solar light. The results showed that the crystallinity of TiO_2 was improved by F-doping. Fluoride ions could prevent the grain growth, and the transformation of anatase to rutile phase was also inhibited. F-doped TiO_2 film exhibited better photocatalytic activity. The high photocatalytic activity of F-doped TiO_2 film may due to extrinsic absorption through the creation of oxygen vacancies rather than the excitation of the intrinsic absorption band of bulk TiO_2.

Lin *et al*. [13] studied the degradation of 4-chlorophenol in TiO_2, WO_3, SnO_2, TiO_2/WO_3 and TiO_2/SnO_2 systems and found that TiO_2/WO_3 increased the band edge wavelength to 475 nm and the gap energy decreased reduced to 2.61 eV. Although the specific surfaces area of TiO_2/WO_3 decreased due to its larger size as compared to either TiO_2 or WO_3, the 4-chlorophenol degradation efficiency significantly increased as compared to single TiO_2 or WO_3 system at 435 nm wavelength. The TiO_2/WO_3 degradation of 4-chlorophenol at 369 nm was inhibited. For TiO_2/SnO_2, the degradation efficiency also suffered at 369 nm, and only slightly increased as

compared to the single TiO_2 or SnO_2 system.

Shchukin *et al*. [14] synthesized nanocrystalline bicomponent TiO_2-In_2O_3 powder and studied the photodegradation of 2-chlorophenol in water. From the results, it found that photocatalytic activity increased with decreasing In_2O_3. The concentrations of the main aromatic intermediate products (chlorohydroquinone and catechol) were considerably lower for TiO_2-In_2O_3 photocatalysts than pure TiO_2. On the basis of various characterizations of the photocatalysts, the reasons invoked to explain the photocatalytic activity enhancement of In_2O_3 included a better separation of photogenerated charge carriers, an improved oxygen reduction and an increased surface acidity inducing a higher extent of adsorption of the aromatics.

Barakat *et al*. [15] studied the photocatalytic degradation of 2-chlorophenol by nanoparticles Co-doped TiO_2. The results revealed that Co-doped TiO_2 exhibited high activity for UV-photocatalytic degradation of 2-chlorophenol. The efficiencies of the 2-chlorophenol photodegradation were 93.4% and 96.4% at solution pH of 9 and 12, respectively. The presence of Co ion in the TiO_2 structure caused a significant absorption shift towards the visible region.

Scopes of the study:

-Sol-gel techniques will be used to synthesize TiO_2 with and without doping.

-All the experiments will be conducted at 1 atm.

-All the photocatalytic processes will be done with synthetic wastewater using 2-chlorophenol as an organic probe in a lab-scale reactor at 25°C.

Methodology:

Materials

-Tetra(n-butoxyl) titanium ($Ti(O\text{-}Bu)_4$) will be purchased from Fluka Chemical Co.

-Sodium tungsten Dihydrate ($Na_2WO_4.2H_2O$) will be optained from Fluka Chemical Co.

-Ammonium florine (NH_4F) will be obtained from merck Chemical Co.

-Tetraamineplatinum(II) nitrate ($Pt(NH_4)_4(NO_3)_2$) will be from Sigma-Aldrich Co.

-2-chlorophenol will be from Fluka Chemical Co.

-H_2SO_4 and NaOH will be used to adjust/control the pH.

-All reagents will be prepared by using the demineralized water.

Experimental

The experimental works will be divided into two parts as follows :

Part 1: TiO_2 Synthesis

Without doping

Synthetic TiO_2 without doping will be synthesized by slowly adding 0.05 mole of tetra (n-butoxyl) titanium into 70 mL anhydrous alcohol controlling at 4°C to prepare a clear tetra (n-butoxyl) titanium ethanol solution. At the same time, 20 ml of distilled water will be added into 20 ml of anhydrous ethanol alcohol to make ethanol aqueous solution. Tetra (n-butoxyl) titanium ethanol solution and ethanol aqueous solution will be mixed together for 1 hour and then

122

the acid or base catalyst will be added into the solution. Mixed liquor will be thoroughly mixed to undergo hydrolytic condensation for the required period. After that the resulting precipitate will be put into an oven to dry at 110°C for 2 hours. Finally TiO_2 powder will be calcined at appropriate temperature and maintained at that temperature at selected time interval. The overall procedure of synthetic TiO_2 is illustrated in the Figure 5 below.

Doping with tungsten (W/TiO_2)

The W/TiO_2 will be synthesized following the similar procedures as mentioned above; however, appropriate amount of $Na_2WO_4.2H_2O$ will be added to the ethanol aqueous solution before mixing with the tetra (n-butoxyl) titanium ethanol solution.

Doping with fluorine (F/TiO_2)

In this experiment, all procedures will be similar to the case of tungsten doping except the NH_4F will replace the $Na_2WO_4.2H_2O$.

Doping with platinum (Pt/TiO_2)

In this experiment, all procedures will be similar to the case of tungsten doping except the $Pt(NH_4)_4(NO_3)_2$ will replace the $Na_2WO_4.2H_2O$.

Optimization of TiO_2 Synthesis

-Effect of calcination temperature

Calcine temperature will be varied from 150 to 500°C .

-Effect of ramp rate

During the calcination, the temperature will be raised at different rate from 1 to 4 and 9°C/min.

-Effect of catalyst type

From literature survey, it was found that good catalytic property is governed by two major opposing physical properties: crystallinity and surface area of the photocatalysts. The high crystallinity helps to prolong the recombination rate, hence, strongly increases the activity of the photocatalyst. The high surface area helps to facilitate adsorption of the target molecules onto the surface of the catalyst [16]. From these reasons, effect of catalyst type which will be categorized into 2 groups will be studied. Firstly, acid group including HNO_3, H_2SO_4, H_3PO_4 and HCl will be used. Secondly, base group in which the diethanolanime will be used as the catalyst.

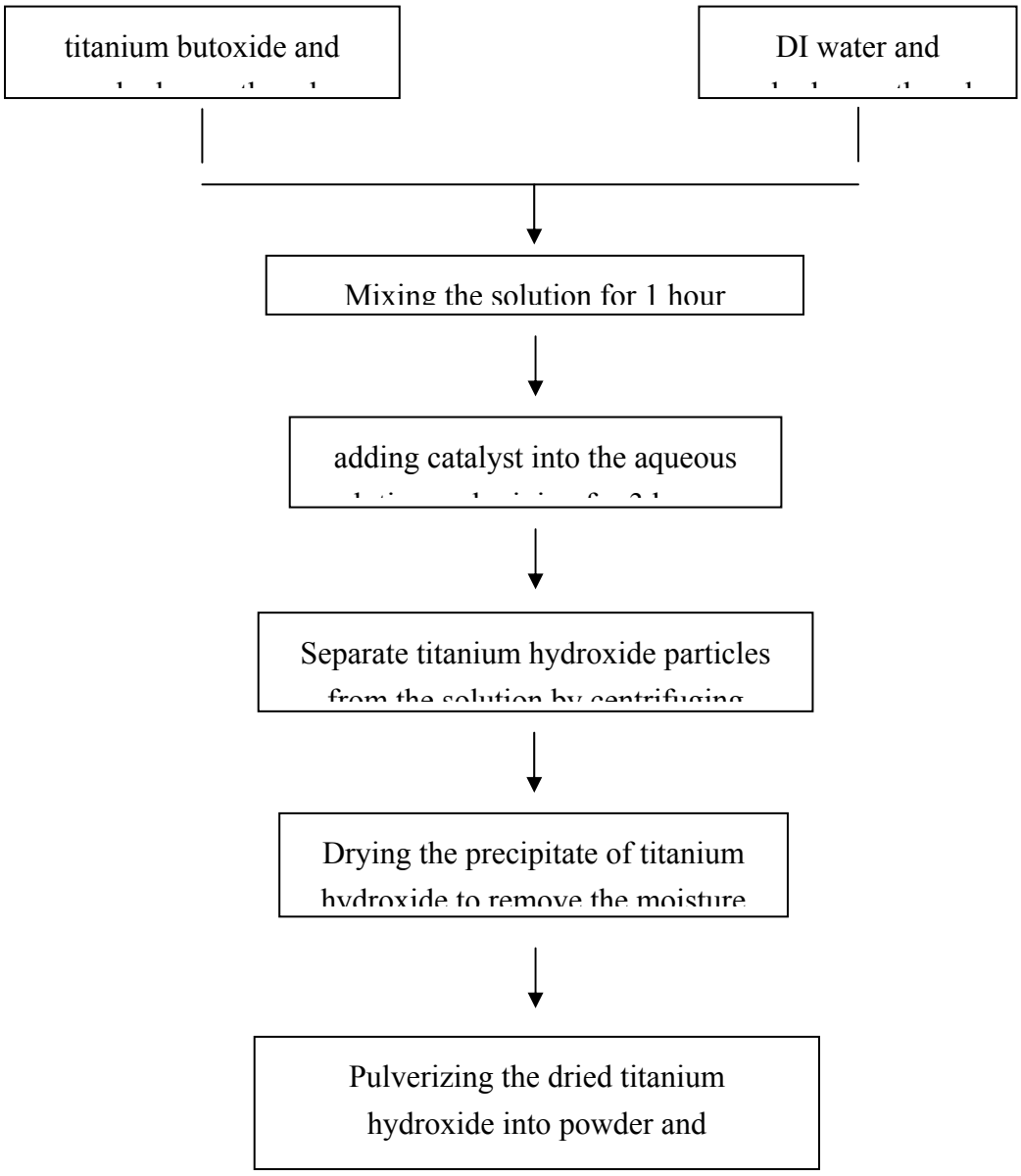

Figure 5 Schematic for TiO_2 synthesis.

Part 2: Determination of the TiO_2 activity

The photocatalytic activity will be evaluated by the oxidation of 2-chlorophenol over the visible light, which will be carried out in a batch mode reactor. Synthetic TiO_2 of 1 g will be mixed in 1 liter solution of 0.01-0.1 mM 2-chlorophenol. Prior to irradiation, the suspension will be stirred for 30 minutes to allow for the adsorption onto the TiO_2 surface reach equilibrium. Laser emitting diodes (LEDs) will provide the lights in visible range, i.e., either blue (430-530nm), green (470-570nm), or red (580-670nm. The residue 2-chlorophenol will be measured which represents

124

the activity of the synthetic TiO_2. The pH and temperature were controlled through out the experimental period. The following scenarios will be performed to determine the effect on TiO_2 property and 2-chlorophenol degradation:

-2-Chlorophenol adsorption onto TiO_2 surface

-Effect of TiO_2 dose

-Effect of light wavelength

-Effect of light intensity

-Effect of pH

-Effect of 2-chlorophenol concentration

3. Analytical methods

-Scanning electron microscopy (SEM) will be used to observe the particulate morphology of synthetic TiO_2.

-X-ray diffraction (XRD) will be performed to get the crystal structure of synthetic TiO_2.

-Brunauer-Emmett-Teller (BET) will be used to determine the surface area and pore size distribution of the synthetic TiO_2.

-UV-VIS spectrophotometer will be used to analyze the absorption spectrographs of the synthetic TiO_2 photocatalyst.

-Point of zero charge(PZC) will be determined the surface charge of synthetic TiO_2.

-4-aminoantipyrine colorimetric method will be used to analyze residual concentration of 2-chlorophenol. One ml of buffer solution, 1 ml of 4-amino-antipyrine solution, 1 ml of potassium ferric cyanide solution will be added into the 2-chlorophenol water sample and mixed together to produce a color reaction product. The color intensity representing the 2-chlorophenol concentration will be measured by a UV-vis spectrophotometer.

References:

1. Smyth, J. R. TiO_2 group. Mineral Structure and Property Data [online]. 2008. available from: http://ruby.colorado.edu/~smyth/min/tio2.html [2008, july 20]
2. Photocatalysis.Visible-Light Photocatalysis: A Cleaner Way of Life [online]. 2005. available from: http://dev.nsta.org/evwebs/1952/photocatalysis.htm[2008, july 20]
3. Watts, R.J. (1998) **Hazardous Wastes**, John Wiley & Son Inc., New York : 354
4. Chang, H.T., Wu, N.M. and Zhu, F. (2000) **A Kinetic model for Photocatalytic Degradation of Organic Contaminants in thin - film TiO_2 Catalyst**. Water Research**,** 34: 407-416.
5. Chen, C.W., Dong, C.D., and Liao, Y.L. (2003) **Photocatalytic degradation of 2,4-dichlorophenol in aqueous TiO_2 suspensions.** Asian-Pacific Regional Conference on Practical Environmental Technologies. A2-55-A2-61
6. Lu, M.C., Roam, G.D., Chen, J.N., and Huang, C.P. (1993) **Factors affecting the photocatalytic degradation of dichlorvos over titanium dioxide supported on glass**. Journal of Photochemistry and Photobiology A: Chemistry**,** 76: 103-110
7. Chemat technology. sol-gel technology[online]. 1998. available from: http://www.chemat.com/html/solgel.html [2008, july 20]

8. Callahan, M.A., Slimak W., Gabel,N.W., May, I.P., Foeler, C.F., Freed, J.R., Jennings, P., Durfee, R.L., Whitemore, F.C., Maestri B., Mabey, N.R., Holt, B.R., and Gould, C. **Water-related Environmental Fate of 129 Priority** US Environmental Protection Agency, Washington DC, 1979.

9. Liu, J., Yang, R. and Li, S. A. (2005). **Preparation and characterization of the TiO_2-V_2O_5 photocatalyst with visible-light activity**. Rare Metals, 25: 636-641

10. Huang, L. H., Sun,C. and Liu, Y. L. (2007). **Pt/N-codoped TiO_2 nano tubes and its photocatalytic activity under visible light.** Applied surface science, 253: 7029-7035.

11. Ishibai, Y., Sato,J., Nishikawa, T. and Miyagishi, S. (2007). **Synthesis of visible-light active TiO_2 photocatalyst with Pt-modification: Role of TiO_2 substrate for high photocatalytic activity**. Applied Catalysis B: Environmental, 79: 117-121

12. Xu, J., Ao, Y., Fu, D. and Yuan, C. (2008). **Low-temperature preparation of F-doped TiO_2 film and its photocatalytic activity under solar light**. Applied Surface Science, 254: 3033–3038

13. Lin, C. F., Wu, C.H. and Onn, Z.N. (2008). **Degradation of 4-chlorophenol in TiO_2, WO_3, SnO_2, TiO_2/WO_3 and TiO_2/SnO_2 systems**. Journal of Hazardous Materials1, 54: 1033–1039

14. Shchukin, D., Poznyak S., Kulak A. and Pichat P.(2004) **TiO_2 -In_2O_3 photocatalysts: preparation, characterisations and activity for 2-chlorophenol degradation in water.** Journal of Photochemistry and Photobiology A : Chemistry, 162 :423–430

15. Barakat, M.A., Schaeffer, H., Hayes, G. and Ismat-Shah, S. (2005) **Photocatalytic degradation of 2-chlorophenol by nanoparticles Co-doped TiO_2.** Applied Catalysis B: Environmental, 57: 23–30

16. Kanna, M. and Wongnawa, S. (2008) **Mixed amorphous and nanocrystalline TiO_2 powders prepared by sol-gel method: Characterization and photocatalytic study**. Materials Chemistry and Physics, 110: 166–175

行政院國家科學委員會補助國內專家學者出席國際學術會議報告

99 年 5 月 5 日

報告人姓名	盧明俊	服務機構及職稱	嘉南藥理科技大學教授
時間 會議 地點	2009.11.30-12.2 紐西蘭北帕默斯頓	本會核定 補助文號	NSC96-2628-E-041-002-MY3
會議 名稱	(中文) 水與工業 2009 研討會 (英文) Water & Industry 2009 Conference		
發表 論文 題目	(中文) 比較各種不同芬頓程序氧化 2,6-二甲基苯胺 (英文) Comparison of 2,6-dimethylaniline oxidation in different Fenton processes		

一、 參加會議經過

IWA 為國際知名學術性組織，所出版的 Water Research 學術地位崇高，此外，除了年會上所發表之論文外，另有專門技術學群之研討會配合召開。，此次於紐西蘭舉辦 2009 水與工業 2009 研討會（**Water & Industry 2009 Conference**），主要是希望透過相關論文的發表，促進國際交流，使工業廢水的水質獲得改善，此次行程如下:

日	日期		停留城市	時間	狀態	服務
六	11月28日	出發	台北桃園(TPE) 台北桃園(TPE) 第一航站	1200	CX 421 經濟艙(L)	直飛 波音 777
		抵達	香港(HKG) 香港國際機場(HKG) 第一航站	1350	機位OK	01小時 50分鐘 午餐
六	11月28日	出發	香港(HKG) 香港國際機場(HKG) 第一航站	1525	CX 117 經濟艙(L)	直飛 空中巴士 340-300
	11月29日	抵達	奧克蘭(AKL) 奧克蘭(AKL)	0730	機位OK	11小時 05分鐘 餐點

日 11月29日 出發 奧克蘭(AKL) 奧克蘭(AKL) 1000 NZ 8345 直飛
DOMESTIC TERMINAL 經濟艙(V)迪哈維DHC-8-300 DASH 8/8Q
抵達 北帕默斯頓 (PMR) 北帕默斯頓(PMR) 1105 機位OK 渦輪螺旋槳
01小時 05分鐘
奧克蘭(AKL) - 北帕默斯頓 (PMR) 實際飛行: /AIRNZ LINK

四 12月03日 出發 北帕默斯頓 (PMR) 北帕默斯頓(PMR) 1155 NZ 8334 直飛
經濟艙(Q)迪哈維DHC-8-300 DASH 8/8Q
抵達 奧克蘭(AKL) 奧克蘭(AKL) 1300 機位OK 渦輪螺旋槳
DOMESTIC TERMINAL 01小時 05分鐘
北帕默斯頓 (PMR) - 奧克蘭(AKL) 實際飛行: /AIRNZ LINK

四 12月03日 出發 奧克蘭(AKL) 奧克蘭(AKL) 1440 CX 108 直飛
經濟艙(L)波音 747-400
抵達 香港(HKG) 香港國際機場(HKG) 2040 機位OK 11小時 00分鐘
第一航站 餐點

四 12月03日 出發 香港(HKG) 香港國際機場(HKG) 2220 CX 408 直飛
第一航站 經濟艙(L)空中巴士 330
抵達 台北桃園(TPE) 台北桃園(TPE) 2355 機位OK 01小時 35分鐘
第一航站 免費茶點

首先，由台北桃園抵達香港國際機場後需換機，改搭空中巴士，於 11 小時以後的隔日抵達紐西蘭的奧克蘭，再換小飛機迪哈維抵達北帕默斯頓，最後搭出租車抵達住宿處。

本次研討會共分 3 天，各國學者、專家參加人數計約 100 多人，同時有兩個會場舉

辦兩類不同類別的 Oral 論文發表，會議主題如下：

1. 工業廢水的物理程序
2. 生物程序
3. 高級技術程序
4. 廢棄物減量
5. 環境政策與管理
6. 個案研究

會場全部以英文報告和討論，另有 1 個 Poster 會場同時舉行，會場是在當地 Massey 大學科學學院中的一棟研究大樓裡面。本人是以口頭報告展示研究成果，篇名為”比較各種不同芬頓程序氧化 2,6-二甲基苯胺”，安排在第 3 天的最後一場，會議中與來自各國學者充分討論與交換意見。另外本次會議也與來自山東大學之教授（照片中之三位女士）及來自台灣之博士後研究員（照片左一及左二）交流。

二、 與會心得

電-芬頓法與流體化床-芬頓法為可改善傳統 Fenton 法產生大量的化學污泥而衍伸出來的新 Fenton 法。電-芬頓法是利用電解還原的方式使 Fe^{3+}在陰極還原為 Fe^{2+}作為催化劑，催化過氧化氫以產生氫氧自由基，提高有機物氧化效率。此法適合處理高濃度 COD 且難生物分解的有機廢液，且反應過程幾乎不會產生鐵污泥。流體化床-芬頓是藉由流體化床-芬頓處理槽中進行 Fenton 反應，反應後產生之鐵氧化物會沉積於擔體上並結晶，在擔體上形成之鐵氧化物亦具有異相催化效果，進而達到化學污泥減量及低處置成本之效益。

實際廢水中的化學物質成份複雜，常含有大量及多種類的陰離子，其存在於 Fenton 反應中會

對系統的反應能力造成極大的影響 Fenton 反應對陰離子的存在很敏感，其中以 PO_4^{3-}對 Fenton 系統的影響最大，主要原因為 PO_4^{3-}會與系統中的鐵或亞鐵離子產生錯合物，降低鐵離子的催化能力，因而使系統無法有效去除苯胺。另外 Cl^-會和 Fe^{3+}作用產生複合物，但 Fe^{3+}複合物並無法有效和 H_2O_2 作用，因此，阻礙了氫氧自由基的形成，尚有 Cl^-亦會和有機物競爭氫氧自由基，此些原因皆造成處理效率下降。本次研討會中，多種工業廢水處理程序被提出討論，然而對於高濃度具有毒性之工業廢水，仍以 Fenton 系列之技術最有應用之潛力。

三、攜回資料名稱及內容

1.研討會論文集: 主要是收錄研討會全部文章的電子檔。

2.研討會摘要集: 主要內容是收錄研討會之摘要。

Comparison of 2,6-dimethylaniline oxidation in different Fenton processes

Ming-Chun Lu[*], Yao-Hui Huang[**] and Wang-Ping Ting[***]

[*] *Department of Environmental Resources Management, Chia Nan University of Pharmacy and Science, Tainan 717, Taiwan.* (E-mail: mmclu@mail.chna.edu.tw)
[**] *Sustainable Environment Research Center, National Cheng Kung University, Tainan 701, Taiwan.* (E-mail: yhhuang@mail.ncku.edu.tw)
[***] *Energy and Environment Research Laboratories, Industrial Technology Research Institute, Hsinchu 31040, Taiwan.* (E-mail: pp0406@yahoo.com.tw)

Abstract Fenton technologies for wastewater treatment have shown their worthiness in the field of toxic compounds elimination. The study explored the effects of hydrogen peroxide concentration and UV light on the oxidation processes. However, total mineralization through these technologies is expensive compared with biological ones. Therefore, partial chemical oxidation of toxic wastewaters with Fenton processes followed by biological units may increase the application possibility of Fenton technologies. Consequently, the detection of oxidation intermediates and their biodegradable efficiencies after treatment by Fenton, electro-Fenton and photoelectro-Fenton processes were investigated in the study.

2,6-Dimethylaniline (2,6-DMA) was the target compound in this study. Results show that the UV light promoting efficiency, $r_{PE\text{-}F}/r_{E\text{-}F}$, were 2.01, 2.56 and 2.66 while the initial concentration of hydrogen peroxide increased from 15 to 20 and 25 mM, respectively. It can be concluded that the UV irradiation promoted the 2,6-DMA degradation significantly. Biodegradability results show that for electro-Fenton and photoelectro-Fenton processes, the ratios of BOD_5/TOC increased with time of reaction. It means that the 2,6-DMA can be successfully detoxified in the electro-Fenton and photoelectro-Fenton processes. Some organic intermediates; i.e. aminobenzene, nitrobenzene, 2,6-dimethylphenol, phenol and oxalic acid were detected in the different oxidation processes.
Keywords: 2,6-dimethylaniline; electro-Fenton process; photoelectro-Fenton process

INTRODUCTION

2,6-Dimethylaniline (2,6-DMA) is used mainly as an intermediate in the manufacture of azo dyestuffs and pharmaceuticals agents. Large amounts of aromatic amine compounds have been produced for the synthesis of dyes and released into the environment as waste during their manufacture and use Although 2,6-DMA has been produced and applied for a long time, little information is available on its toxicology and environmental behavior (Ting et al., 2009).

Recently, more demanding requirements imposed by law to the treatment plants have forced on the development of new alternatives, like stronger oxidizing agents or advanced oxidation processes (AOPs). AOPs are defined as the oxidation processes that generate hydroxyl radicals in sufficient quantity for wastewater treatment (Walling, 1975). The Fenton reaction is a widely used and studied catalytic process based on an electron transfer between hydrogen peroxide and ferrous ions acting as a homogeneous catalyst. The process may be applied on the treatment of wastewaters, sludge, and contaminated soils for reducing toxicity, improving biodegradability, and removing odor and color (Lu, 1999&2003). During the Fenton process, hydrogen peroxide is catalyzed by ferrous ions to produce hydroxyl radicals (Walling, 1975).

$$Fe^{2+} + H_2O_2 \rightarrow Fe^{3+} + OH^- + {}^{\bullet}OH \qquad k = 53\sim76\ M^{-1}s^{-1} \qquad (1)$$

This reaction is propagated from ferrous ion regeneration mainly by the reduction of the produced ferric species with hydrogen peroxide (Walling, 1975).

$$H_2O_2 + Fe^{3+} \rightarrow Fe^{2+} + {}^{\bullet}H_2O + H^+ \qquad k = 0.01\ M^{-1}s^{-1} \qquad (2)$$

However, in the Fenton chain reactions, the rate constant of equation (1) is between 53 and 76 $M^{-1}s^{-1}$ (Rigg et al., 1954; Metelitsa, 1971; Walling, 1975), while that of equation (2) is only 0.01 $M^{-1}s^{-1}$ (Walling, 1975). This means that ferrous ions are consumed more rapidly than they are produced. However, the iron species need to be removed leading to production of large amount of ferric hydroxide sludge, which requires additional separation and disposal processes.

An electrochemical application method in the Fenton processes, named the electro-Fenton method, has been reported. Different authors have shown that in aqueous mediums, several non-biodegradable organic pollutants can be detoxified in both the Fenton and electro-Fenton processes (Sirés et al., 2007a&2007b; Brillas et al., 2003). Furthermore, electro-Fenton methods with UV irradiation are also being developed for wastewater treatment, so-called photoelectro-Fenton process (Boye et al., 2002; Flox et al., 2007). The process is irradiated with UV light under electro-Fenton conditions. The action of this irradiation is complex and can be described as: (i) the production of a greater amount of hydroxyl radicals from the photoreduction of $Fe(OH)^{2+}$, the predominant Fe^{3+} species in acid medium, by equation (3) and (ii) the photolysis of complexes of Fe(Ⅲ) with generated carboxylic acids, as shown in equation (4) (Exposito et al., 2007).

$$Fe(OH)^{2+} \xrightarrow{h\nu} Fe^{2+} + {}^{\bullet}OH \qquad (3)$$

$$R(CO_2) - Fe(\text{Ⅲ}) + h\nu \rightarrow R({}^{\bullet}CO_2) + Fe(\text{Ⅱ}) \rightarrow {}^{\bullet}R + CO_2 \qquad (4)$$

Although advanced oxidation technologies for wastewater treatment show high efficiency but work at high consume of energy and reagents. AOPs were classified as expensive treatment option, but the cost can be minimized and optimized such as integration of chemical and biological treatment processes. Partial chemical oxidation of a toxic wastewater may increase its biodegradability up to high levels. Therefore, detection of intermediates and biodegradable efficiencies for Fenton, electro-Fenton and photoelectro-Fenton processes were investigated in the study.

MATERIALS AND METHODS

Chemicals and analytical method

2,6-DMA (purity, 98%), ferrous sulfate and hydrogen peroxide (purity, 35%) were manufactured by Merck. The rest of the used reagents were at least reagent grade. All the preparations and experiments were conducted at 30±2 ^{o}C. The 2,6-DMA was analyzed by an HP4890 gas chromatography with a flame ionization detector and an HP-5 column (0.53 mm in inside diameter, 15 m long). The concentration of hydrogen peroxide was analyzed using a titanium sulfate spectrophotometric method (Roland et al., 1997). Biodegradability was measured by the 5-day biochemical oxygen demand (BOD_5) analysis. TOC was determined with an Elementer-liquid TOC total organic carbon analyzer (Germany). The intermediates were detected by a gas chromatography mass spectrometry (GC-MS) using an HP 6890 gas chromatography and an HP 5975 mass spectrometer. DB-5MS capillary column (30 m x 0.25 mm i.d., 0.25 lm film, from J&W, USA) was used. The GC temperature program was as follows: 40 °C for 2 min, followed by a 15 °C/min ramp to 280 °C, and hold for 5 min.

Experimental apparatus

The cylindrical reactor (radius: 6.5 cm and height: 35 cm) was operated at a constant current mode. The total volume of the reactor was 3.5 liters. The anode used was a titanium net coated with RuO_2/IrO_2 (DSA), and the cathode was made of stainless steel. The double electrode cell had a DSA anode with an

inside diameter of 7 cm, and the cathode had 2 cm and 13 cm stainless steel walls.

Electro-Fenton process

Solutions with 1 mM 2,6-DMA (corresponding to 96 mg/L total organic carbon (TOC)) and 50 mM $NaClO_4$ as background electrolyte were treated by all Fenton processes for comparison. The ferrous ions were added after the pH was adjusted to the desired value. The pH of the solution was not controlled during the reaction. In the meantime, the power supply was turned on, and hydrogen peroxide was added to initiate the reaction. Fenton reaction was stopped instantly by adding NaOH to the reaction mixtures after sampling. The samples were filtered with Toyo 0.45 μm mixed cellulose ester filters to remove precipitates before analysis.

Photoelectro-Fenton process

The irradiation source was a set of sixteen 3 W UV lamps (Sunbeamtech Com) fixed inside a cylindrical Pyrex tube (allowing wavelengths $\lambda>320$ nm to penetrate). In addition to all the experimental conditions mentioned above, UV lights with maximum wavelength of 360 nm was irradiated inside the reactor, supplying a photoionization energy input of 48 W to the solution.

RESULTS AND DISCUSSION

Degradation of 2,6-DMA

The degradation of 2,6-DMA was explored by electro-Fenton and photoelectro-Fenton processes. To compare the performance of different oxidation processes, three indexes: (i) the stoichiometric efficiency (E), (ii) the rate constant (k_{obs}) and (iii) UVA-promoted efficiency ($r_{PE\text{-}F}/r_{E\text{-}F}$) were evaluated. An index, E, is defined as below:

$$E\ (mM/mM) = \Delta[\text{pollutant}]/\Delta[H_2O_2] \quad (5)$$

To evaluate the effect of UVA light on the degradation of 2,6-DMA, electro-Fenton and photoelectro-Fenton processes were compared at different concentrations of hydrogen peroxide (15, 20 and 25 mM). Table 1 indicates that higher hydrogen peroxide concentrations induced faster 2,6-DMA degradation, but reduce E. These phenomena may be due to the hydroxyl radical scavenging effect of hydrogen peroxide as shown by equation (6) (Walling, 1975; Rigg., 1954).

$$H_2O_2 + {}^{\bullet}OH \rightarrow H_2O + {}^{\bullet}HO_2 \quad k = 2.7\times10^7\ M^{-1}s^{-1} \quad (6)$$

Table 1 Comparison of various oxidation processes by Stoichiometric efficiency (E) and kinetic constant (k_{obs})

$[H_2O_2]$ (mM)	Electro-Fenton process			Photoelectro-Fenton process		
	C/C_0 (%)	E (mM/mM)	K_{obs} (min^{-1})	C/C_0 (%)	E (mM/mM)	K_{obs} (min^{-1})
15	61	0.0548	0.0096	28	0.1122	0.0194
20	50	0.0457	0.0123	12	0.0744	0.0314
25	43	0.0320	0.0153	9	0.0489	0.0408

Experimental conditions: [2,6-DMA] =1 mM; Fe^{2+}=1 mM; H_2O_2= 20 mM; pH_i=2.0; $NaClO_4$= 50 mM; CD_a= 7.6 A/m^2; CD_c=7.1 A/m^2; 48 W UVA irradiation; reaction time=60 min

The degradation of 2,6-DMA in the electro-Fenton and photoelectro-Fenton processes follows pseudo-first-order kinetics in which the *k* value is determined by the following expression:

$$\ln C / C_0 = kt \tag{7}$$

where C_0 represents the initial concentration of the organic compound, and C represents the concentration of the organic compound at time, t. The first-order rate constants (k_{obs}) were determined from the slopes of the plots of $\ln([2,6\text{-DNA}]_t/[2,6\text{-DNA}]_0)$ vs. time ($R \geq 0.95$). The k_{obs} values for 2,6-DMA degradation in each process were determined as shown in Table 1. The degradation rate of electro-Fenton process with UV irradiation would be faster than that without it. The photoelectro-Fenton process exhibited a good ability on the degradation of organic contaminants in this work. It is due to the fact that ferrous ion catalyst can be regenerated through the photoreduction of ferric ions, and then catalyzes hydrogen peroxide to produce highly reactive hydroxyl radicals. These findings confirm that UV light contributed the additional generation of hydroxyl radicals in the photoelectro-Fenton process.

Table 2 UVA irradiation promoting the efficiency of 2,6-DMA oxidation

$[Fe^{2+}]$ (mM)	$[H_2O_2]$ (mM)	$r_{E\text{-}F}$	$r_{PE\text{-}F}$	$r_{PE\text{-}F}/r_{E\text{-}F}$
1	15	0.0096	0.0194	2.01
1	20	0.0123	0.0314	2.56
1	25	0.0153	0.0408	2.66

Experimental conditions: [2,6-DMA] =1 mM; Fe^{2+}=1 mM; H_2O_2= 20 mM; pH_i=2.0; $NaClO_4$= 50 mM; CD_a= 7.6 A/m^2; CD_c=7.1 A/m^2; 48 W UVA irradiation

The role of UVA irradiation in promoting the oxidation efficiency of 2,6-DMA could be clearly illustrated with the values obtained in Table 2. The ratios of UVA irradiation promoting the efficiency on the initial rates of 2,6-DMA could be obtained as follows:

$$r_{PE\text{-}F}/r_{E\text{-}F} = \text{Initial rate of PE-F /Initial rate of E-F} \tag{8}$$

Where $r_{PE\text{-}F}$ represents the initial rate of the photoelectro-Fenton process and $r_{E\text{-}F}$ represents the initial rate of the electro-Fenton process. The initial oxidation rate by hydroxyl radicals of organic compound in the electro-Fenton and photoelectro-Fenton processes can be expresses as equation (9) and (10), respectively (Valentine et al., 1998):

$$-d[C_{E-F}]/dt = k_{OH}[^{\bullet}OH][C_{E-F}] = r_{E-F} \tag{9}$$

$$-d[C_{PE-F}]/dt = k_{OH}[^{\bullet}OH][C_{PE-F}] = r_{PE-F} \tag{10}$$

where $C_{E\text{-}F}$ and $C_{PE\text{-}F}$ are the concentrations of 2,6-DMA in the electro-Fenton and photoelectro-Fenton processes, and the k_{OH} represents the rate constants for the reaction between hydroxyl radicals and organic compound. The ratios ($r_{PE\text{-}F}/r_{E\text{-}F}$) of UVA promoting the efficiency were 2.01, 2.56 and 2.66 while the initial concentration of hydrogen peroxide increased from 15 to 20 and 25 mM, respectively. It can be concluded that the UVA irradiation can promote the 2,6-DMA degradation.

Biodegradability of 2,6-DMA in different oxidation processes

Fenton, electro-Fenton and photoelectro-Fenton processes were conducted for 2 hours to investigate the

biodegradability of the treated mixtures. Fig. 1 shows the biodegradability based on BOD_5/TOC in each process at various reaction times. The BOD test measures organic pollutant concentrations indirectly in terms of an equivalent oxygen demand by biological oxidation of the organic matter. However, not all organic materials are biologically degradable. Conversely, the BOD/TOC (molar ratio) evaluation measures the amount of total organic carbon decomposable by microorganisms. A high BOD/TOC ratio means high degree of biodegradation. An increase in the BOD_5 of a sample due to the different treatment would indicate a greater amenability to biodegradation. Thus, an increase in BOD_5/TOC ratio after Fenton, electro-Fenton and photoelectro-Fenton processes were indicative of improved biodegradability due to enhancement in the proportion of TOC amenable to biological mineralization.

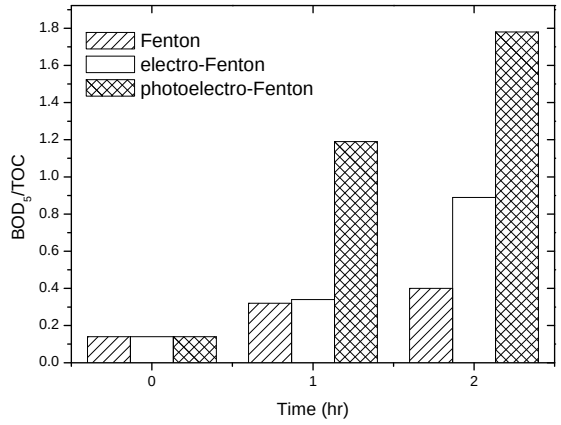

Fig. 1. BOD_5/TOC ratios of treated mixtures by Fenton, electro-Fenton and photoelectro-Fenton processes at 1 mM of 2,6-DMA, 1 mM of Fe^{2+}, 20 mM of H_2O_2, 48 W UVA irradiation, CD_a= 7.6 A/m^2 and CD_c=7.1 A/m^2.

Reaction pathway for 2,6-DMA mineralization

Hydroxyl radicals react with organic compounds by the addition to double bonds possessing sufficient electron density, by hydrogen abstraction from alkyl groups or hydroxyl groups, or electron transfer. Therefore, aminophenols should be generated during the addition reaction with hydroxyl radicals. Brillas et al. (1998) reported that different oxidation reactions led to the formation of nitrobenzene and benzoquinonimine. Benzoquinonimine produced benzoquinone. The oxidation of phenol leads to hydroquinone, which can be further degraded to either benzoquinone. The destruction of nitrobenzene with the release of NO_3^-, benzoquinone and 1,3,4-trihydroxybenzene gives maleic, fumaric and oxalic acids.

In this study, the formation of aminobenzene, nitrobenzene, 2,6-dimethylphenol, phenol and oxalic acid were detected by GC-Mass in this study. Therefore, the degradation mechanism of 2,6-DMA is proposed in Fig. 2.

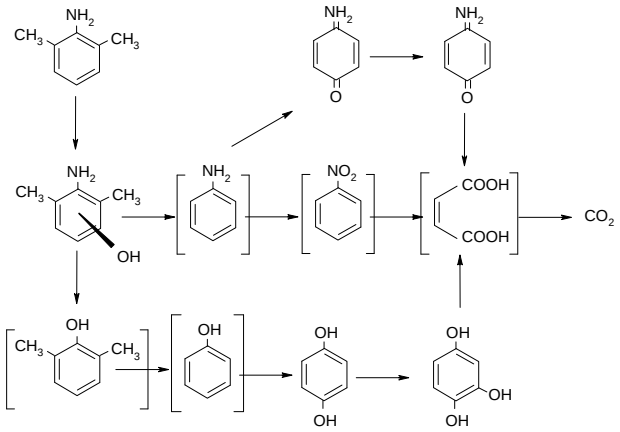

Fig. 2. Proposed reaction pathways for the mineralization of 2,6-DMA in the Fenton processes.

CONCLUSIONS

In the degradation of 2,6-DMA, the performances of the electro-Fenton and photoelectro-Fenton methods are significantly superior to that of the Fenton process. Higher hydrogen peroxide concentrations induced faster 2,6-DMA degradation, but reduce E. These phenomena may be due to the hydroxyl radical scavenging effect of hydrogen peroxide. The electro-Fenton oxidation under UV irradiation accelerated the degradation rate higher than that in electro-Fenton method. These findings confirm that the significant combination (photoelectrochemical/Fenton reagent) led to the formation of additional recycling of ferrous catalyst and hydroxyl radicals. The intermediates, aminobenzene, nitrobenzene, 2,6-dimethylphenol, phenol and oxalic acid, were detected in this study. IN addition, based on the BOD_5/TOC ratios, it reveals that 2,6-DMA can be successfully detoxified in the electro-Fenton and photoelectro-Fenton processes. Some organic intermediates; i.e. were detected.

ACKNOWLEDGEMENT

The authors would like to thank the National Science Council of Taiwan for financially supporting this research under contract No. NSC96-2628-E-041-002-MY3.

REFERENCES

Boye B., Dieng M. M. and Brillas E. (2002). Degradation of herbicide 4-chlorophenoxyacetic acid by advanced electrochemical oxidation methods. Environ. Sci. Technol., 36, 3030-3035.

Brillas E., Mur E., Sauleda R., Sanchez L., Peral J., Domenech X. and Casado J. (1998). Aniline mineralization by AOP's: anodic oxidation, photocatalysis, electro-Fenton and photoelectro-Fenton processes. Appl. Catal. B: Environ., 16, 31-42.

Brillas E., Baños M.Á. and Garrido J.A. (2003). Mineralization of herbicide 3,6-dichloro-2-methoxybenzoic acid in aqueous medium by anodic oxidation, electro-Fenton and photoelectro-Fenton, Electrochimica. Acta., 48, 1697-1705.

Exposito E., Sanchez-Sanchez C.M. and Montiel V. (2007). Mineral iron oxides as iron source in electro-Fenton and photoelectro-Fenton mineralization processes. J. Electrochem. Soc., 154, E116-E122.

Flox C., Garrido J.A., Rodríguez R.M., Cabot P.L., Centellas F., Arias C. and Brillas E. (2007). Mineralization of herbicide mecoprop by photoelectro-Fenton with UVA and solar light, Catal. Today, 129, 29-36.

Lu M.-C., Lin C.-J., Liao C.-H., Huang R.-Y. and Ting W.-P.(2003). Dewatering of activated sludge by Fenton's reagent, Adv. Environ. Res., 7, 667-670.

Lu M.-C., Chen J.-N. and Chang C.-P.(1999). Oxidation of dichlorvos with hydrogen peroxide using

ferrous ion as catalyst. J. Hazard. Mater. , 65 , 277-288.
Metelitsa D.I. (1971) Mechanisms of the hydroxylation of aromatic compounds. Russ. Chem. Rev. 40, 563-580.
Rigg T., Taylor W. and Weiss J. (1954). The rate constant of the reaction between hydrogen peroxide and ferrous ions. J. Chem. Phys., 22, 575-577.
Roland S., Ingbert S. and Hans-Henning S. (1997). Fluorometric determination of low concentrations of H2O2 in water: Comparison with two other methods and application to environmental samples and drinking-water treatment. Wat. Res., 31, 1371–1378.
Safarzadeh-Amiri A., Bolten J.R. and Cater S.R.(1996). The use of iron in advanced oxidation processes. J. Adv. Oxid. Technol, 118-26.
Sirés I., Arias C., Cabot P.L., Centellas F., Garrido J.A., Rodríguez R.M. and Brillas E. (2007). Degradation of clofibric acid in acidic aqueous medium by electro-Fenton and photoelectro-Fenton. Chemosphere, 66, 1660-1669.
Sirés I., Garrido J.A., Rodrígues R.M., Brillas E., Oturan N. and Oturan M.A. (2007b). Catalytic behavior of the Fe^{3+}/Fe^{2+} system in the electro-Fenton degradation of the antimicrobial chlorophene. Appl. Catal. B-Environ. 72 382-394.
Ting W.-P., Lu M.-C., and Huang Y.-H. (2009). Kinetics of 2,6-dimethylaniline degradation by electro-Fenton process. J. Hazard. Mater. 161, 1464-1490.
Valentine R.L. and Wang H.C.A. (1998). Iron oxide surface catalyzed oxidation of quinoline by hydrogen peroxide. J. Environ. Eng., 124, 31-38.
Walling C. (1975) Fenton's reagent revisited. Acc. Chem. Res. 8 121-131.